IMPROVED DROUGHT EARLY WARNING AND FORECASTING TO STRENGTHEN PREPAREDNESS AND ADAPTATION TO DROUGHTS IN AFRICA

DEWFORA

A 7th Framework Programme Collaborative Research Project

Testing of drought indicators at Pan-African level

WP6-D6.3

August 2012

Coordinator: Deltares, The Netherlands

Project website: www.dewfora.net

FP7 Call ENV-2010-1.3.3.1

Contract no. 265454

Page intentionally left blank

DOCUMENT INFORMATION

Title	Testing of drought indicators at Pan-African level
Lead Author	Gustavo Naumann, Paulo Barbosa
Contributors	Emanuel Dutra, Florian Pappenberger, Fredrik Wetterhall
Distribution	PP: Restricted to other programme participants (including the Commission Services)
Reference	WP6 – D6.3

DOCUMENT HISTORY

Date	Revision	Prepared by	Organisation	Approved by	Notes
06/08/2012		G. Naumann and P.Barbosa	JRC		
03/08/2012		Gilbert Ouma	ICPAC		
15/06/2012		Gustavo Naumann	JRC		
15/06/2012		Paulo Barbosa	JRC		
14/06/2012		Emanuel Dutra	ECMWF		
14/06/2012		Florian Pappenberger	ECMWF		
14/06/2012		Fredrik Wetterhall	ECMWF		
10/05/2012		Gustavo Naumann	JRC		

ACKNOWLEDGEMENT

The research leading to these results has received funding from the European Union's Seventh Framework Programme (FP7/2007-2013) under grant agreement N°265454

Page intentionally left blank

Summary

This study investigates the potential of implementing different drought indicators to improve drought monitoring capabilities at continental scale. It is the first of a series of deliverables referring to continental Africa that will be followed by D6.4 (Integration of Drought Vulnerability and Hazard into Risk Maps at the Pan-African Level), D6.5 (Integration of Drought Forecasting Tools for Africa into the Pan-African Map Server) and D6.6 (Development and Implementation of the Pan-African Map Server). Several global datasets based on re-analysis, gridded observation, and remote sensing data were tested. At regional level the capabilities of each indicator and dataset on five regions on the African continent (Oum-er-Rbia, Eastern Nile, Niger, Limpopo and the Great Horn of Africa) were compared. A more exhaustive analysis on these case studies will be provided in D6.2 (Implementation of improved methodologies in comparative casec studies. Final Report for each Case Study).

The five precipitation datasets used in this study were the ERA – Interim reanalysis (0.5°x0.5° resolution from 1979 to 2010), the Tropical Rainfall Measuring Mission (TRMM) satellite monthly rainfall product 3B43 (0.25°x0.25° resolution from 1998 to 2010), the Global Precipitation Climatology Centre (GPCC) gridded precipitation dataset V.5 (1°x1° resolution from 1901 to 2010), the Global Precipitation Climatology Project (GPCP) Global Monthly Merged Precipitation Analyses (2.5°x2.5° resolution from 1979 to 2010), and the Climate Prediction Center Merged Analysis of Precipitation (CMAP, 2.5°x2.5° resolution from 1979 to 2010).

The set of indicators proposed included the Standardized Precipitation index (SPI), the Standardized Precipitation-Evaporation Index (SPEI), the Standardized Run-off index (SRI), the Soil Moisture Anomalies (SMA), the Normalized Difference Water Index NDWI, the fraction of Absorbed Photosynthetically Active Radiation (fAPAR) and the growing season length (GSL) anomalies.

This report evaluates the ability of the different datasets and derived indicators in representing drought conditions at continental level, by analysing its intensity, duration and spatial extent.

A comparison of the annual cycle and monthly precipitation time series using the different datasets shows a general agreement in the timing of the precipitation peaks, including in the Great Horn of Africa area that has two rainy seasons. The main differences are observed thus in the ability to represent the magnitude of the wet seasons and extremes. Moreover, for the areas that are under drought, all the datasets agree with the time of drought onset and

recovery although this agreement varies with the threshold selected to define the drought conditions, and there are sometimes disagreements on the area affected.

The comparative analysis between TRMM, ERAI, GPCP and GPCC datasets suggests that it is feasible to use TRMM time series for reliable drought monitoring over Africa. The main advantage of this dataset is mainly due to its high spatial resolution. However, higher discrepancies in SPI estimations are shown in mountainous areas and in areas with low in situ station density.

All the drought indicators analysed at continental level showed a good agreement in North West and Southern Africa, while a low agreement was observed in Central Africa.. A good agreement is also observed between SPI-3 TRMM and SPI-3 ERAI in east Africa. The low agreement of the indicators over Central Africa reflects the high uncertainty present in the precipitation datasets.

The comparison between different SPI estimations suggest that the main sources of error are due to the uncertainties in the datasets (lack of ground information, estimation algorithms, parameterization of the convection, etc.) rather than the estimation of the distribution parameters.

Finally, the integrated use of two different sources of information in the Horn of Africa, meteorological and remote sensing derived vegetation indices, shows great potential to synergistically monitor drought events.

Page intentionally left blank

TABLE OF CONTENTS

List of figures

List of tables

Page intentionally left blank

1. INTRODUCTION

The monitoring and assessment of drought conditions requires understanding of regional historical droughts as well as of the impacts on human activities during their occurrence. Traditional methods for drought monitoring and assessment are mainly based on water supply indices derived from precipitation time-series alone. However, the lack of reliable and up-to-date precipitation data in many regions of the continent hinder the development of effective real-time drought monitoring and early warning systems at Pan-African level.. The sparse spatial distribution of rain gauges and the short or incomplete rainfall historical records pose further problems. This lack of information may lead to significant errors in the estimation of statistical parameters needed for deriving water supply indices from precipitation time-series.

Procedures for drought detection and assessment have a particular level of uncertainty associated to the data and models used. In order to better understand the extent, severity and impact of a drought in a region, it is first necessary to improve the quality of these procedures by using the best available data, theoretical assumptions and model formulations.

Examination and selection of the data to be used often constitute a more complicated task than the calculation of the index itself. Also, one of the main concerns when choosing a baseline period is that this baseline should represent normal or expected conditions (and include no climatic drifts), since most users of a drought indicator assume that the baseline represents such conditions. Usually a drought index that measures departures from normal conditions requires historical observations longer than 30 years to calculate stable baseline statistics (WMO, 2011). However, in some areas of the world the availability of quality information to calculate these statistics and to compute the drought indices in near-real time is almost impossible.

The DEWFORA project aims to implement an operational early warning system, over Africa. The main goals of the project are to build up a system that could provide local and regional stakeholders with a practical decision-support tool in order to better assess drought impacts, to quantify spatial extent of drought risk, and to improve early warning systems in Africa.

Many drought-prone regions in Africa have complicated terrain and limited rain gauge data. Many countries in the region have seen recent famines that affected millions of people. Because crops are dependent on rainfall in these drought-prone regions, improvements in drought monitoring and early warning will extend our capacity to detect, anticipate, and mitigate famine.

The main objective of this study is to evaluate the capabilities of different drought indicators in detect the timing, duration and extension of droughts across Africa. In order to do this, four different rainfall datasets, each available on a monthly basis, were analysed over four river basins in Africa (Oum er-Rbia, Limpopo, Niger, and Eastern Nile) as well as for the Great Horn of Africa and at continental level. The four precipitation datasets used were the ERA-INTERIM Reanalysis (approximately 0.7°x0.7° and was interpolated to 0.5°x0.5°), the Tropical Rainfall Measuring Mission (TRMM) satellite monthly rainfall product 3B43 (0.25°x0.25°), the Global Precipitation Climatology Centre (GPCC) gridded precipitation dataset V.5 (0.5°x0.5°), and the Global Precipitation Climatology Project (GPCP) Global Monthly Merged Precipitation Analyses (2.5°x2.5°). The set of hydro-meteorological indicators proposed included the Standardized Precipitation index (SPI), the Standardized Precipitation-Evaporation Index (SPEI), the Standardized Run-off index (SRI), and Soil Moisture Anomalies (SMA). These were further compared with the growing season length (GSL) anomalies for the different geographical regions analysed.

The vegetation remote sensing derived indicators, Normalized Difference Water Index NDWI, and fraction of Absorbed Photosynthetically Active Radiation (fAPAR) were further analysed in order to assess their capacity to monitor drought during the 2010-2011 drought event in the Great Horn of Africa. A step by step analysis of this drought scenario in the Great Horn of Africa and its linkage with impacts and decision making process were further developed with a special focus in Kenya.

2. CASE STUDIES DESCRIPTION

The DEWFORA project has a clear focus on the testing and implementation of existing and developed methodologies on drought monitoring and forecasting. Within the WP6 a demonstrative continental Pan-African system will be developed, focusing on a pre-operational drought monitoring and forecasting system. As a first step, and in order to set up the continental monitoring system a set of drought indicators and datasets were tested.

In addition to the continental case study, other regions were used in order to provide in depth analysis of drought monitoring at different spatial scales. The regions selected for the analysis are the four case studies defined in DEWFORA (see D6.1 for a more detailed description) plus the Great Horn of Africa (GHA) region. The size and geographical extent of the boxes delimiting the case study areas are provided in Table 2-1 and Figure 2-1.

Region	Area (10^6xKm^2)	Longitude-Latitude	TRMM Grid cells	GPCC Grid cells	ERA-I and GPCP Grid cells
A - Oum er-Rbia	0.49	[10ºW-0ºE]X[31ºN-35ºN]	640	36 (0.52, 0.65)	160
B - Niger	1.48	[10ºW-0ºE]X[6ºN-18ºN]	1920	120 (0.23,.70)	480
C - Eastern Nile	1.23	[30ºE-40ºE]X[7ºN-17ºN]	1600	100 (0.23,0.75)	400
D - Limpopo	0.94	[25ºE-34ºE]X[26ºS-20ºS]	1224	54 (0.56, 0.44)	216
E -GHA	2.22	[40ºE-52ºE]X[2ºS-12ºN]	2880	180 (0.15, 0.85)	720

Table 2-1 Geographical extent of the African regions and number of grid cells analysed for each dataset. For GPCC, the percentage of stations per grid and the percentage of pixels without stations are respectively shown between brackets.

2.1 REGION A: OUM ER-RBIA BASIN

The Oum er-Rbia Basin is a river basin of strategic importance in Morocco. It represents 7% of the total area of Morocco and contains 14% of the population. The basin has diverse economic activities, including irrigated and rain-fed agriculture,

mining, and numerous large manufacturing industries. The basin also provides water transfers to large cities, including Casablanca and Marrakech.

2.2 REGION B: NIGER BASIN

The Niger river is the third longest river in Africa (4180 km) and its basin (2,117,700 km2) encompasses nine countries in West and Central Africa. About 30% of the basin is located in Mali, one of the poorest countries in the world. The main economic activities in Mali are agriculture and fishing. The agricultural sector employs about 80% of the work force, even though less than 2% of the land is arable. For this reason, livelihood and welfare in Mali depends largely on the timely onset and intensity of the annual monsoon.

2.3 REGION C: EASTERN NILE BASIN

The Nile River is the longest river in the world (6650 km); its basin covers 3,400,000 km^2 and encompasses ten countries in east and central Africa. From the socio-economic and political points of view, the Nile Basin can be regarded as one of the most important basins in Africa. Water management in the basin has historically been a controversial issue and cause of tensions between the countries, which often have a sole dependency on the Nile as a water resource.

2.4 REGION D: LIMPOPO BASIN

The Limpopo River located in central-southern Africa, is about 1,750 km long and has a drainage basin of 415,000 km^2, covering four countries: Botswana, Mozambique, South Africa and Zimbabwe. The basin experiences a short and intense rainy season, with highly unreliable rainfall, which leads to frequent droughts. Poverty is widespread and people are extremely vulnerable to the effects of drought on crop failure. Starvation and malnutrition are common occurrences. About one million people in the basin currently rely on food aid (Love et al., 2006).

2.5 REGION E: GREAT HORN OF AFRICA

The Greater Horn of Africa comprises 10 countries: Burundi, Djibouti, Eritrea, Ethiopia, Kenya, Rwanda, Somalia, Sudan, Uganda, and Tanzania. The annual cycle in the majority of the GHA region is quite complex and experiences a bimodal rainfall pattern associated with the progression of the intertropical convergence zone (ITCZ)

across the region. The rainfall during the period October–December, or “short rain” season, is generally associated with larger interannual variability in comparison to the “long rains” of March-May (Camberlin and Philippon 2002).

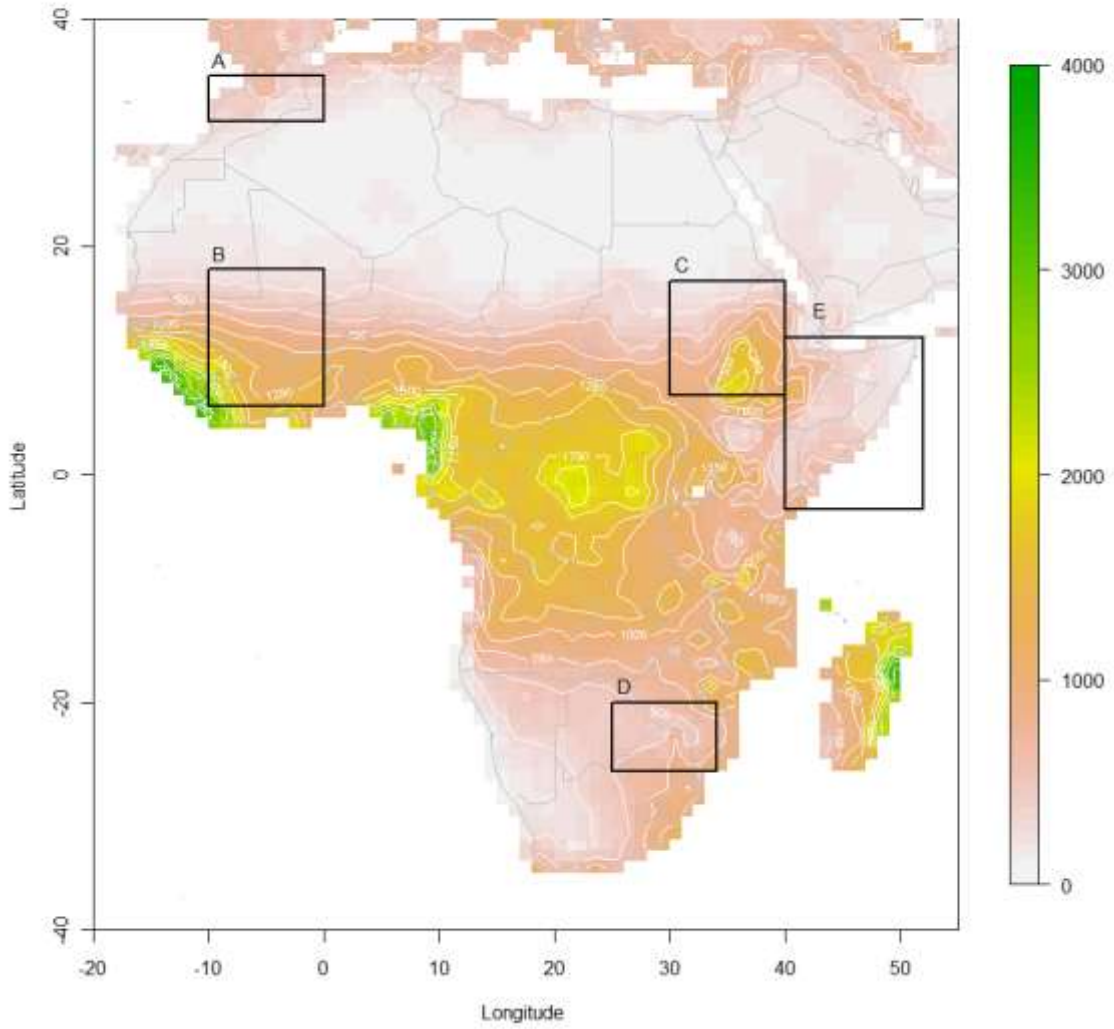

Figure 2-1 Annual mean precipitation for GPCC dataset and African regions used in this analysis. (A) Oum er-Rbia, (B) Niger, (C) Eastern Nile, (D) Limpopo and (E) Great Horn of Africa.

Several droughts were recorded during the lasts years having different degrees of severity and impacts. As detailed in D2.2, during the period 1981/82 to 2008/09 the Southern Africa region recorded 14 seasons of drought, the North Africa - Maghreb Region 18 seasons, West Africa-Niger Basin 4 seasons, East Africa- Nile Basin 21 seasons, the Ethiopian Plateau 10 seasons and the East Africa- Nile Basin Equatorial Lakes Region 15 seasons. However, the droughts for the East Africa- Nile Basin and Ethiopian Plateau were poorly recorded over this period.

2.6 DATASETS DESCRIPTION

Table 2-2 synthesizes the characteristics of the different precipitation datasets used in this study followed by a more detailed description and by a short spatial analysis of each dataset.

Datasets	resolution	period	Source	delay
ERA INTERIM	0.5ºx0.5º	1979-present	ECMWF Reanalysis	½ month
TRMM 3B-43 **v.6 (v.7 when available)**	0.25ºx0.25	1998-present	RSE (combination 3B-42, CAMS and/or GPCC)	1/2 months
GPCC **v.5 (Combined)**	0.5ºx0.5º (1ºx1º)	1901-2010 (-present)	In-situ data	1 month
GPCP **v.2.2**	2.5ºx2.5º	1979-2010	RSE (merged from microwave, infrared and sounder data and precipitation gauge analyses (GPCC).	irregular
CMAP	2.5ºx2.5º	1979-2009	RSE (GPI, OPI,S SM/I scattering, SSM/I emission and MSU + NCEP/NCAR Reanalysis)	irregular

Table 2-2 Description of global datasets available in near-real time and could be used for monitoring precipitation conditions at continental level. Note: The hyperlink to access the entire data are associated at each dataset name.

2.6.1 ERA-INTERIM REANALYSIS

The ECMWF ERA-Interim (ERAI) reanalysis is the latest global atmospheric reanalysis produced by ECMWF extending from 1 January 1979 to the present date. See Dee et al. (2011) for detailed descriptions of the atmospheric model used in ERAI, the data assimilation system, the observations used, and various performance aspects. The ERAI configuration has a spectral T255 horizontal resolution (about 0.7°x0.7° in the grid-point space) with 60 model levels. For the present application, the monthly means of precipitation were spatially interpolated (bilinear) to a regular 0.5°x0.5° grid. Further details and analysis of ERAI precipitation and its application to drought indices can be found in D4.1, D4.2 and D4.3.

2.6.2 TRMM B3-43

TRMM Multi-Satellite Precipitation Analysis (TMPA; computed at monthly intervals with the TRMM 3B-43 dataset for the period 1998-2010) combines the estimates generated by the TRMM and other satellites product (3B-42) with the Climate Anomaly Monitoring System (CAMS) gridded rain gauge data, produced by NOAA's Climate Prediction Center, and/or with the global rain gauge product produced by the Global Precipitation Climatology Center (GPCC). The output product represents monthly rainfall at 0.25°x0.25° spatial resolution.

The TRMM satellite has proved to be useful for precipitation monitoring in regions, such as areas of Central Africa, where station data is difficult to obtain or where there is poor station coverage (Jenkins 2000). In fact, TRMM precipitation products have been extensively validated at ground sites around the world, some of these in Africa. Nicholson et al. (2003) show that TRMM estimations are in excellent agreement with gauge data over West Africa on monthly to seasonal timescales with a root mean square (RMS) error of around 1mm/day at monthly resolution.

Adeyewa and Nakamura (2003) conducted a 36-month climatological assessment of the TRMM-PR, 3B43, and Global Precipitation Climatology Project (GPCP) satellite products over the major climatic regions in Africa. The study shows that 3B43 closely matches rain gauge data, suggesting that the goal of the algorithm was largely achieved. Dinku et al. (2007) studied a relatively dense station network over the Ethiopian highlands to evaluate the performance of different satellite products over complex topography in the tropics. The authors found that for those evaluated at a monthly time scale, CPC Merged Analysis of precipitation (CMAP) and TRMM 3B43 performed very well with a bias less than 10% and an RMS of about 25%. The TMPA estimation provides reasonable performance at monthly scales, but has lower skill in correctly specifying moderate and light event amounts at short time intervals, in common with other fine scale estimators (Huffman et al. 2007).

2.6.3 GPCC

The version 5 of the GPCC full reanalysis (Rudolph et al. 1994) during the period 1951 to 2010 was used in this study. This dataset is based on quality-controlled precipitation observations from a large number of stations (up to 43,000 globally) with irregular coverage in time.

The Monitoring Product of monthly precipitation for global climate monitoring is based on SYNOP and monthly CLIMAT reports received in near-real time via GTS from ca. 7,000 –8,000 stations (after high level QC) and is available within 2 months after the observation month. This is the GPCC product with the longest history: Operational monthly analysis started in 1986 and has continuously been updated every month since then. The analyses are based on automatic and intensive manual quality-control of the input data. The GPCC Monitoring Product is the *in situ* component to the satellite-gauge combined precipitation analyses of GPCP (Huffman et al. 1995, Adler et al. 2003) and of CMAP (Xie and Arkin 1997). It also supports regional climate monitoring.

The Full Data Reanalysis Product is of much higher accuracy compared to the GPCC near real-time products mentioned above. Therefore, its application is recommended for hydrometeorological model verification and water cycle studies, e.g. in context of UNESCO, GEWEX, and GTN-H (Global Terrestrial Network for Hydrology). This analysis product is based on all stations, near real-time and non-real-time, in the GPCC data base supplying data for the individual month for which a climatological normal is available (for details see Precipitation Climatology). The GPCC Full Data Reanalysis Product Version 6 covers the period from 1901 to 2010.

2.6.4 GPCP

The Global Precipitation Climatology Project (GPCP) was established by the World Climate Research Program (WCRP) to address the problem of quantifying the distribution of precipitation around the globe over many years. The general approach is to combine the precipitation information available from each of several sources into a final merged product, taking advantage of the strengths of each data type. The microwave estimates are based on Special Sensor Microwave/Imager (SSM/I) data from the Defence Meteorological Satellite Program (DMSP, United States) satellites that fly in sun-synchronous low-earth orbits. The infrared (IR) precipitation estimates are computed primarily from geostationary satellites (United States, Europe, Japan), and secondarily from polar-orbiting satellites (United States). Additional low-Earth orbit estimates include the Atmospheric Infrared Sounder (AIRS data from the NASA Aqua, and Television Infrared Observation Satellite Program (TIROS) Operational Vertical Sounder (TOVS) and Outgoing Longwave Radiation Precipitation Index (OPI) data from the NOAA series satellites. The gauge data are assembled and analyzed by the Global Precipitation Climatology Centre (GPCC) of the Deutscher

Wetterdienst and by the Climate Prediction Center of NOAA. The latest version of GPCP v2.2 available from January 1979 to December 2010 in a regular 2.5°x2.5° grid was used in this study.

2.6.5 CMAP

The CPC Merged Analysis of Precipitation ("CMAP") is a technique which produces pentad and monthly analyses of global precipitation in which observations from raingauges are merged with precipitation estimates from several satellite-based algorithms (infrared and microwave). The analyses are on a 2.5° x 2.5° latitude/longitude grid and extend back to 1979. For further information refer to Xie and Arkin, 1997.

2.6.6 Spatial analysis of the different datasets

The datasets analysed are mainly based on in-situ data (GPCC), remote sensing estimations (TRMM, GPCP and GPCC) and global circulation model (ERAI-I). Although each dataset relies on his primarily source of data those are not completely independent (TRMM and GPCP are mainly based on remote sensing data and GPCP uses GPCC over land). Figure 2-2 shows the mean annual precipitation for the ERA-I, GPCC, GPCP, CMAP and TRMM datasets over Africa. An overall agreement is shown between datasets with respect to average and interannual variability as well as the mean spatial patterns of annual precipitation. These datasets agree on the north-south gradient from the desert areas to the tropical savannahs in the Sahel and rainforests related to a precipitation maximum due the location of the Intertropical Convergence Zone (ITCZ). The main differences are observed in the tropical area and un-gauged areas. Also, there exists a tendency in ERA-I in overestimate precipitation in the tropical rainforest. For more details, refer to Deliverable D4.2.

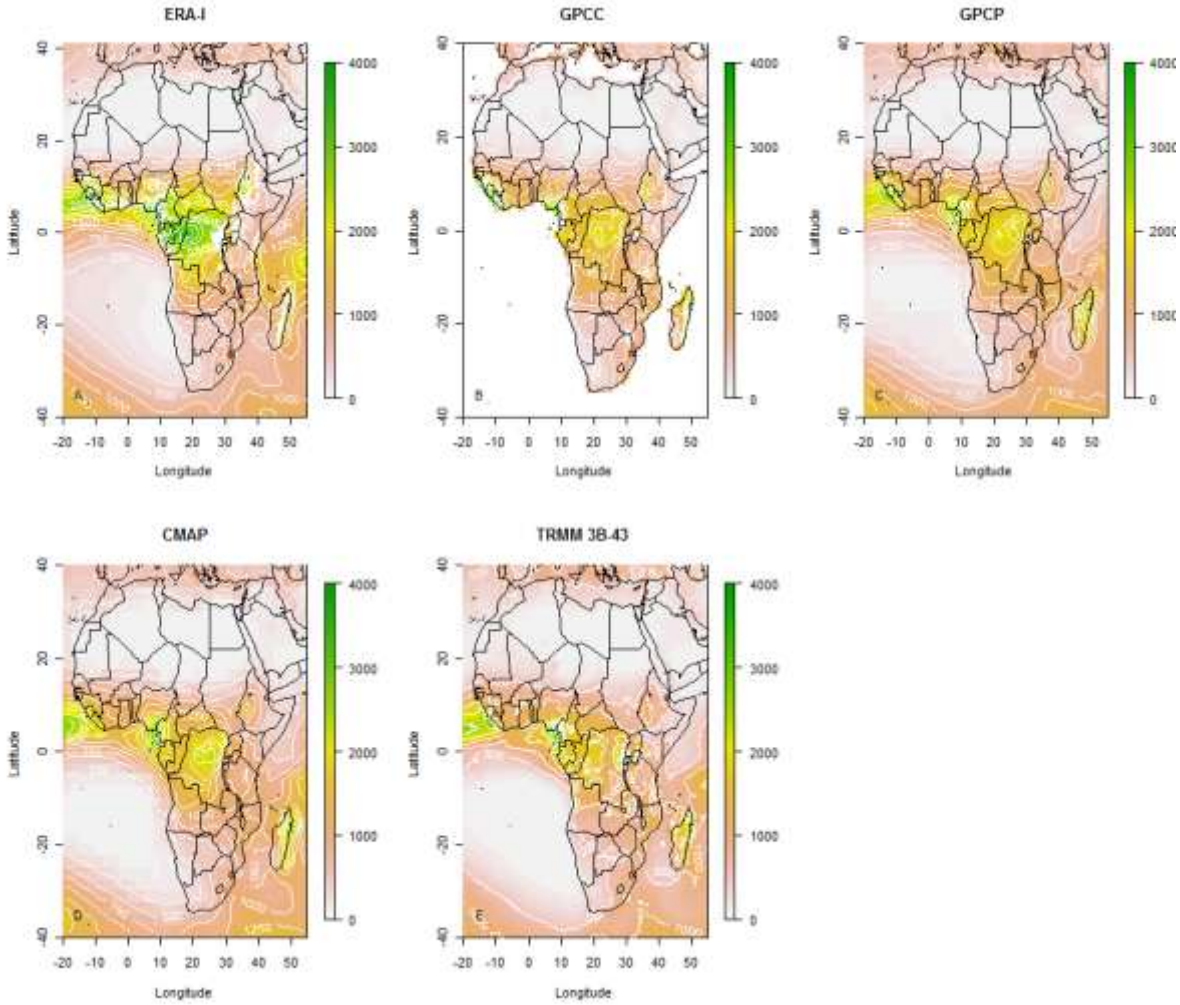

Figure 2-2 Mean annual precipitation (mm/year) from different datasets for the common period 1998-2010.

3. DROUGHT INDICATORS

3.1 STANDARDIZED PRECIPITATION INDEX (SPI)

The Standardized Precipitation Index (SPI) was developed by McKee et al. (1993, 1995) to provide a spatially and temporally invariant measure of the precipitation deficit (or surplus) for any accumulation timescale. It is computed by fitting a parametric Cumulative Distribution Function (CDF) to a homogenized precipitation time-series and applying an equi-probability transformation to the standard normal variable. This gives the SPI in units of number of standard deviations from the median.

Typically, the gamma distribution is the parametric CDF chosen to represent the precipitation time-series (e.g. McKee et al. 1993, 1995; Lloyd-Hughes and Saunders 2002; Husak et al. 2007) since it has the advantage of being bounded on the left at zero and positively skewed (Thom 1958; Wilks 2002). Moreover, Husak et al. (2007) have shown that the gamma distribution adequately models precipitation time-series in roughly 98% of locations over Africa. In this study we use the Maximum-Likelihood Estimation (MLE) method to estimate the parameters of the gamma distribution.

A reduction in precipitation with respect to the normal precipitation amount is the primary driver of drought, resulting in a successive shortage of water for different natural and human needs. Since SPI values are given in units of standard deviation from the standardised mean, negative values correspond to drier periods than normal and positive values correspond to wetter periods than normal. The magnitude of the departure from the mean is a probabilistic measure of the severity of a wet or dry event (Table 3-1).

Since the SPI can be calculated over different rainfall accumulation periods, different SPIs allow for estimating different potential impacts of a meteorological drought:

- SPIs for short accumulation periods (e.g., SPI-1 to SPI-3) are indicators for immediate impacts such as reduced soil moisture, snowpack, and flow in smaller creeks;
- SPIs for medium accumulation periods (e.g., SPI-3 to SPI-12) are indicators for reduced stream flow and reservoir storage; and
- SPIs for long accumulation periods (SPI-12 to SPI-48) are indicators for reduced reservoir and groundwater recharge, for example.

The exact relationship between accumulation period and impact depends on the natural environment (e.g., geology, soils) and the human interference (e.g., existence of irrigation schemes). In order to get a full picture of the potential impacts of a

drought, SPIs of different accumulation periods should be calculated and compared. A comparison with other drought indicators is needed to evaluate actual impacts on the vegetation cover and different economic sectors.

Definition of SPI classes	
SPI ≤ -2	Extremely dry
-2 < SPI ≤ -1.5	Severely dry
-1.5 < SPI ≤ -1	Moderately dry
-1 < SPI ≤ 1	Near normal
1 < SPI ≤ 1.5	Moderately wet
1.5 < SPI ≤ 2	Severely wet
SPI ≥ 2	Extremely wet

Table 3-1 Definition of Standard Precipitation Index (SPI) classes

3.2 STANDARDIZED PRECIPITATION-EVAPORATION INDEX (SPEI)

The Standardized Precipitation evapotranspiration index (SPEI, Vicente-Serrano et al. 2010) is based on precipitation and temperature data, and it has the advantage of combining time multiscale properties (like the SPI) with the capacity to include the effects of temperature variability on drought. The calculation involves a climatic water balances, the accumulation of deficit/surplus at different time scales, and adjustment to a log-logistic probability distribution, SPEI is similar to SPI, but it includes the role of temperature via the potential evapotranspiration (PET) that is calculated following (Thornthwaite 1948). In the current work, we used ERAI 2-meters temperature to derive PET, and the index is calculated as P-PET over the different time-scales and normalized (like the SPI) using the log-logistic probability distribution.

3.3 STANDARDIZED RUNOFF INDEX (SRI)

The standardized runoff index (SRI) follow the same concept has the SPI, defined as the unit standard normal deviate associated with the percentile of hydrologic runoff accumulated over a specific duration (Shukla and Wood 2008). As for the SPI and SPEI, different distributions can be used to fit the data. In the current application we used the Gamma function applied to ERAI simulated monthly means of runoff.

3.4 SOIL MOISTURE ANOMALIES (SMA)

Soil moisture anomalies were derived from ERAI simulations by removing the mean annual cycle. Further standardization, could be achieved by fitting the soil moisture distribution to a probability distribution (similar procedure to SPI, SPEI or SRI) such as the Beta (Sheffield et al. 2004) or just a simple z-score (Dutra et al. 2008). In the current work we kept only the anomalies since a proper standardization would require further research on the topic that has not been so widely used as in the SPI case.

3.5 START OF GROWING SEASON (SOS) AND GROWING SEASON LENGTH (GSL)

The yearly values of Start of the Growing Season (SOS) and Growing Season Length (GSL) were derived for each image pixel of the study area using the algorithms of the “Phenolo” package developed at the EC Joint Research Centre. The methodology is similar to the method described in Reed et al. (1994). While Reed et al. (1994) determine a general lag based on a priori knowledge about the average phenology of the study area, Phenolo is strictly data driven using for each individual pixel the time series itself to determine the parameters for each annual growth cycle. Hence, it is independent of a priori knowledge on average phenology in an area and thus is able to accommodate both a large variation of climatic conditions, and local land cover and land use characteristics. In order to generate results comparable between data sources with different time aggregation windows, the first processing step involves interpolation to daily values smoothed through a 5 day moving average filter. Then a median filter within a 50-day moving window is applied to the time series in order to identify and remove short peaks and drop-offs due to noise as caused for instance by clouds. The interpolation and smoothing window sizes are parameterised to adjust to local variations resulting in the reference time series on which the phenological parameters are to be computed. For further information, refer to Ivits et al., 2012.

In order to compute the indicators, NDVI data at a spatial resolution of 8 km×8 km and a temporal resolution of 15 days were acquired from the Global Inventory Monitoring and Mapping Studies (GIMMS) group. The time span of the data covered January 1982 to December 2010 from the NOAA/AVHRR satellite series (NOAA 7, 9, 11, 14, 16 and 17) (Tucker et al., 2005). The SOS and GSL are determined as the intersections of the reference time-series and a forward and backward lagged moving average curve. For each pixel the forward and backward lag is defined by the average length of the non-growing season based on an estimation of the growing season length (GSL) derived from the reference time-series. Where single yearly growing seasons occur, season length is constrained by the points in time where indicators of vegetation intensity signals are minimal. Between two subsequent signal minima, the signal above the line connecting the minimal values is interpreted as a histogram, of which mean and standard deviation are determined. The obtained mean value is effectively passing through the “barycentre” of the area, delimited by the NDVI signal and the baseline connecting the minima. By default, the estimated objective season length (GSL) is defined to be two times the standard deviation computed from the barycentre of the area expressed in days. One standard deviation was taken as the default value because it describes 68.2% of the statistical population with normal distribution, which is considered a good approximation of vegetation signal in case of a single season. The size of the moving average window, i.e. the lag, used to obtain the forward and backward shifted moving average filtered time series is the yearly complement of GSL.

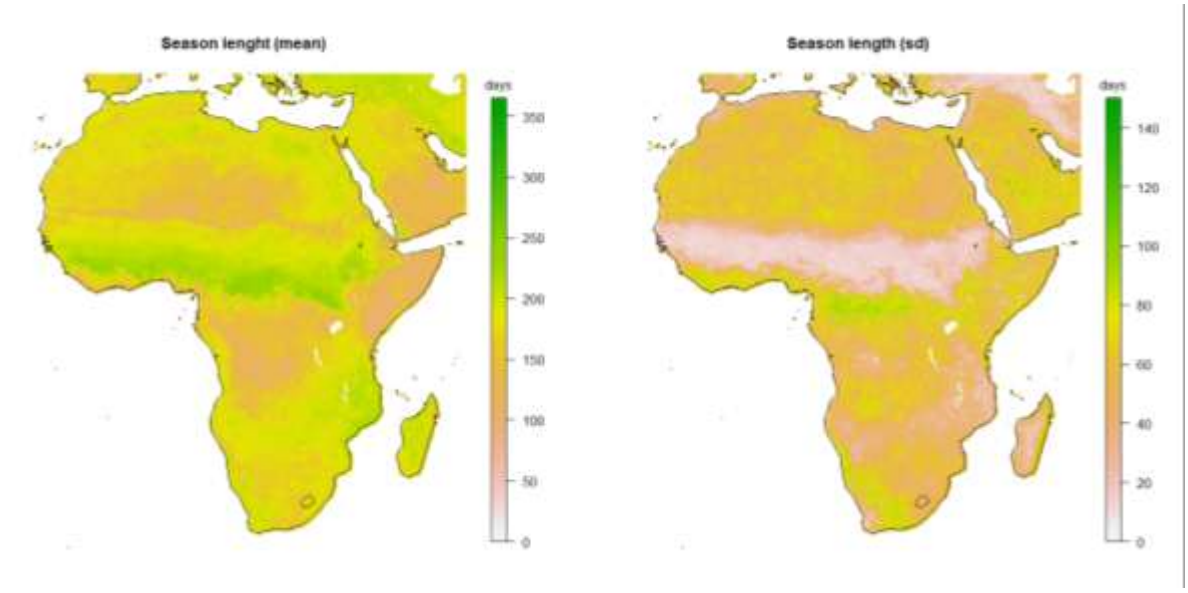

Figure 3-1 Mean composite and standard deviation of Growing Season length for the period 1982-2010, based on NDVI.

As observed in Figure 3-1 there are a wide range of growing season length across the continent, ranging between 50 to more than 300 days. Also, there are some regions where variability can reach more than 100 days, mainly in central Africa (Cameroon, Central Africa Republic).

3.6 NORMALIZED DIFFERENCE WATER INDEX (NDWI)

The Normalized Difference Water Index (NDWI) (Gao, 1996) is a satellite-derived index from the Near-Infrared (NIR) and Short Wave Infrared (SWIR) channels. The SWIR reflectance reflects changes in both the vegetation water content and the spongy mesophyll structure in vegetation canopies, while the NIR reflectance is affected by leaf internal structure and leaf dry matter content but not by water content. The combination of the NIR with the SWIR removes variations induced by leaf internal structure and leaf dry matter content, improving the accuracy in retrieving the vegetation water content (Ceccato et al. 2001). The amount of water available in the internal leaf structure largely controls the spectral reflectance in the SWIR interval of the electromagnetic spectrum. SWIR reflectance is therefore negatively related to leaf water content (Tucker 1980).

Its usefulness for drought monitoring and early warning has been demonstrated in different studies (e.g., Gu et al., 2007; Ceccato et al., 2002). It is computed using the near infrared (NIR) and the short wave infrared (SWIR) reflectance, which makes it sensitive to changes in liquid water content and in spongy mesophyll of vegetation canopies (Gao, 1996; Ceccato et al., 2001).

The Normalized Difference Water Index (NDWI) is a remote sensing derived index estimating the leaf water content at canopy level.

- Geographic coverage: available for Africa
- Spatial scale: 1.2km
- Temporal scale: every 10 days aligned on the first day of each month, which corresponds to 3 images per month (day 1-10, day 11-20, day 21-last day of month).
- Data source: MODIS spectral bands 2 and 6 are provided by the German Aerospace Centre (DLR) and pre-processed by the FOREST Action (IES, JRC).
- Frequency of data collection: every day
- Baseline statistics: The archive of NDWI covers the period from January 2006 to current day.

NDWI anomalies are produced for every 10-day period as follows:

$$NDWI\ anomaly_t = \frac{x_t - \bar{x}}{\sigma} \quad \text{3–1}$$

where X_t is the NDWI of the 10-day period t of the current year and, $\bar{X}$ is the long-term average NDWI and σ is the standard deviation, both calculated for the same 10-day period t using the available time series (see baseline statistics).
NDWI anomalies are produced only for pixels that have at least five years of data for the given 10-day period.

3.7 FRACTION OF ABSORBED PHOTOSYNTHETICALLY ACTIVE RADIATION (FAPAR)

The Fraction of Absorbed Photosynthetically Active Radiation (fAPAR) represents the fraction of the solar energy which is absorbed by the vegetation. fAPAR is a biophysical variable directly correlated with the primary productivity of the vegetation, since the intercepted PAR is the energy (carried by photons) underlying the biochemical productivity processes of plants. fAPAR is one of the Essential Climate Variables recognized by the UN Global Climate Observing System (GCOS) and by the FAO Global Terrestrial Observing System (GTOS) as of great potential to characterize the climate of the Earth.
Due to its sensitivity to vegetation stress, fAPAR has been proposed as a drought indicator (Gobron et al. 2005 and 2007). Indeed droughts can cause a reduction in the vegetation growth rate, which is affected by changes either in the solar interception of the plant or in the light use efficiency.

The MERIS Global Vegetation Index (MGVI) is a remote sensing derived index estimating fAPAR at canopy level.

- Geographic coverage: available for Africa
- Spatial scale: 1.2km
- Temporal scale: every 10 days aligned on the first day of each month, which corresponds to 3
- Images per month (day 1-10, day 11-20, day 21-last day of month).
- Data source: MGVI data are delivered as a subscription service within the Service Support
- Environment (SSE) of the European Space Agency. This service is called "MGVI Catalogue Search and Download" and can be access via this link: http://services.eoportal.org/portal/service/ShowServiceInfo.do?serviceId=7180CB90&categoryId=89802980
- Frequency of data collection: every 10 days

fAPAR is difficult to measure directly but can be inferred from models describing the transfer of solar radiation in plant canopies, using Earth Observation information as input data. fAPAR estimates are retrieved using EO information by numerically inverting physically-based models. The fAPAR estimates used within the DESERT Action are operationally produced by the European Space Agency (ESA). They are derived from the multispectral images acquired by the Medium Resolution Imaging Spectrometer (MERIS) onboard ENVISAT by means of the MERIS Global Vegetation Index (MGVI) algorithm, developed at the JRC (Pinty B. et al, 2002; Gobron et al. 2004). The MGVI anomalies were computed as for the NDWI anomalies above.

4. INTER-COMPARISON OF DROUGHT INDICATORS

4.1 METHODOLOGY

4.1.1 Mean Absolute error

The Mean Absolute Error (MAE) measures the average magnitude of the errors in a set of different estimations of a certain indicator. It measures *accuracy* for continuous variables without considering their direction of the error. Also, this quantity is usually used to measure how close forecasts or predictions are to the eventual outcomes. The MAE is the average of the absolute values of the differences between simulated and the corresponding observation.

$$MAE = \frac{1}{n}\sum_{i=1}^{n}|sim_i - obs_i| \qquad \textbf{4–1}$$

n represents the number of pairs occurrences of the simulated (sim) and observed (obs) indicators.

4.1.2 Index of agreement

The Index of Agreement (d) developed by Willmott (1981) as a standardized measure of the degree of model prediction error and varies between 0 and 1. A value of 1 indicates a perfect match, and 0 indicates no agreement at all (Willmott, 1981).

The index of agreement can detect additive and proportional differences in the observed and simulated means and variances; however, it is overly sensitive to extreme values due to the squared differences (Legates and McCabe, 1999).

$$d = 1 - \frac{\sum(obs - sim)^2}{\sum(|sim - \overline{obs}| + |obs - \overline{obs}|)^2} \qquad \textbf{4–2}$$

4.1.3 Percent bias

Percent bias (PBIAS) measures the average tendency of the simulated values to be larger or smaller than their observed ones.

$$Bias(\%) = 100\frac{\sum(sim - obs)}{\sum(obs)} \quad \text{4–3}$$

The optimal value of PBIAS is 0.0, with low-magnitude values indicating accurate representation of drought indicators. Positive values indicate overestimation bias, whereas negative values indicate model underestimation bias. Must be take into account that this metric depends on which dataset is considered to represent the observations.

4.1.4 Spearman correlation coefficient

The Spearman correlation is simply the Pearson correlation coefficient computed using the ranks of the data. Conceptually, Pearson correlation coefficient applied, but to the ranks of the data rather than to the data values themselves. The Spearman coefficient is a more robust and resistant alternative to the Pearson product-moment correlation coefficient (Wilks, 2002).

In practice it is not necessary to use the equation of Pearson coefficient to compute the Spearman rank correlation. Because the data are ranks, they consist simply of all the integers from 1 through the sample size n. Taking advantage of this information, computation of the Spearman rank correlation can be simplified to:

$$\rho = 1 - \frac{6\sum d_i^2}{n(n^2 - 1)} \quad \text{4–4}$$

where di is the difference in ranks between the i^{th} pair of data values. In cases of ties, where a particular data value appears more than once, all of these equal values are assigned their average rank before computing the di's.

4.2 COMPARISON OF THE GLOBAL DATASETS

For all the datasets and regions the mean annual cycle of precipitation (Figure 4-1) shows a good agreement in the days of onset and end of the rainy season, also for the GHA region which are characterized by two rainy seasons. However for the

intensity the results are more heterogeneous. At Limpopo and Oum er-Rbia there is a good agreement between datasets, meanwhile for the basins located between the tropics the discrepancies are higher with the overestimation of ERAI in the Blue Nile Basin and GHA (where TRMM datasets tends to underestimate the peaks) and an underestimation at Niger basin.

Also the density of gauges is playing a role in determining the agreement or not between datasets. The most gauged regions (Oum er-Rbia and Limpopo according to Table 2-1) are those with the lower dispersion in terms of annual cycle. By coincident, those two regions (Oum er-Rbia and Limpopo) are also away from the tropical region, and their precipitation variability is mainly controlled by synoptic variability, while in the tropical region small-scale convective event play are important. In these regions, model uncertainties (for example land-atmosphere coupling), satellite retrievals and poor gauge cover contribute to the large spread in the mean annual cycles.

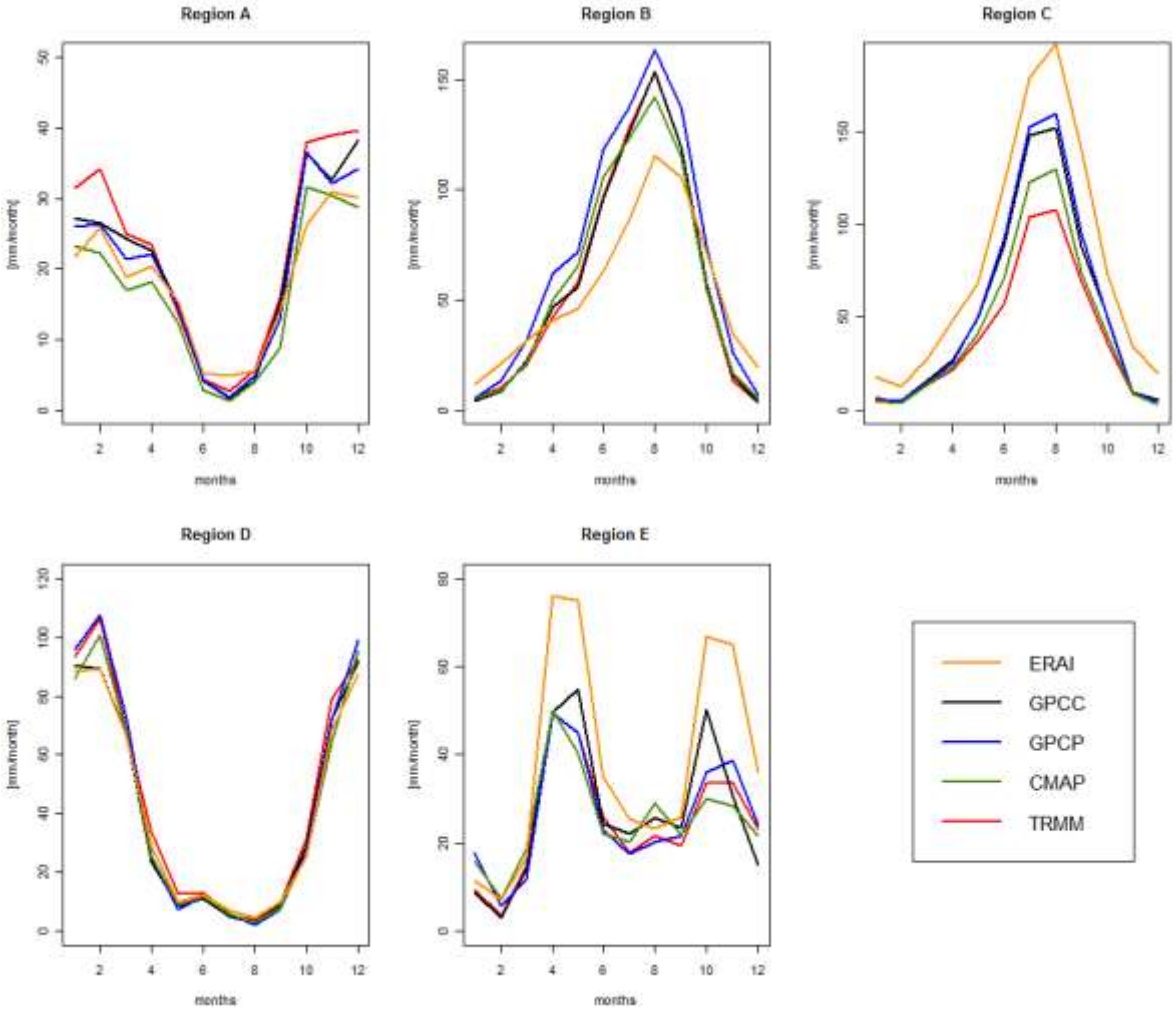

Figure 4-1 Mean annual cycle of precipitation from the different datasets averaged over the five regions defined in Figure 2-1 [A) Oum er-Rbia, B) Inner Niger Delta, C) Blue Nile and D) Limpopo basin and E) Great Horn of Africa] for the common period 1998-2010.

To further examine the series of these five datasets, we examined time series of monthly precipitation for the five regions. Figure 4-2 contain the time series of the monthly means, while the monthly mean correlations, Mean Absolute Error (MAE) and bias of the time series of each dataset are summarized in Table 4-1. A comparison of the monthly time series shows a general agreement in the timing of the peaks also for the GHA were there are two rainy seasons. The bigger differences are again in the magnitude of the peaks; effect also was reflected in the mean annual cycles.

In order to assess the degree of dependence between datasets the Spearman's rank correlation, was performed. This non-parametric test was chosen because its exact sampling distribution can be obtained without requiring knowledge of the joint probability distribution of the variables analyzed. Also, the rank correlations rely only on the local differences of the two series compared (equation 4-4), thus the influence of the annual cycle is not considered in the analysis. For the monthly mean the datasets fit each other well with correlation coefficients over all regions usually greater than 0.8. The CMAP dataset is that shows lower agreement with values below 0.7 in some regions.

According to the other indicators, Oum er-Rbia, Niger and Limpopo areas shows the lower disagreement between datasets with MAEs values below 10 mm/month. The bias in those two regions is below 20 % in all the cases except when TRMM and CMAP are compared (30%).

The worst performance of ERAI is observed at Blue Nile and GHA regions. At this regions the overestimations of monthly precipitation could be around 40 mm/month and the bias could reach 90% in the first region and stay around 50% in the second. This tendency of the reanalysis to overestimate the precipitation in the tropical regions was also depicted in D4.2.

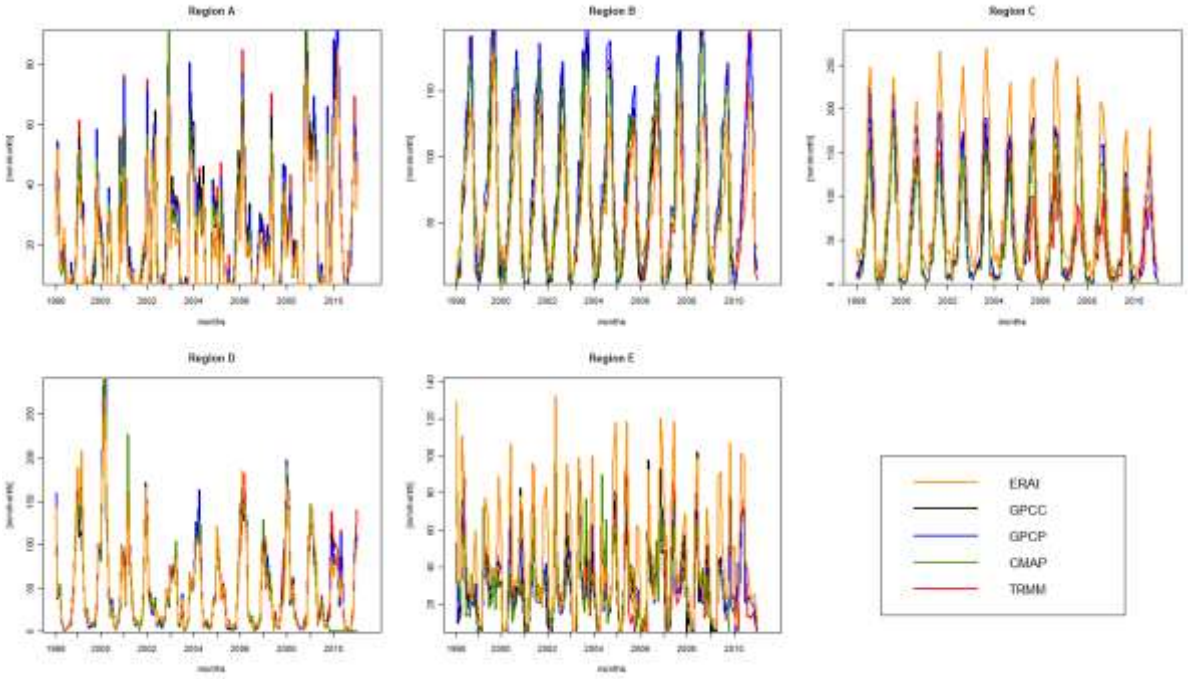

Figure 4-2 Monthly times series of precipitation from the different datasets averaged over the five regions [A) Oum er-Rbia, B) Inner Niger Delta, C) Blue Nile and D) Limpopo basin and E) Great Horn of Africa] for the common period 1998-2010.

REGION A: Oum er-Rbia

		TRMM	GPCC	GPCP	CMAP	ERAI
Spearman coefficient	TRMM	1.00	0.99	0.99	0.74	0.95
	GPCC	0.99	1.00	0.99	0.94	0.95
	GPCP	0.99	0.99	1.00	0.73	0.95
	CMAP	0.74	0.94	0.73	1.00	0.68
	ERAI	0.95	0.95	0.95	0.68	1.00
MAE (mm/month)	TRMM	0.00	2.54	2.94	7.82	7.31
	GPCC	2.54	0.00	2.53	4.66	6.66
	GPCP	2.94	2.53	0.00	6.52	5.70
	CMAP	7.82	4.66	6.52	0.00	7.01
	ERAI	7.31	6.66	5.70	7.01	0.00
BIAS (%)	TRMM	0.00	2.70	6.70	42.80	26.30
	GPCC	-2.60	0.00	4.20	23.10	24.40
	GPCP	-6.20	-4.00	0.00	33.90	18.40
	CMAP	-30.00	-18.70	-25.30	0.00	-11.60

	ERAI	-20.80	-19.60	-15.50	13.10	0.00

REGION B: Niger

		TRMM	GPCC	GPCP	CMAP	ERAI
Spearman coefficient	TRMM	1.00	0.99	0.98	0.80	0.94
	GPCC	0.99	1.00	0.99	0.97	0.95
	GPCP	0.98	0.99	1.00	0.82	0.95
	CMAP	0.80	0.97	0.82	1.00	0.78
	ERAI	0.94	0.95	0.95	0.78	1.00
MAE (mm/month)	TRMM	0.00	5.85	13.67	13.89	23.16
	GPCC	5.85	0.00	11.57	6.90	22.18
	GPCP	13.67	11.57	0.00	16.76	25.80
	CMAP	13.89	6.90	16.76	0.00	25.79
	ERAI	23.16	22.18	25.80	25.79	0.00
BIAS (%)	TRMM	0.00	-1.90	-14.50	7.20	8.00
	GPCC	1.90	0.00	-14.10	-1.00	8.30
	GPCP	17.00	16.40	0.00	25.40	26.40
	CMAP	-6.70	1.00	-20.30	0.00	0.70
	ERAI	-7.40	-7.70	-20.90	-0.70	0.00

REGION C: Blue Nile

		TRMM	GPCC	GPCP	CMAP	ERAI
Spearman coefficient	TRMM	1.00	0.94	0.93	0.82	0.93
	GPCC	0.94	1.00	1.00	0.97	0.97
	GPCP	0.93	1.00	1.00	0.85	0.97
	CMAP	0.82	0.97	0.85	1.00	0.86
	ERAI	0.93	0.97	0.97	0.86	1.00
MAE (mm/month)	TRMM	0.00	17.61	17.44	15.33	43.99
	GPCC	17.61	0.00	2.66	12.08	29.90
	GPCP	17.44	2.66	0.00	14.27	30.05
	CMAP	15.33	12.08	14.27	0.00	43.42
	ERAI	43.99	29.90	30.05	43.42	0.00
BIAS (%)	TRMM	0.00	-23.70	-22.40	-0.60	-48.10
	GPCC	31.00	0.00	1.90	22.50	-32.30

	GPCP	28.90	-1.90	0.00	28.20	-33.10
	CMAP	0.60	-18.40	-22.00	0.00	-47.80
	ERAI	92.80	47.60	49.50	91.70	0.00

REGION D: Limpopo

		TRMM	GPCC	GPCP	CMAP	ERAI
Spearman coefficient	TRMM	1.00	0.98	0.97	0.76	0.96
	GPCC	0.98	1.00	0.99	0.91	0.98
	GPCP	0.97	0.99	1.00	0.79	0.97
	CMAP	0.76	0.91	0.79	1.00	0.79
	ERAI	0.96	0.98	0.97	0.79	1.00
MAE (mm/month)	TRMM	0.00	7.03	8.39	12.57	10.38
	GPCC	7.03	0.00	5.05	8.32	8.11
	GPCP	8.39	5.05	0.00	9.93	8.80
	CMAP	12.57	8.32	9.93	0.00	12.78
	ERAI	10.38	8.11	8.80	12.78	0.00
BIAS (%)	TRMM	0.00	8.90	6.70	20.60	9.00
	GPCC	-8.20	0.00	-3.30	1.80	-1.50
	GPCP	-6.30	3.40	0.00	13.00	2.10
	CMAP	-17.00	-1.80	-11.50	0.00	-9.60
	ERAI	-8.20	1.50	-2.10	10.60	0.00

REGION E: GHA

		TRMM	GPCC	GPCP	CMAP	ERAI
Spearman coefficient	TRMM	1.00	0.82	0.88	0.72	0.84
	GPCC	0.82	1.00	0.90	0.84	0.83
	GPCP	0.88	0.90	1.00	0.70	0.92
	CMAP	0.72	0.84	0.70	1.00	0.61
	ERAI	0.84	0.83	0.92	0.61	1.00
MAE (mm/month)	TRMM	0.00	9.82	6.59	9.25	17.81
	GPCC	9.82	0.00	8.20	9.38	17.05
	GPCP	6.59	8.20	0.00	9.62	16.40
	CMAP	9.25	9.38	9.62	0.00	22.72
	ERAI	17.81	17.05	16.40	22.72	0.00

BIAS (%)	TRMM	0.00	-4.20	1.70	11.20	-34.00
	GPCC	4.40	0.00	7.10	8.40	-30.90
	GPCP	-1.70	-6.60	0.00	9.30	-35.10
	CMAP	-10.10	-7.80	-8.50	0.00	-40.60
	ERAI	51.50	44.70	54.10	68.40	0.00

Table 4-1 Spearman correlation coefficient, mean absolute error and bias (%) between the different precipitation datasets averaged over each region for the common period 1998-2010. All correlations are significant at 99%.

4.3 SPI ESTIMATION USING TRMM 3B-43

When the availability of in situ data is scarce, it is necessary to determine whether to use longer, but spatially sparse time-series, or shorter time-series with higher spatial resolution. Prior studies suggest that within-station substitution with a moderate length history (about 10 years) performs better than spatial interpolation of long time series for representing the spatial–temporal variability of large-scale climatology, such as time-averaged precipitation (Willmott et al. 1996). In this way, Rhee and Carbone (2011) studied the effect of drought estimation with limited precipitation data across different climatic regions in United States. They show that the Standardized Precipitation Index (SPI) values based on short-term records generally produced smaller cross-validation mean absolute errors values than the spatially interpolated SPI values when the lengths of records were equal to or longer than 10 years for all SPI time scales. This relation was high even when the lengths of records were only 5 years. These results using short-term records show that including as many stations with moderate lengths of records (at least 10 years) can improve the representation of spatial–temporal variability of drought. The authors also perform an analysis using 5.5 years of the Tropical Rainfall Measuring Mission (TRMM) 3B43 record. They stated that the TRMM data could not outperform the spatially interpolated daily precipitation in most regions. However, in some regions (like mountainous regions or those without in situ measurements) the use of remote sensing derived data (even with 5.5 years record length) could outperform spatial interpolation of long term gauge data.

As a step towards the implementation of a cost-effective drought early warning system in many under-gauged regions around Africa, this section describes and tests an approach of un-biased SPI estimation using TRMM 3B43 data over Africa. In

order to quantify bias and uncertainties a non-parametric bootstrap approach was performed.

Here we use a non-parametric bootstrap method to estimate the parameters and confidence intervals of the gamma distribution. This is done for aggregated precipitation for the 3-month time-scale over the 12-year time-series of the TRMM 3B43 dataset from 1998 to 2010.

Consider that a random sample of observations, $X=\{X_1,X_2,\ldots,X_n\}$ is used to obtain a sample estimate θ_s of a parameter of interest θ, which can be the shape or scale parameter that define the gamma distribution for X. The purpose of bootstrap simulation is to estimate uncertainty (bias and variance) associated with the sample estimate θ_s. According to Efron and Tibshirani (1993), a random sample size of size n is drawn with replacement from the original sample.

Using the k^{th} bootstrap sample of b bootstrap simulations and denoting by

$$X(k) = \{X_1^*, X_2^*, \ldots, X_n^*\} \quad , k=1,2,\ldots,b \qquad 4–5$$

a new bootstrap estimate θ_k^* of θ_s can be obtained. The set of $\theta^*=\{\theta_1^*, \theta_2^*,\ldots, \theta_b^*\}$, constitutes the sampling distribution of θ_s. The bootstrap estimate of the bias is given as

$$Bias = (\theta_m^* - \theta_s) \qquad 4–6$$

where θ_m^* represents the average of all bootstrap estimates θ^*. This leads to the bias corrected estimator of the parameter θ

$$\theta = \theta_s - Bias = 2\theta_s - \theta_m^* \qquad 4–7$$

The variance S of θ_s is estimated as

$$S(\theta_s) = \frac{1}{b-1}\sum_{k=1}^{b}(\theta_k^* - \theta_m^*)^2 \qquad 4–8$$

This is a statistical resampling technique that does not require preselected distribution or models to fit the data, because the simulations have the same distributional properties of the original dataset. On the other hand, this behaviour may produce spurious fine structure in the original data (Silverman 1986).

In Figure 4-3 it is shown that the confidence interval decreases when the record length of data increases, meaning that the stability of the coefficients that can be estimated with reasonable accuracy increases as the sample size growths. Stability

is usually understood to mean that the fitted distribution (i.e. parameters) and is also applicable to independent future data, so that the parameters would be substantially unchanged if based on a different sample of the same kind of data. Furthermore, the error in the estimation of the scale parameter is greater for dry months (June-August). This result suggests that the error in the estimation is not constant during the year and also that it changes for each climate region, being greater for dry climates.

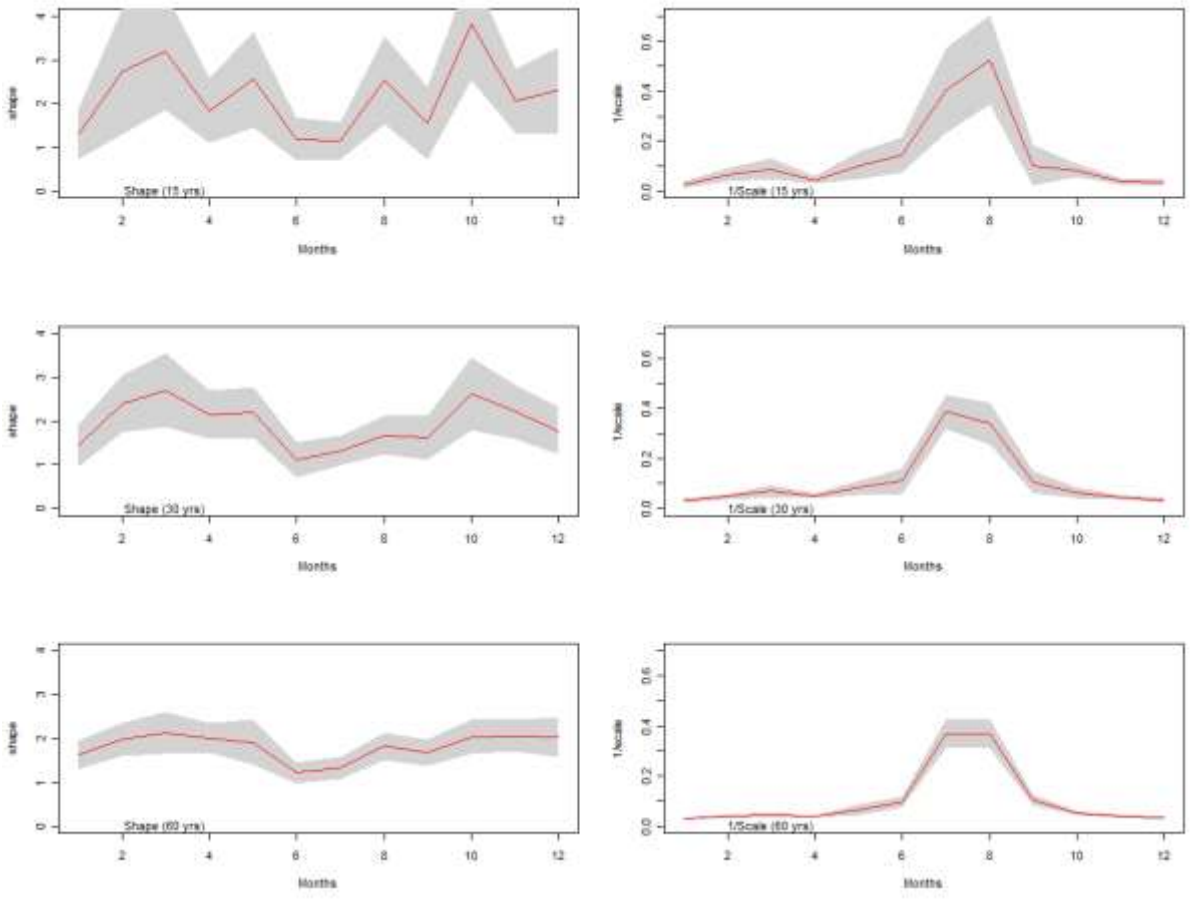

Figure 4-3 Annual cycle of shape and scale Gamma parameters of GPCC precipitation at region A (Oum er-Rbia) for different record length (red) and its uncertainties (light gray).

This lack of stability for the shorter time series could produce greater uncertainties when the drought indices are calculated. Figure 4-4 shows the empirical distribution of the 3-month TRMM averaged precipitation over the Limpopo basin for February. This distribution was fitted using Kernel, Gamma, and unbiased Gamma distribution using the bootstrap technique (equation 4-7). The unbiased estimation fits best (less K-S distance, not shown) compared with the other approaches. Figure 4-4 also

shows the distribution estimation and the family of distributions associated with the bootstrap resampling. It is shown that the members of this could vary widely, but the mode is in general well represented by the majority of members.

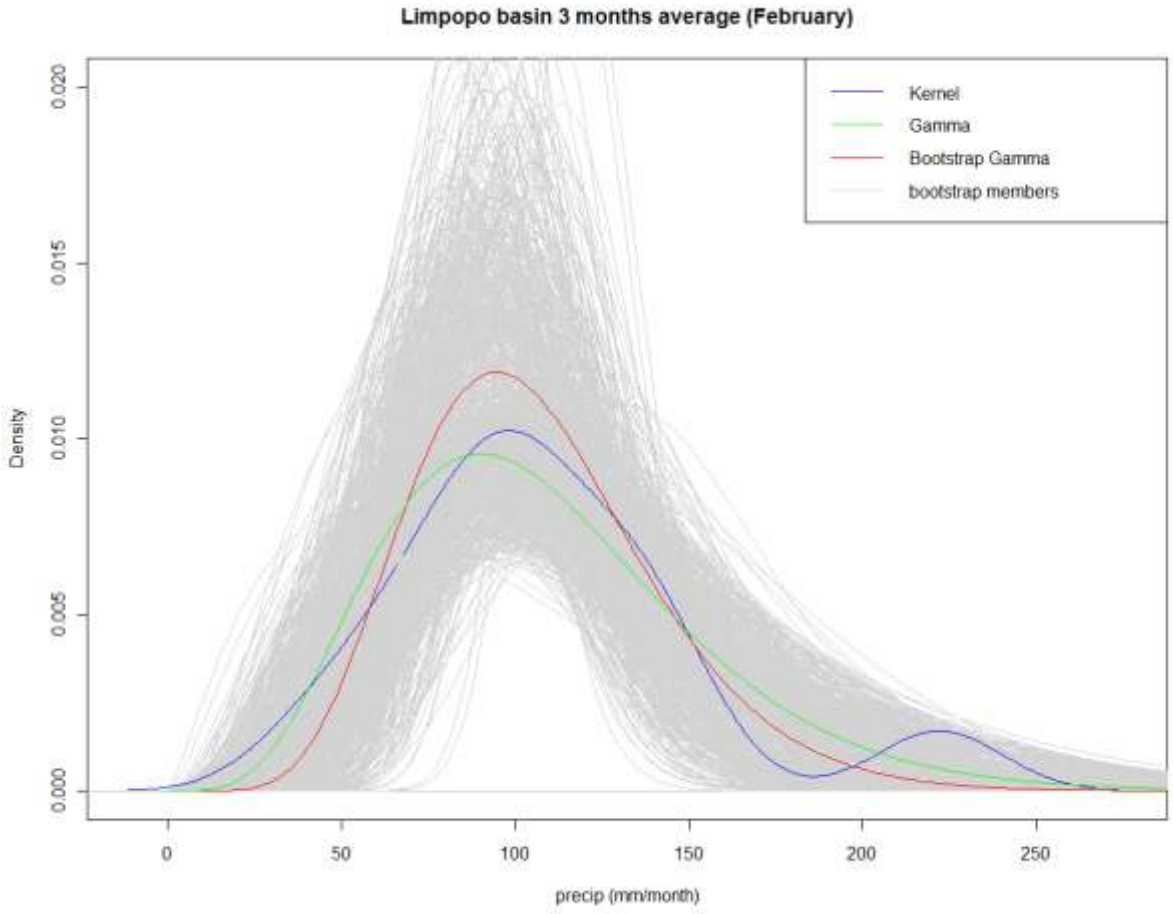

Figure 4-4 Gamma and Kernel probability distribution function of TRMM precipitation at Limpopo Basin (region D).

At Pan-African level, Figure 4-5 shows the spatial distribution of the unbiased shape and scale parameters using 3-monthly averaged TRMM precipitation data. This estimation shows a regional consistency and is in agreement with the findings of Husak et al. (2007). Large shape values tend to follow the ITCZ through each of the monthly maps. Regions with higher shape values indicate that the probability of events drier than average becomes similar to the probability of events wetter than average, since the distribution is more symmetrical. The maxima are located near the coasts of Gabon, Congo and the Democratic Republic of Congo in January, while in July they are located between 0 and 10°N mainly in western and central Africa. The wet seasons in these regions are driven by the ITCZ accompanied by large and consistent rainfall is observations. The areas with higher scale parameters are mainly observed in the poleward borders of the ITCZ where the rainfall could be more

variable. This larger variability is mainly due to fluctuations in the position of the ITCZ across the continent and may give one region heavy rainfall for an extended period of time while causing another to have an abbreviated rainy season.

Figure 4-6 shows the 3-month SPI estimated with unbiased cumulative distribution function (CDF) estimation using 13 years baseline for TRMM (including confidence intervals) and 60 year baseline for GPCC over the four regions. It is shown that in general TRMM exceeds the peaks when compared to GPCC. This means that the main source of error is due to the estimation of the tails of the distribution and this is related with the stability of the time series. However, for most of the time the GPCC estimation is within the TRMM estimation confidence intervals. This is confirmed by the correlation coefficient (r) that is shown in Figure 4-6, which is statistically significant for all river basins. The largest differences are observed for the regions with the most complex orography and lack of in-situ information, namely the Blue Nile basin (B) and the Niger basin (C) respectively. In addition, as shown in Table 2-1, these regions have also the lowest station density per grid, with up to 75% of pixels without any ground observation for the GPCC dataset. This means that more in-situ data are needed in order to improve the GPCC precipitation datasets and the TRMM calibration as well.

The comparative analysis of the four different datasets suggests that is feasible to use short time series of precipitation data with high spatial resolution (0.25°x0.25°) such as the TRMM for reliable drought monitoring over Africa. Furthermore, the bootstrap technique gives an estimate of the SPI uncertainty by providing confidence intervals. The proposed approach for drought monitoring has the potential to be used in support of decision making at continental and sub-continental scales over Africa or other regions that have a sparse distribution of rainfall measurement instruments.

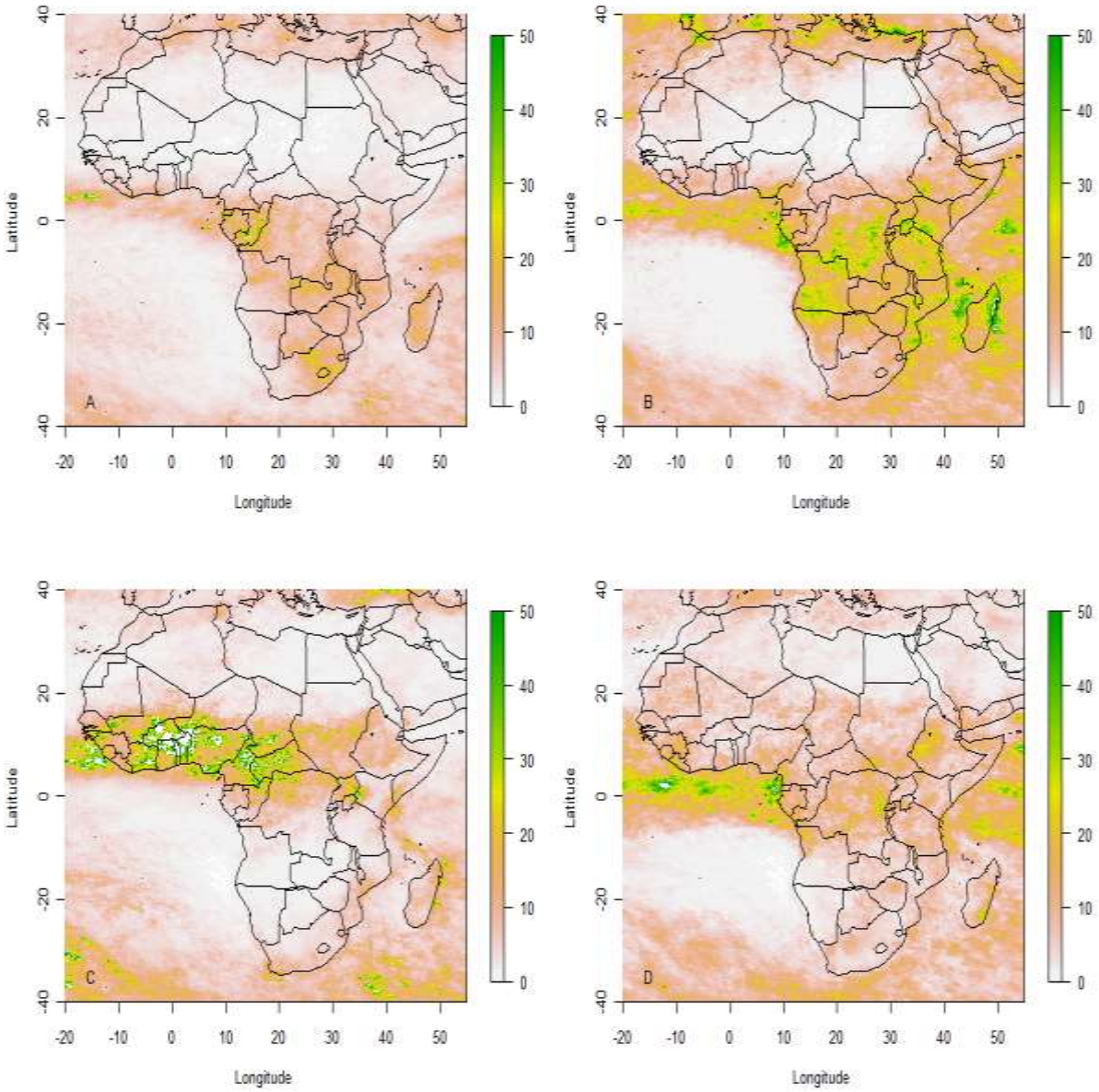

Figure 4-5 Shape and Scale parameters for January and July using unbiased estimation of parameters

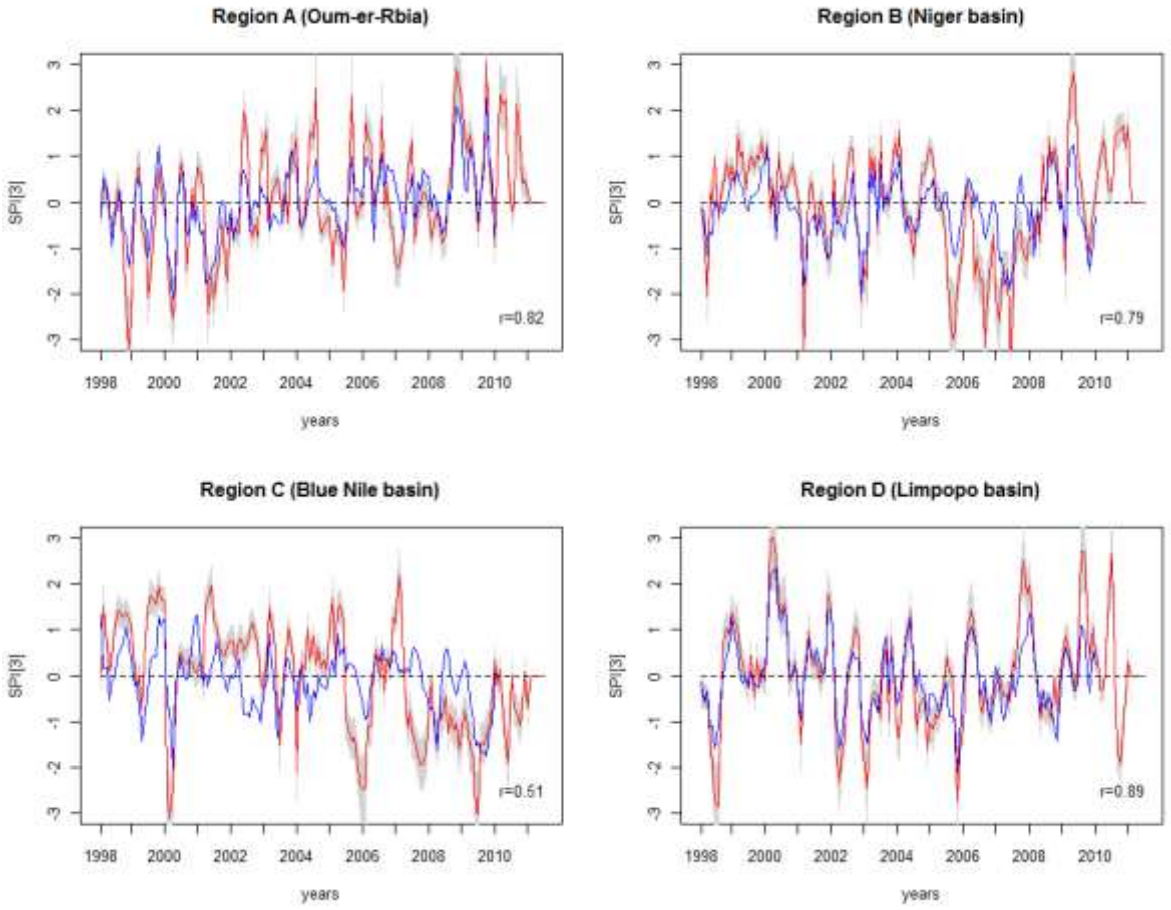

Figure 4-6 3-month SPI time series calculated using 13 year TRMM (red) and 60 year GPCC datasets (blue) and Confidence Intervals (light grey).

4.4 SPATIAL ANOMALIES ANALISYS

In order to set up a Pan-African map server this section is intended to perform a comparison between the different indicators proposed. A number of drought indicators are included to study the comparative behaviour of a range of metrics commonly used. Moreover, the results of this section were compared with the findings in D2.2. A direct quantitative assessment over continental scale is difficult because the lack of an actual validation dataset that represent the ground truth with adequately high spatial or temporal resolution. Two performance metrics are used to diagnose the relative reliability of each drought indicator. One using a spatial anomalies analysis and other based on time series correlation analysis.

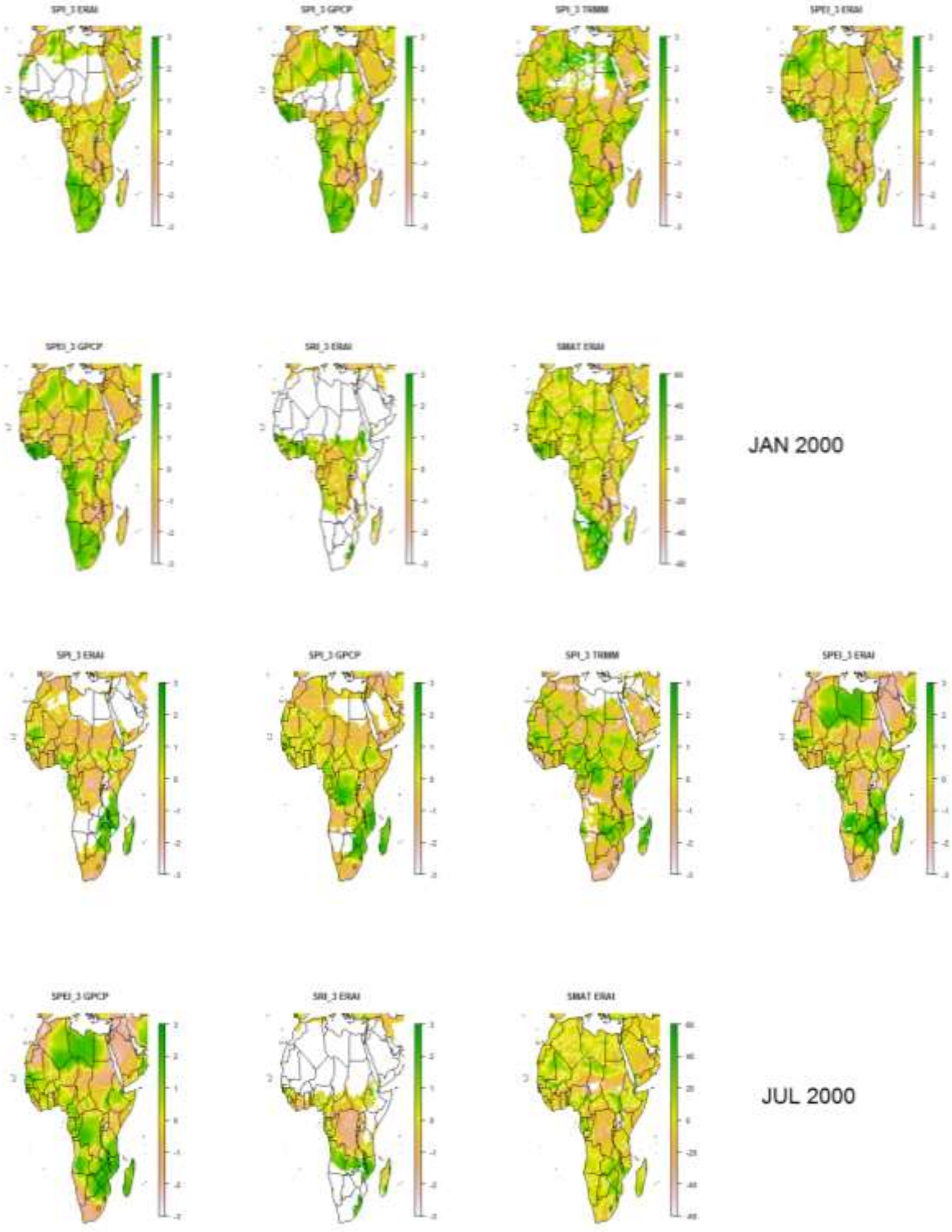

Figure 4-7 Monthly anomalies in SPI-3 (ERAI, GPCP, TRMM), SRI (ERAI) and Soil Moisture Anomalies (SMAT) for January and July 2000.

This analysis doesn't assume that any dataset or indicator are better than the other but allows making an inter-comparison between all of them and detect the time and

regions where all or part of these shows a good agreement. The second will explore the relation between the temporal anomalies of each indicator.

Figure 4-7 to Figure 4-16 describes the monthly patterns of drought over Africa according to the different indicators during the 2000-2009 decade. These maps shows standardized anomalies (SPI-3, SPEI-3 and SRI-3) and anomalies (SMA) computed for January and July of each year. Drought features are generally reflected in more than one index, but this agreement varies depending on the drought type, spatial and time scale. Overall, during the period there is a good spatial correspondence between all the indicators.

During the period analysed there is a good qualitative agreement between SPI-TRMM and SPEI-ERAI with the growing season length anomalies. It's worth to mention that the growing season length is not a monitoring indicator (the onset of the growing season is) but is the only independent dataset analysed while the other datasets are sharing information. This indicator is related with phenological changes on vegetation and is sensible to different climatic variables depending on the region studied. In temperate zones biological activity is mostly controlled by temperature (Menzel, 2002) while at lower latitudes rainfall and evapotranspiration are the main drivers (Linderholm et al., 2005). On the local scale other climatic and micro-climatic variables might explain phenological changes better (Ivits et al., 2012).

In the appendix section are also included a detailed month by month evolution of droughts characterized by the amount of indicators below a certain threshold (Figure 8-1 to Figure 8-20). In almost all the areas there is a good agreement, whit usually more than 3 indicators reporting drought conditions per grid cell. However, there are some cases with only one indicator below the defined threshold mostly over Central Africa.

For instance, during year 2000, it's observed a good agreement between indicators, where all of them are showing drought conditions in central Africa (D.R. of Congo, Kenya Rwanda and part of Tanzania), Somalia and in Morocco. Those droughts also affected the growing season (Figure 4-18), were significant shorter seasons (shorter on more than one standard deviation) were observed at the mentioned areas. A good agreement between indicators including a shorter growing season is also observed during 2003, 2005 (western central Africa) and 2009 (most over eastern Africa) in this area. During 2000 is observed that the onset of the drought in central Africa started in March and it propagates to the south east until the end of July. This drought could be triggered by a weak but early northward movement of the ITF (Inter Tropical Front) and its end was signed by southward retract of it (Lele and Lamb, 2010).

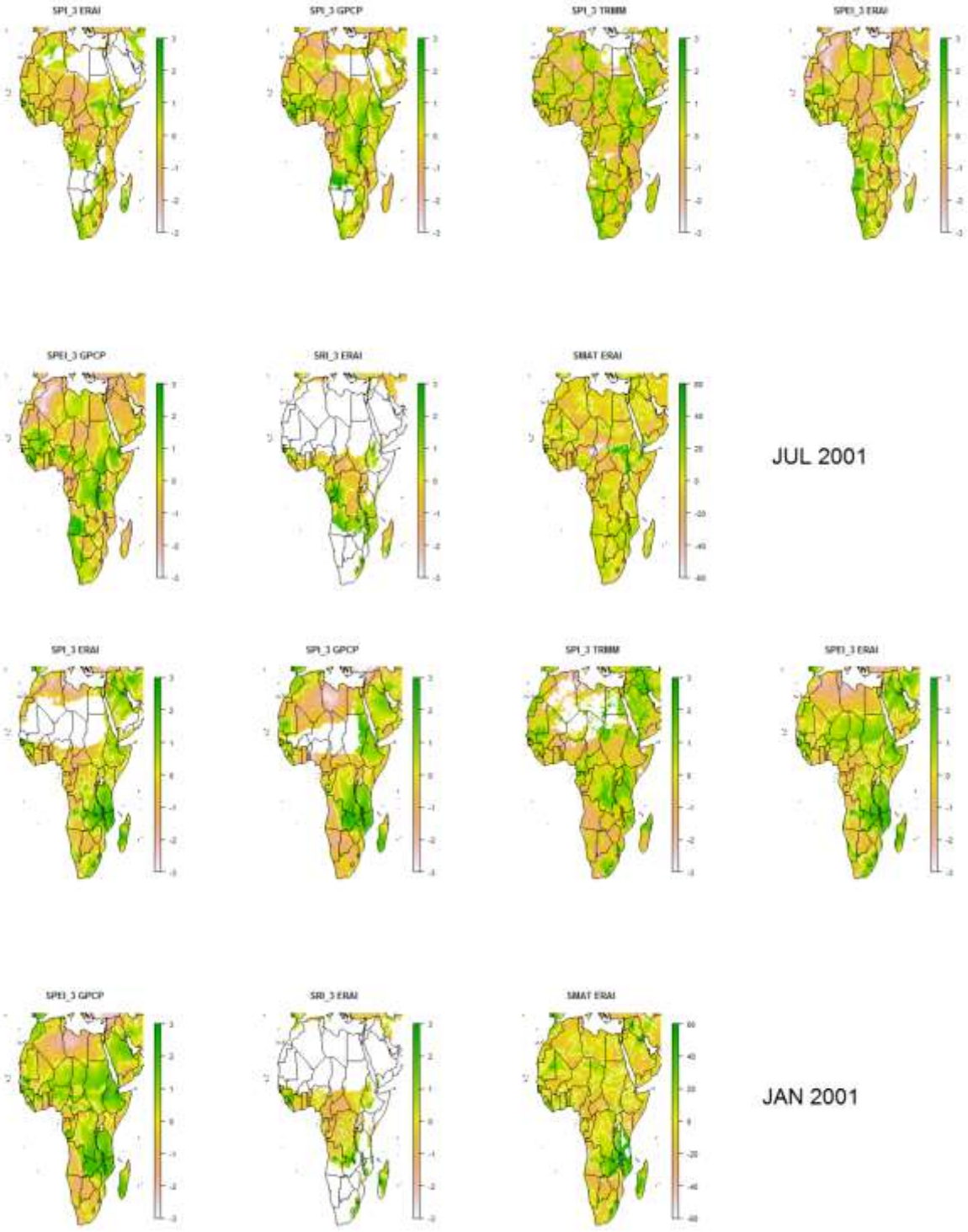

Figure 4-8 same as Figure 4-7 but for year 2001.

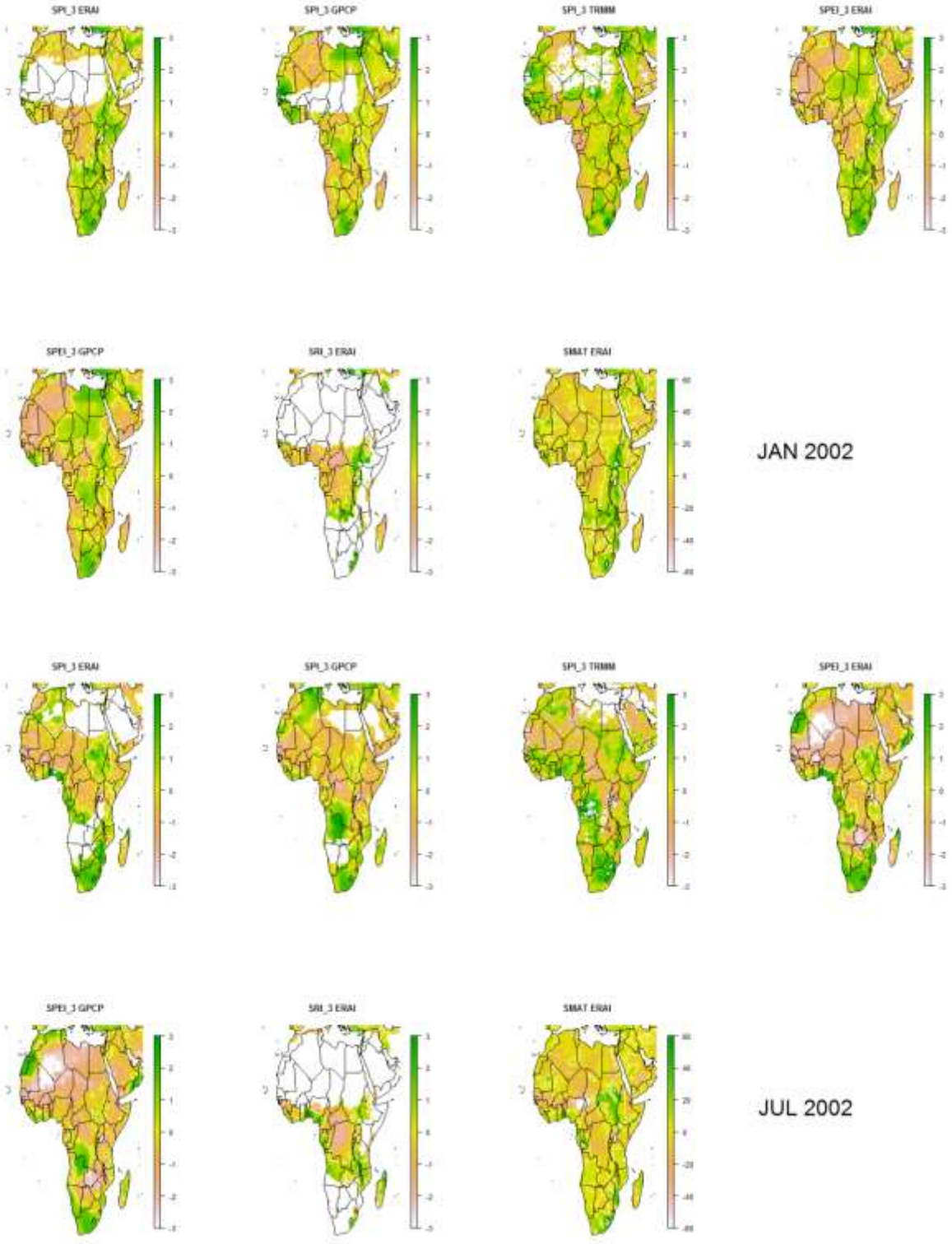

Figure 4-9 same as Figure 4-7 but for year 2002.

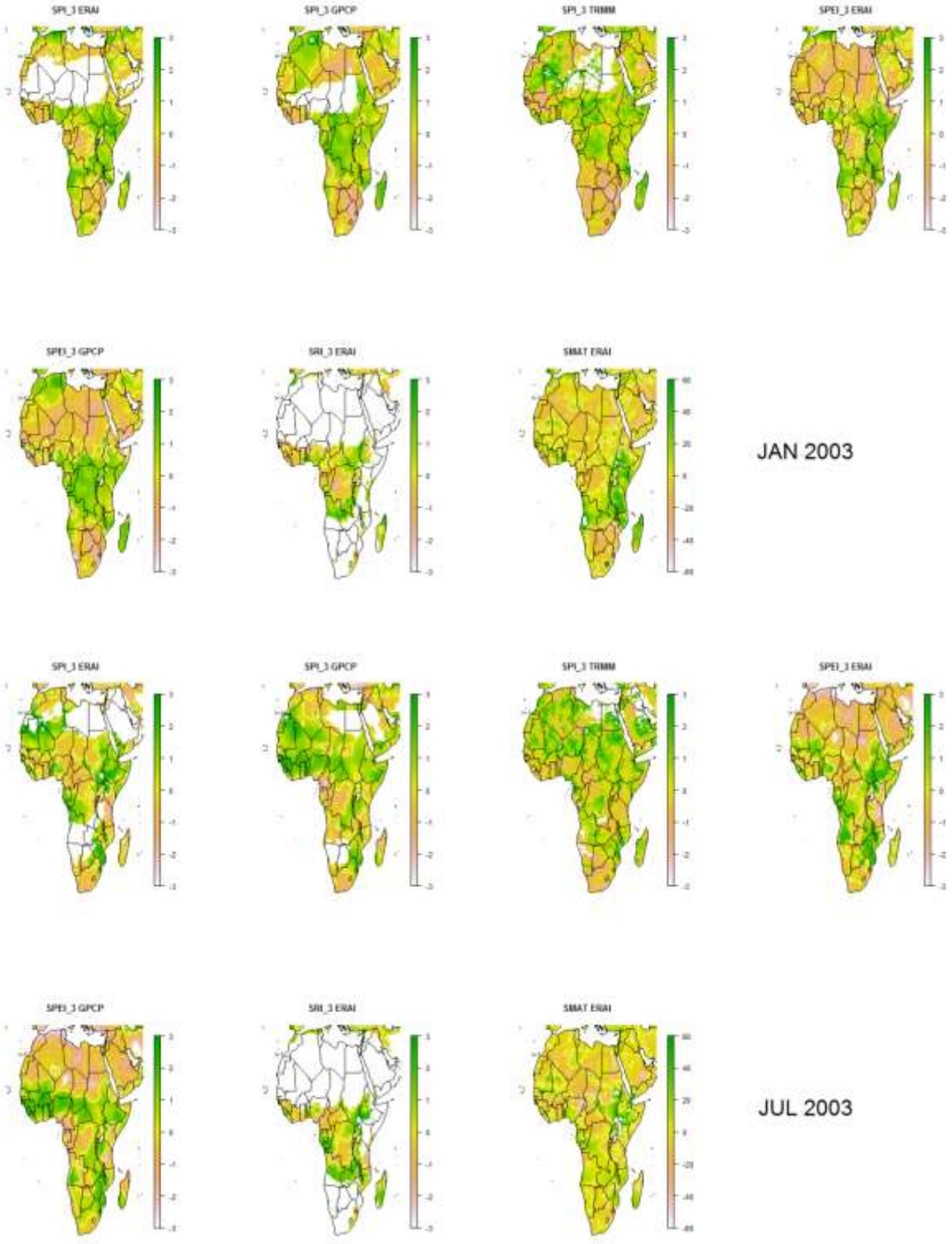

Figure 4-10 same as Figure 4-7 but for year 2003.

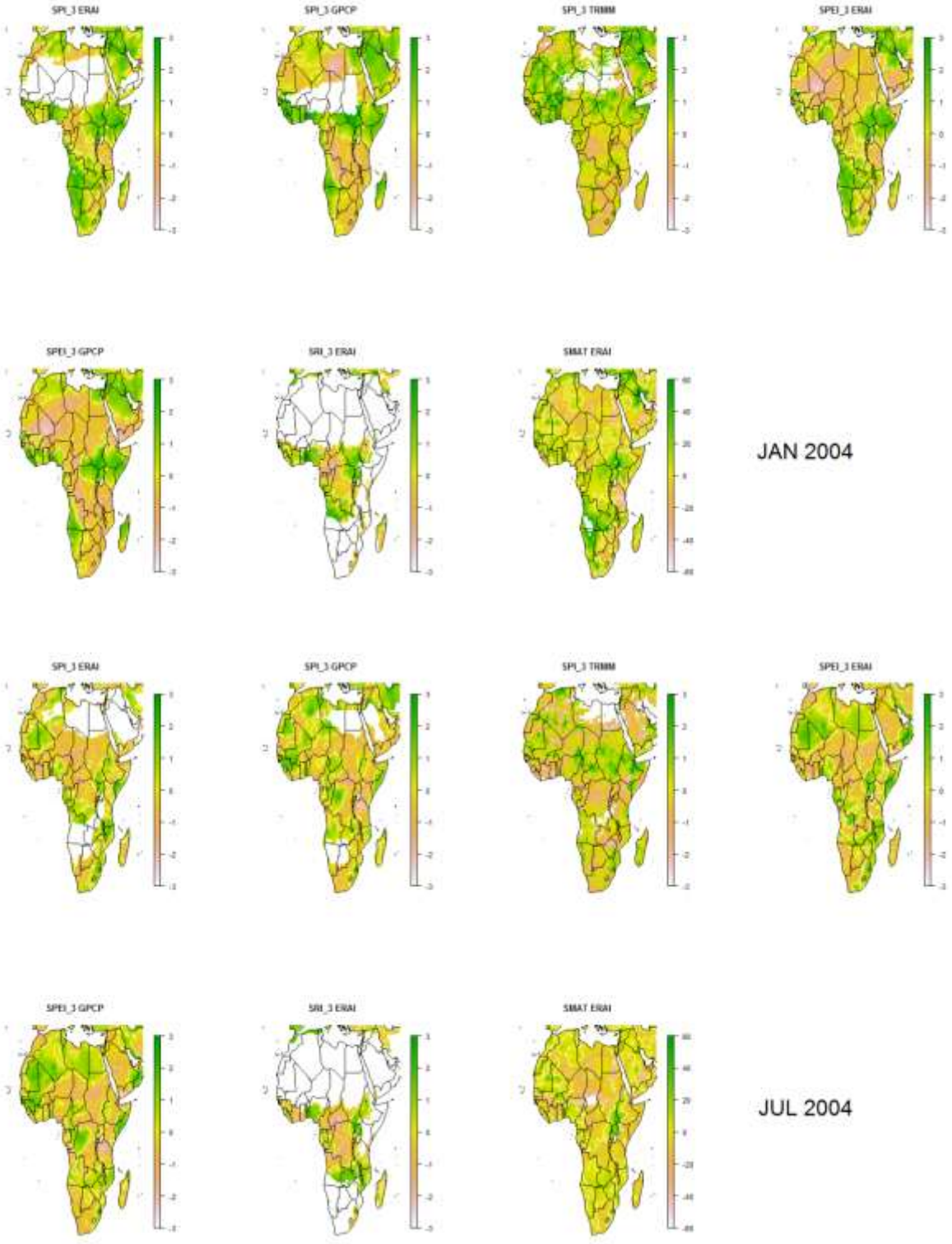

Figure 4-11 same as Figure 4-7 but for year 2004.

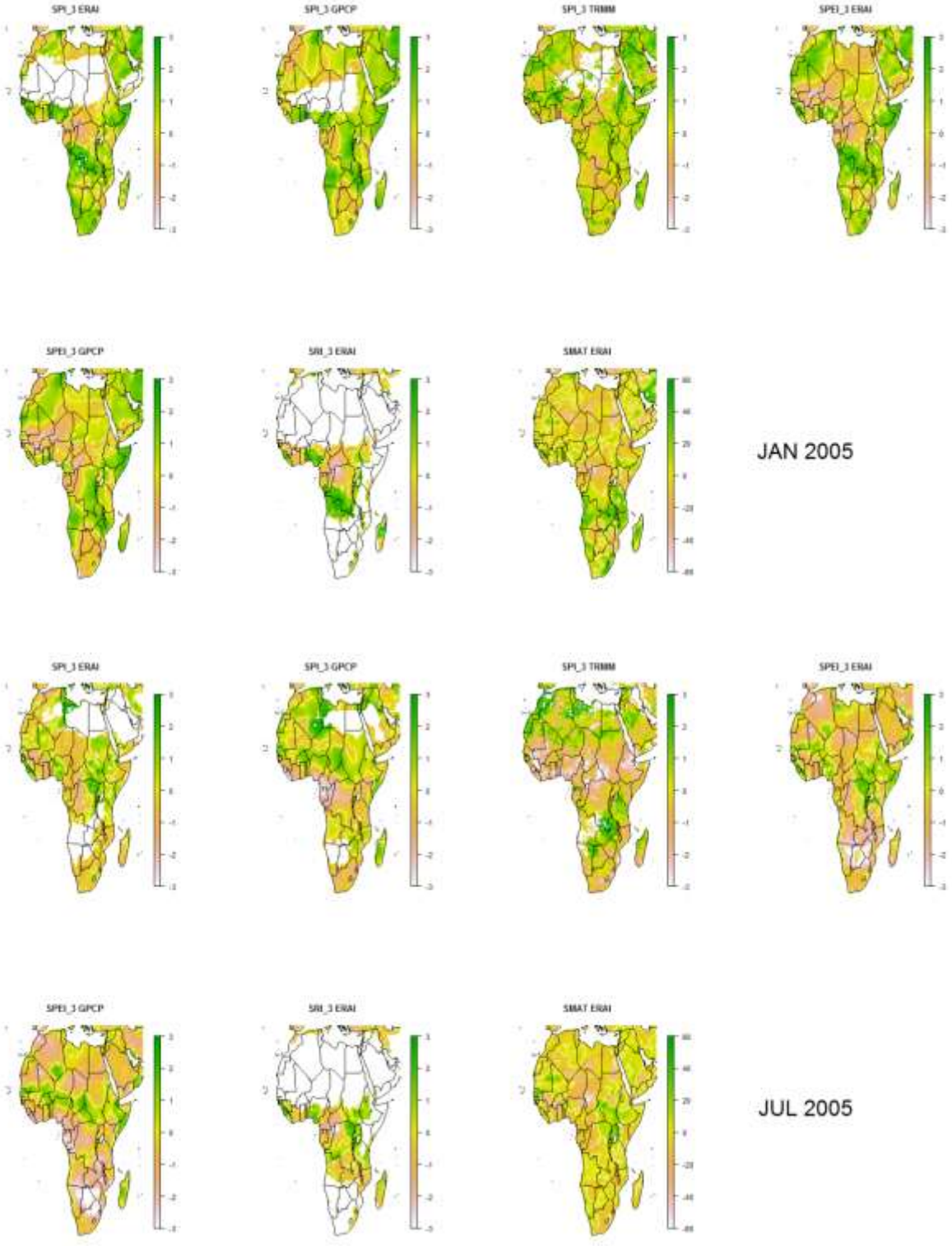

Figure 4-12 same as Figure 4-7 but for year 2005.

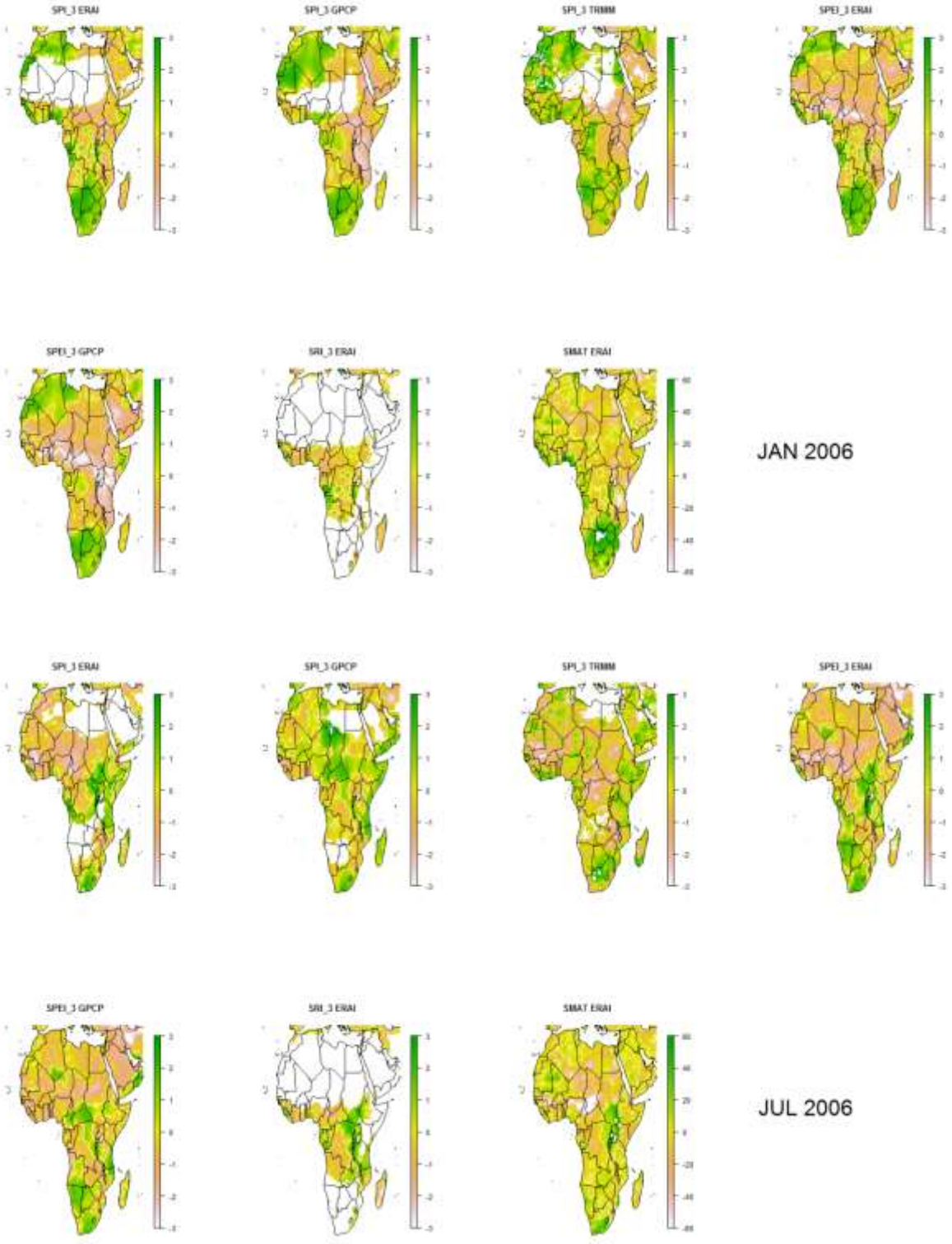

Figure 4-13 same as Figure 4-7 but for year 2006.

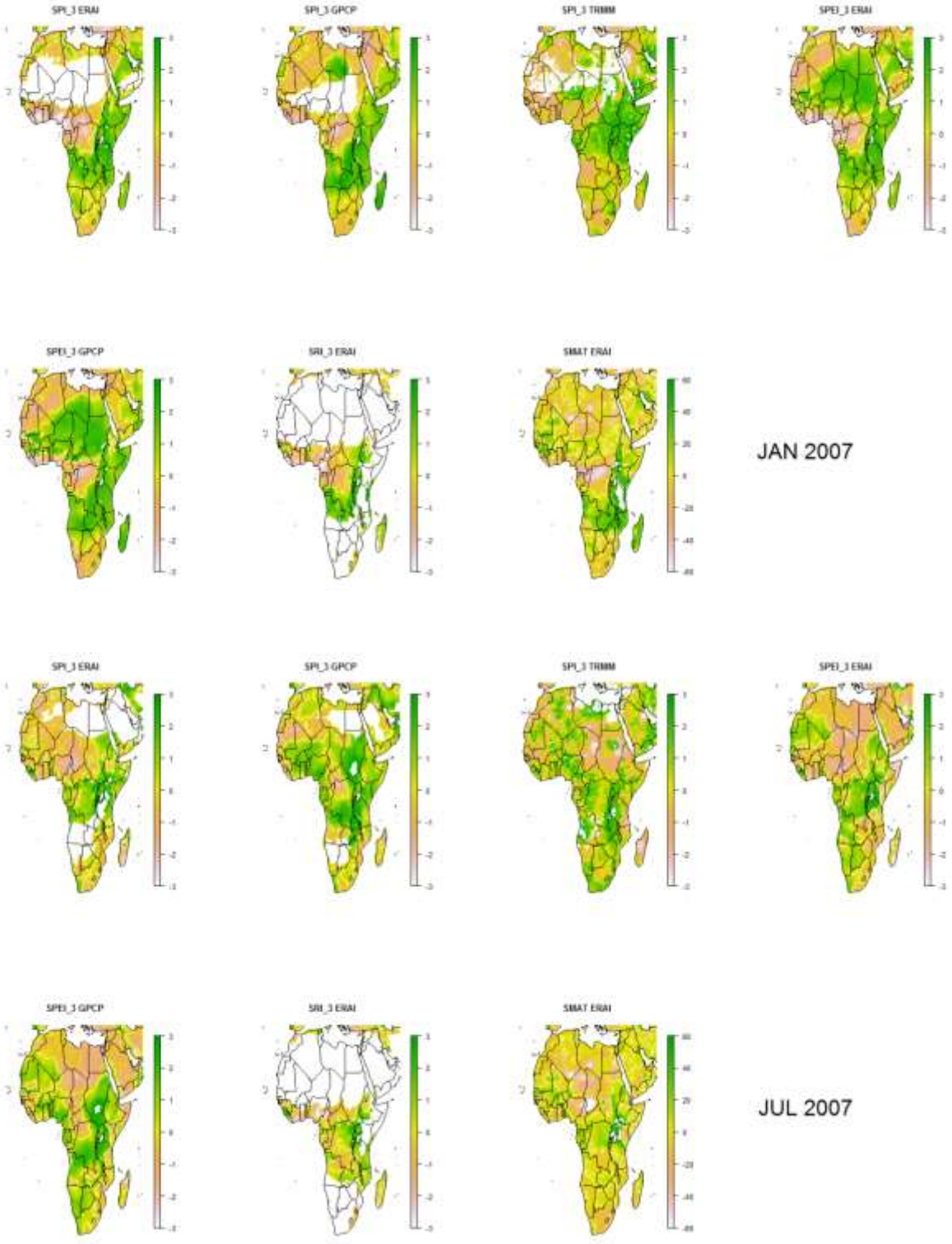

Figure 4-14 same as Figure 4-7 but for year 2007.

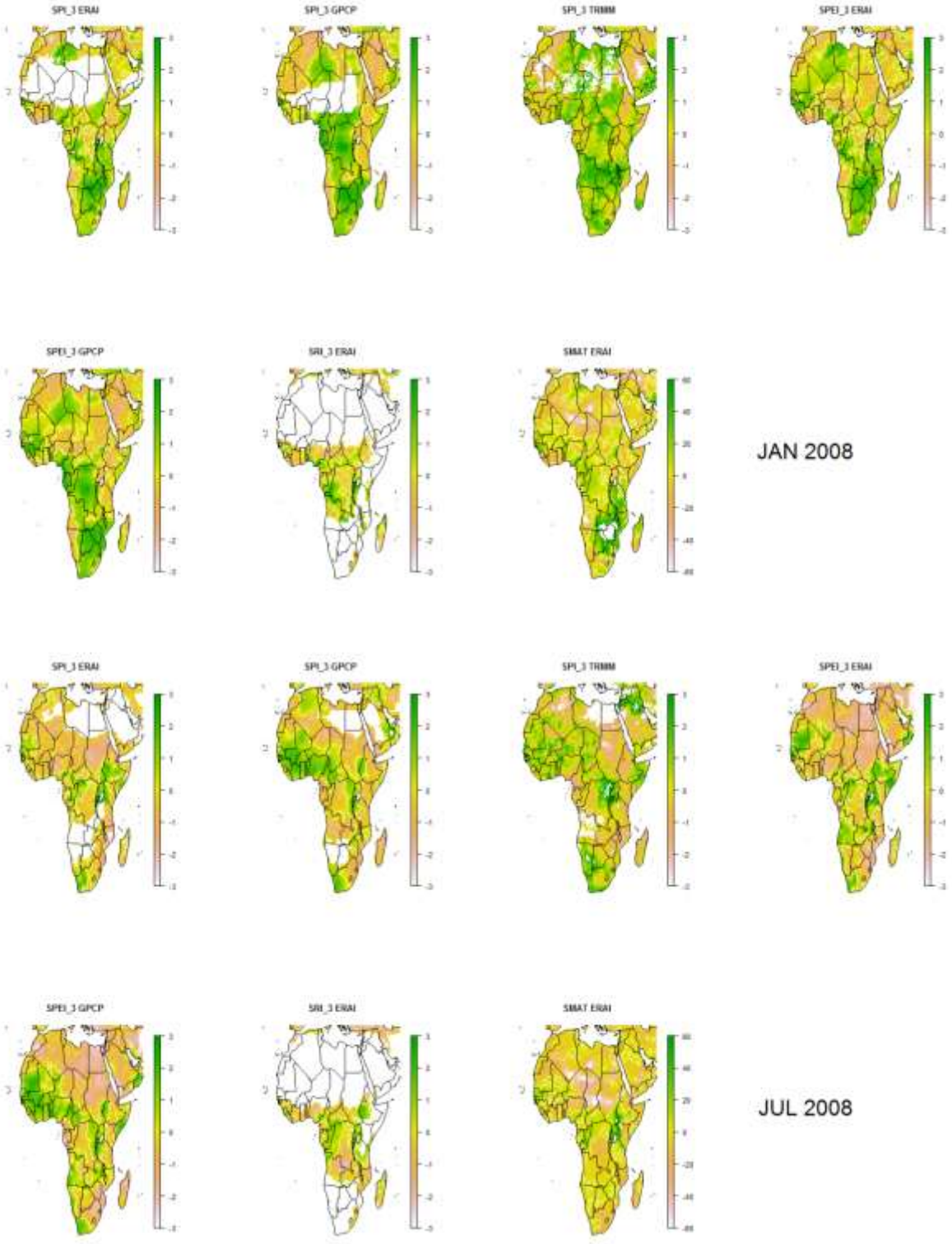

Figure 4-15 same as Figure 4-7 but for year 2007.

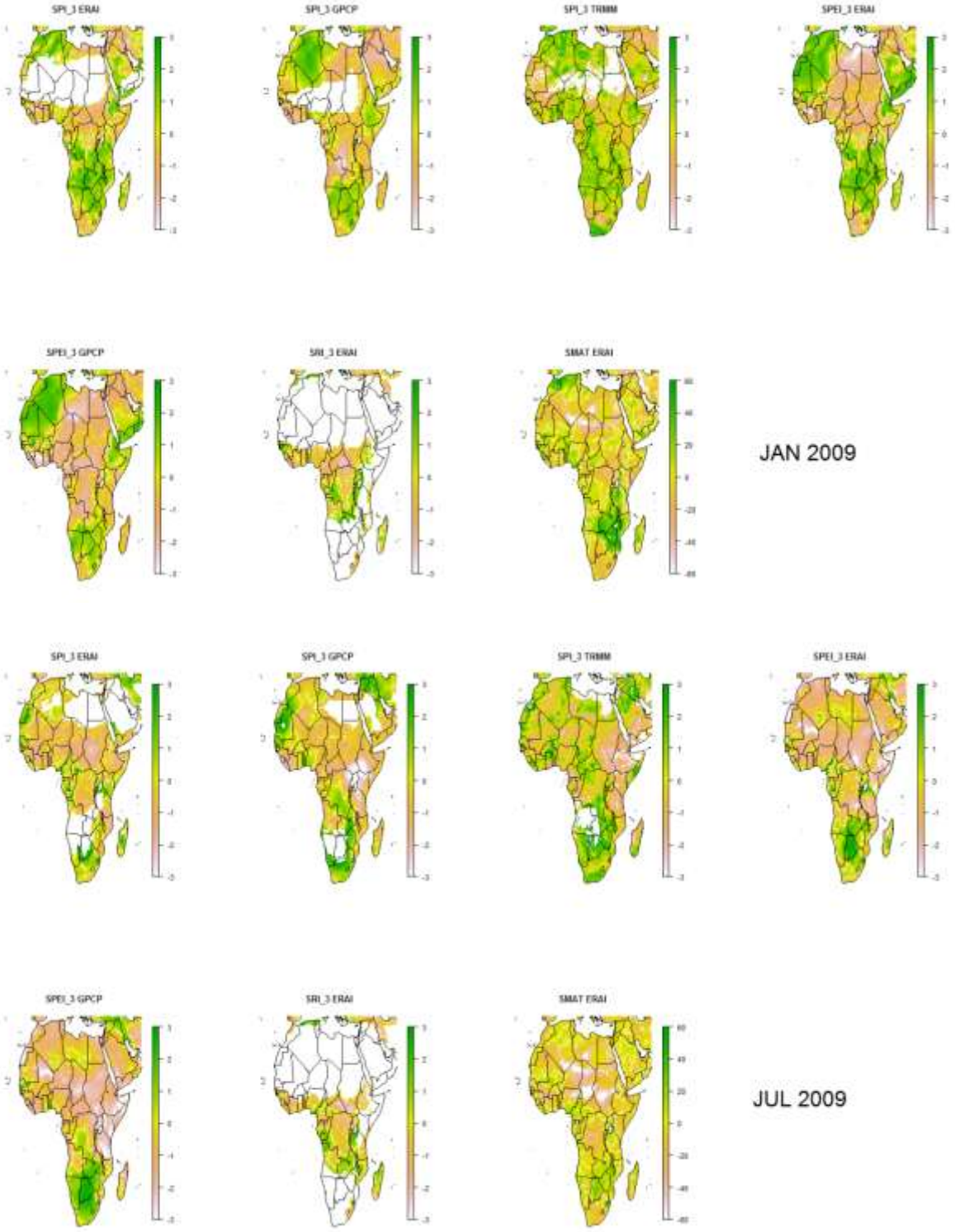

Figure 4-16 same as Figure 4-7 but for year 2009.

Also there exist some differences between the annual and monthly comparison. If we look on impacts, 2006 was the year with more people affected by drought in

Tanzania and Kenya with more than 3.000.000 of people affected directly in each country (D2.2). However no one of the indicators (Figure 4-19, Figure 4-21) shows a clear pattern of drought in this area in the monthly composites. But looking at monthly level, Figure 8-16 and Figure 8-17 show that a drought start to develop between September and October 2005 and persisted until February 2006 in the region. High levels of agreement with almost all the indicators bellow threshold are observed during all the period. The timing of this drought affected the develop growing season with the observed consequences.

During 2001 there all datasets agrees in show drought very dry conditions over North west Africa (Morocco and Ghana, Togo) and over central east (Tanzania, Kenya and north of Madagascar), while all datasets show very wet conditions except for the SMA that presents near normal conditions in this area. In 2002 and 2003 drought conditions were observed by all the indicators, including the growing season length anomalies in Botswana, Mozambique and Zambia.

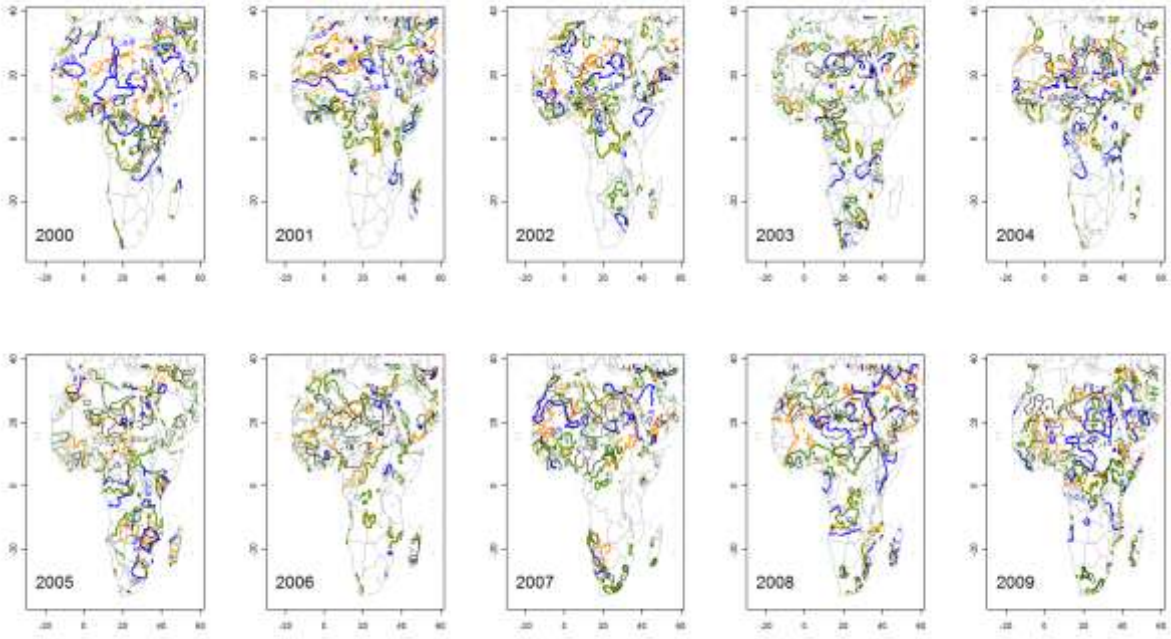

Figure 4-17 Areas of yearly SPI-3 (ERAI in orange and GPCP in blue), SPEI-3 (ERAI in green and GPCP in grey) below -0.5 and Soil Moisture anomalies below -15 mm.

During 2004 the Sahel drought are well represented while there are some discrepancies in South Africa where SPI-TRMM and SPEI-GPCP and SMA indicates dry conditions while the others are in near-normal or slightly wet conditions. According with the findings on deliverable D2.2 (D2.2 Table 12) the period 2003-2005 the SADC area were classified under meteorological and agricultural droughts. 2006 and 2007 are years with normal or wet conditions over the entire continent.

Only SPI-TRMM, SPI-ERAI and SPEI ERAI (Figure 4-17) reflect dry conditions over part of Western Africa (Chad, Niger and Nigeria).

During 2008 a not well defined area of drought are drawn in south-eastern South Africa. This lack of agreement on the annual average are mainly due by the exceptional dry month in October (Figure 8-19) that was registered with a high agreement between indicators over this region. In 2009 the onset of the drought in the Great Horn of Africa is well represented by all the indicators, included the growing season length anomalies. According to Figure 8-20 the dry conditions persist for almost the entire year in this region.

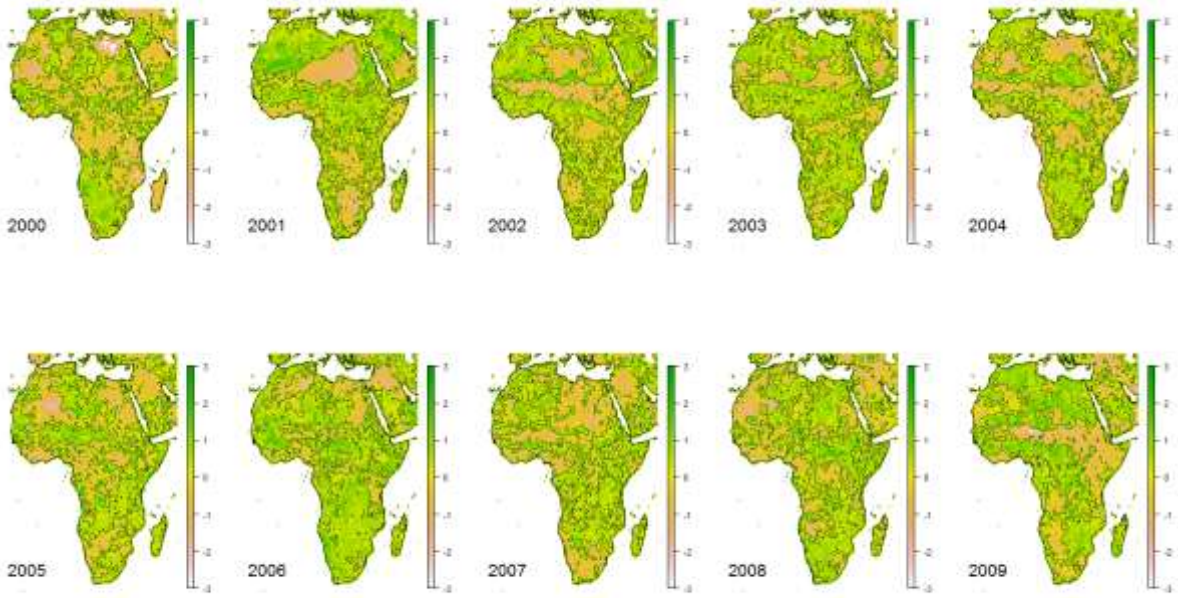

Figure 4-18 Spatial patterns of Standardized Season Length anomalies during the 2000-2009 period.

Another feature is the threshold defined to identify a drought area. The areas with spatial agreement between indicators considering standardized anomalies below 0, -0.5 and -1 are depicted in Figure 4-19 to Figure 4-21. This results show a high dependence between the threshold and the area (agreement between indicators) a drought event. If conditions under normal values are considered there are almost for the entire period one indicator below 0 covering the entire continent. Exceptions are the wet periods observed in southern Africa during the years 2000, 2001 and 2006.

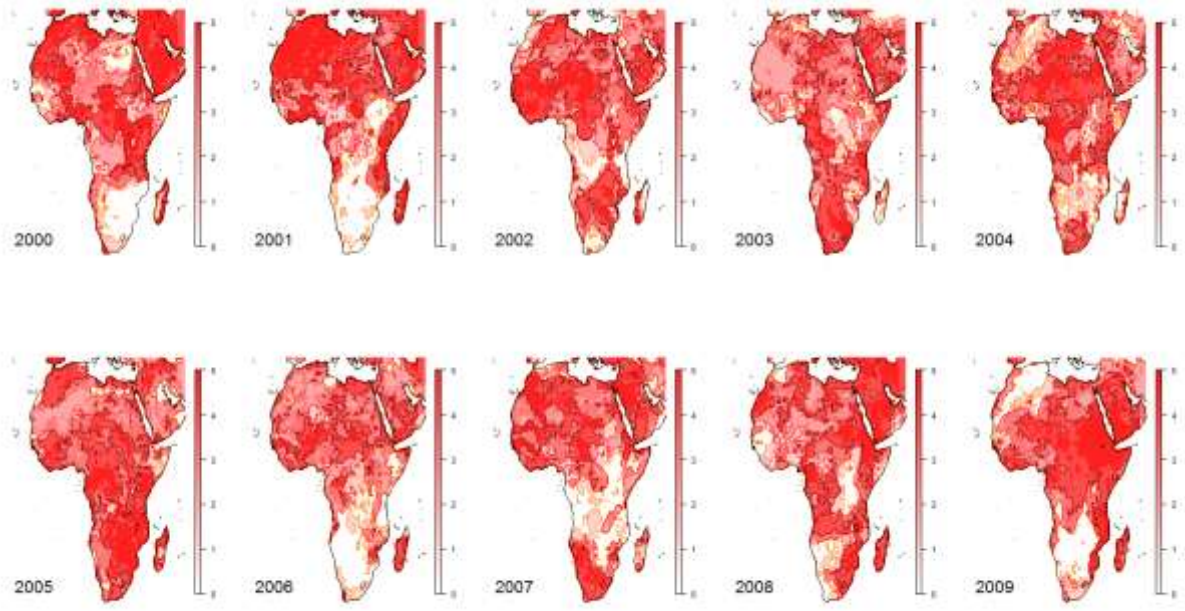

Figure 4-19 Spatial agreement between ERA-I, GPCP and TRMM SPI-3 and ERIA, GPCP SPEI-3 estimations. Grid cells with SPI-3 below 0.0 were considered. Values are ranged between 0 (no dataset with SPI below the threshold) and 5 (all datasets below the threshold).

In the other hand a threshold of -0.5 seems to be more realistic than consider values below -1 in represent drought areas if compared with the anomalies composites itself (Figure 4-19 to Figure 4-21). This seems to be reasonable since consider yearly average values under -1 means that during all the year a region was under severe drought condition or some months with extreme droughts. This was the case for the 2001 drought in Morocco and the 2009 drought in eastern Africa. However it's shown in Section 4.6 that the threshold selected (in particular for values below -1) could trigger greater discrepancies between datasets.

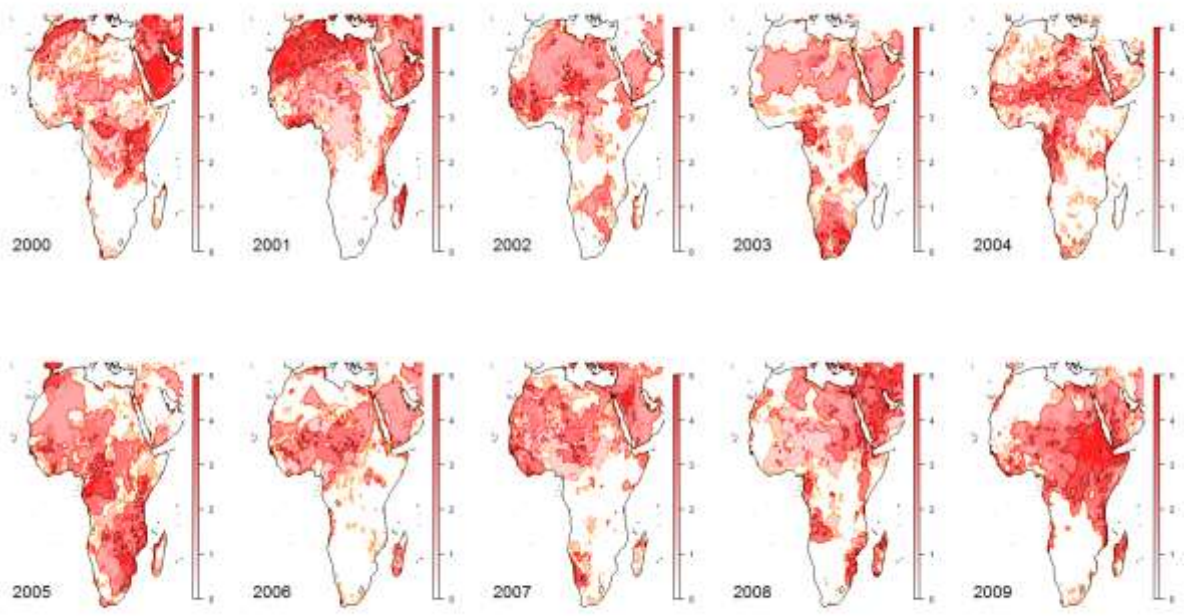

Figure 4-20 Spatial agreement between ERA-I, GPCP and TRMM SPI-3 and ERIA, GPCP SPEI-3 estimations. Grid cells with SPI-3 below -0.5 were considered. Values are ranged between 0 (no dataset with SPI below the threshold) and 5 (all datasets below the threshold).

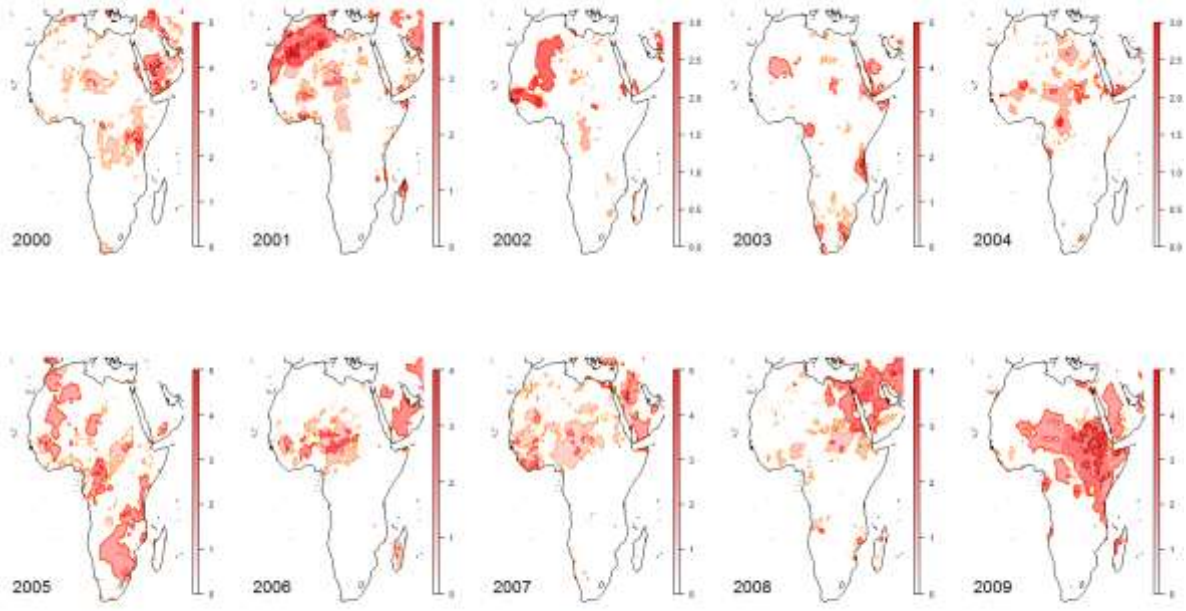

Figure 4-21 Spatial agreement between ERA-I, GPCP and TRMM SPI-3 and ERIA, GPCP SPEI-3 estimations. Grid cells with SPI-3 below -1.0 were considered. Values are ranged between 0 (no dataset with SPI below the threshold) and 5 (all datasets below the threshold).

4.5 TIME SERIES ANOMALIES ANALYSIS

4.5.1 Standardized Precipitation Index (SPI)

As stated in section 2 there is a general good agreement between precipitation datasets, however computation of SPI requires the knowledge of the sample distribution and the estimation of the parameters that defines it are dependent on the baseline period, aggregation period and spatial resolution. In this section time series of SPI-3 using ERAI, GPCC, TRMM and GPCP datasets are analysed at the five regions. Figure 4-22 shows the time series for the 4 estimations at each region and table 4-1 includes a number of metrics that represents the agreement between estimations.

The comparison between SPI estimations tends to resemble the findings on section 2 about agreement between precipitation datasets. This could suggest that the main sources of error are the uncertainties (due by lack of ground information, estimation algorithms, parameterization of the convection, etc.) in the datasets rather than the estimation of the distribution parameters.

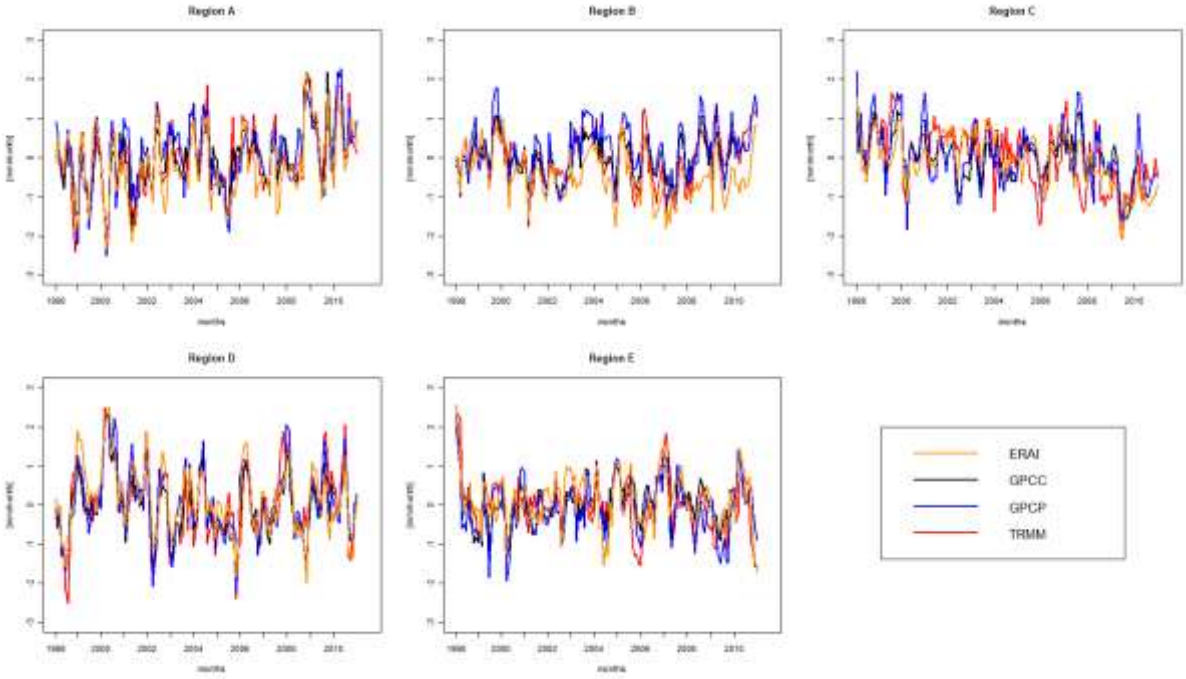

Figure 4-22 3-month SPI times series from the different datasets averaged over the five regions [A) Oum er-Rbia, B) Inner Niger Delta, C) Blue Nile and D) Limpopo basin and E) Great Horn of Africa] for the common period 1998-2010.

In fact, Oum er-Rbia and Limpopo regions are those that exhibit a better agreement between estimations with correlation coefficient mostly greater than 0.8 and the index of agreement between 0.86 and 0.92 (A index of agreement of 1 indicates a perfect match, and 0 indicates no agreement at all). The mean absolute error is usually around 0.3 at these locations but could reach 0.5 at Oum er-Rbia between ERAI and GPCP estimations and 0.46 between TRMM and ERAI at the Limpopo basin.

While for the other regions the discrepancies between datasets are also acceptable with mean absolute errors (MAE) around 0.3 and 0.5 and correlation coefficient/ index of agreement between 0.7 and 0.9. The greater discrepancies are observed at Niger basin, where the mean absolute error between the datasets and ERAI estimation are greater than 0.46, reaching 0.65 if ERAI-GPCP are compared. This discrepancy is also evident in Figure 4-22 where is observed that ERAI underestimates SPI compared with the other datasets mainly during the second half of the period analysed.

REGION A: Oum er-Rbia

		TRMM	GPCC	GPCP	ERAI
Spearman Coefficient	TRMM	1.00	0.89	0.81	0.84
	GPCC	0.89	1.00	0.81	0.81
	GPCP	0.81	0.81	1.00	0.74
	ERAI	0.84	0.81	0.74	1.00
MAE	TRMM	0.00	0.28	0.38	0.37
	GPCC	0.28	0.00	0.35	0.34
	GPCP	0.38	0.35	0.00	0.50
	ERAI	0.37	0.34	0.50	0.00
Index of Agreement (d)	TRMM	1.00	0.95	0.92	0.92
	GPCC	0.95	1.00	0.92	0.92
	GPCP	0.92	0.92	1.00	0.86
	ERAI	0.92	0.92	0.86	1.00

REGION B: NIger

		TRMM	GPCC	GPCP	ERAI
Spearman Coefficient	TRMM	1.00	0.85	0.79	0.71
	GPCC	0.85	1.00	0.91	0.72
	GPCP	0.79	0.91	1.00	0.67

	ERAI	0.71	0.72	0.67	1.00
MAE	TRMM	0.00	0.26	0.38	0.50
	GPCC	0.26	0.00	0.29	0.46
	GPCP	0.38	0.29	0.00	0.65
	ERAI	0.50	0.46	0.65	0.00
Index of Agreement (d)	TRMM	1.00	0.89	0.86	0.76
	GPCC	0.89	1.00	0.91	0.74
	GPCP	0.86	0.91	1.00	0.69
	ERAI	0.77	0.74	0.70	1.00

REGION C: Blue Nile

		TRMM	GPCC	GPCP	ERAI
Spearman Coefficient	TRMM	1.00	0.54	0.53	0.60
	GPCC	0.54	1.00	0.92	0.57
	GPCP	0.53	0.92	1.00	0.67
	ERAI	0.60	0.57	0.67	1.00
MAE	TRMM	0.00	0.54	0.55	0.50
	GPCC	0.54	0.00	0.27	0.41
	GPCP	0.55	0.27	0.00	0.46
	ERAI	0.50	0.41	0.46	0.00
Index of Agreement (d)	TRMM	1.00	0.73	0.75	0.77
	GPCC	0.73	1.00	0.93	0.80
	GPCP	0.75	0.93	1.00	0.82
	ERAI	0.77	0.80	0.82	1.00

REGION D: Limpopo

		TRMM	GPCC	GPCP	ERAI
Spearman Coefficient	TRMM	1.00	0.91	0.84	0.80
	GPCC	0.91	1.00	0.92	0.91
	GPCP	0.84	0.92	1.00	0.88
	ERAI	0.80	0.91	0.88	1.00
MAE	TRMM	0.00	0.28	0.39	0.46
	GPCC	0.28	0.00	0.27	0.33
	GPCP	0.39	0.27	0.00	0.35

	ERAI	0.46	0.33	0.35	0.00
Index of Agreement (d)	TRMM	1.00	0.95	0.92	0.88
	GPCC	0.95	1.00	0.96	0.94
	GPCP	0.92	0.96	1.00	0.94
	ERAI	0.88	0.94	0.94	1.00

REGION E: GHA

		TRMM	GPCC	GPCP	ERAI
Spearman Coefficient	TRMM	1.00	0.58	0.65	0.61
	GPCC	0.58	1.00	0.86	0.58
	GPCP	0.65	0.86	1.00	0.68
	ERAI	0.61	0.58	0.68	1.00
MAE	TRMM	0.00	0.40	0.44	0.44
	GPCC	0.40	0.00	0.29	0.42
	GPCP	0.44	0.29	0.00	0.45
	ERAI	0.44	0.42	0.45	0.00
Index of Agreement (d)	TRMM	1.00	0.78	0.81	0.80
	GPCC	0.78	1.00	0.91	0.80
	GPCP	0.81	0.91	1.00	0.83
	ERAI	0.80	0.80	0.83	1.00

Table 4-2 Spearman correlation coefficient, mean absolute error and bias (%) between the different SPI-3 estimations averaged over each region for the common period 1998-2010. All correlations are significant at 99%.

These results could be used in order to assess an objective selection of the dataset to be used in the map server and to determine a relative error of each estimation. First, the selected dataset could be these with higher index of agreement or lower mean absolute error compared with the others considering each grid cell or region. Second for the selected dataset the average values of mean absolute error could be used in order to determine a confidence interval and make more reliable the drought estimation.

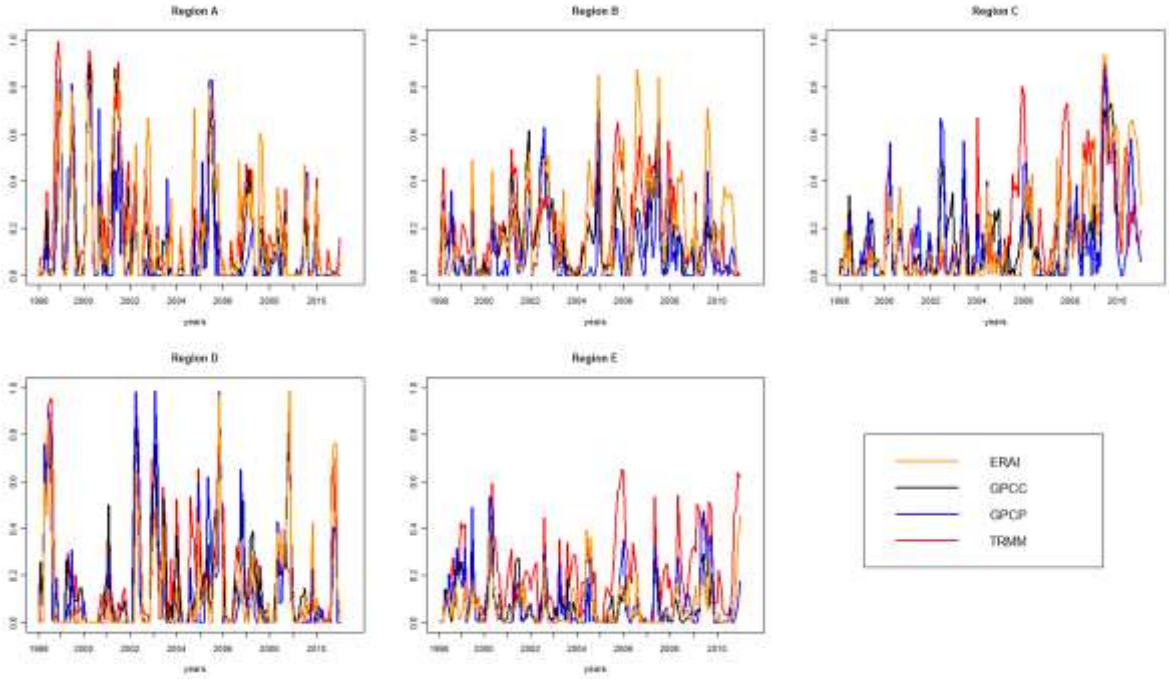

Figure 4-23 Fractional area of each region under 3 month-SPI bellow -1.0

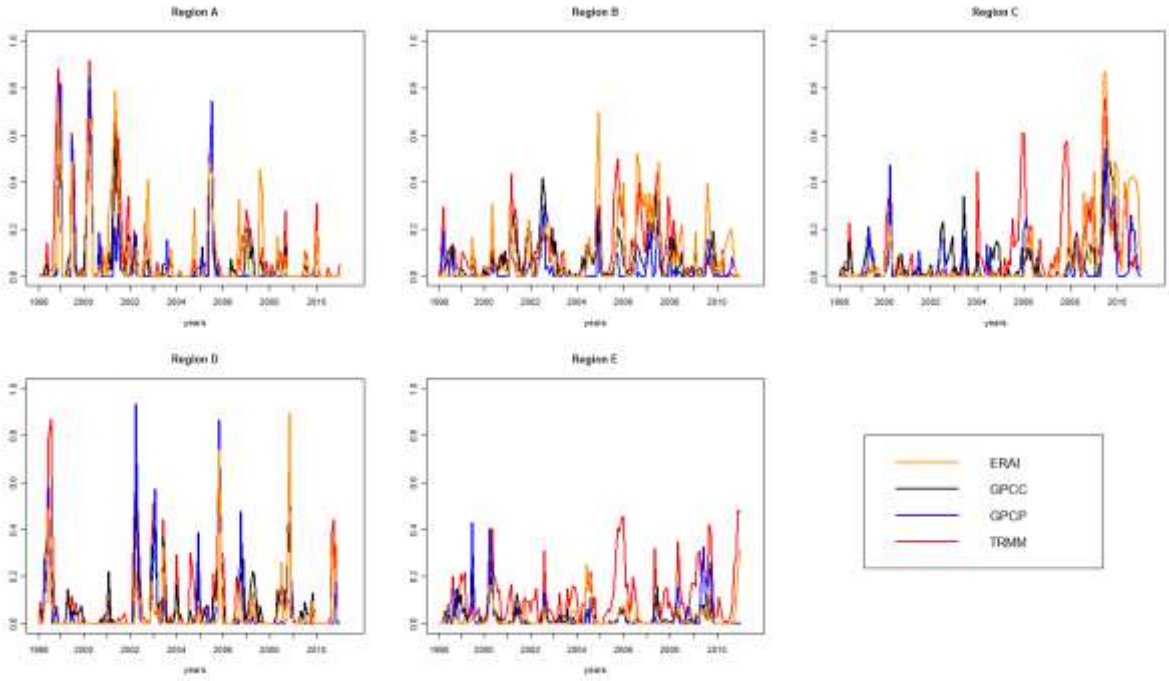

Figure 4-24 Fractional area of each region under 3 month-SPI bellow -1.5

Regarding the areas that are under drought, all the datasets agrees with the certain time of onset and recovery but there are sometimes disagreements on the area affected and also this agreement tends to be dependent on the threshold. Figure 4-23 and Figure 4-24 shows the monthly fractional area under SPI below -1.0 and -1.5 respectively.

There is a general better agreement if the areas covered by SPI below -1.0 are considered. In this analysis the Great Horn of Africa presents more discrepancies reaching a difference of more than 50% between GPCC and TRMM during the 2005/2006 period.

For values below -1.5 and in regions with better agreement (Oum er-Rbia and Limpopo basins) the only discrepancies are for the 2002 in Limpopo and 2005 drought in Morocco, where the GPCP estimation tends to overestimate the area affected in around 20 %, while TRMM shows the same behaviour for the 1998 drought at Limpopo basin. Here ERA-I are 20% over the other estimations during 2008 while during 2007 is the only dataset that present significant areas affected. For the other regions and considering extreme droughts, is difficult to find some agreement, mainly at regions Blue Nile and GHA.

In order to define how the threshold defined could affect the agreement between datasets a correlation analysis was performed between different thresholds of SPI and the areas affected by droughts by regions. Figure 4-25 shows that for almost all regions (except for Oum er-Rbia where this relationship is almost constant) there are an inverse relation between the agreement of the area defined under dry conditions and the value of SPI defined as threshold. In other words, the differences in the estimations of each sample distributions are highlighted while more extreme cases are considered. A solution to reduce this effect is to consider a lower threshold to define areas (namely no below than -0.8 or -1).

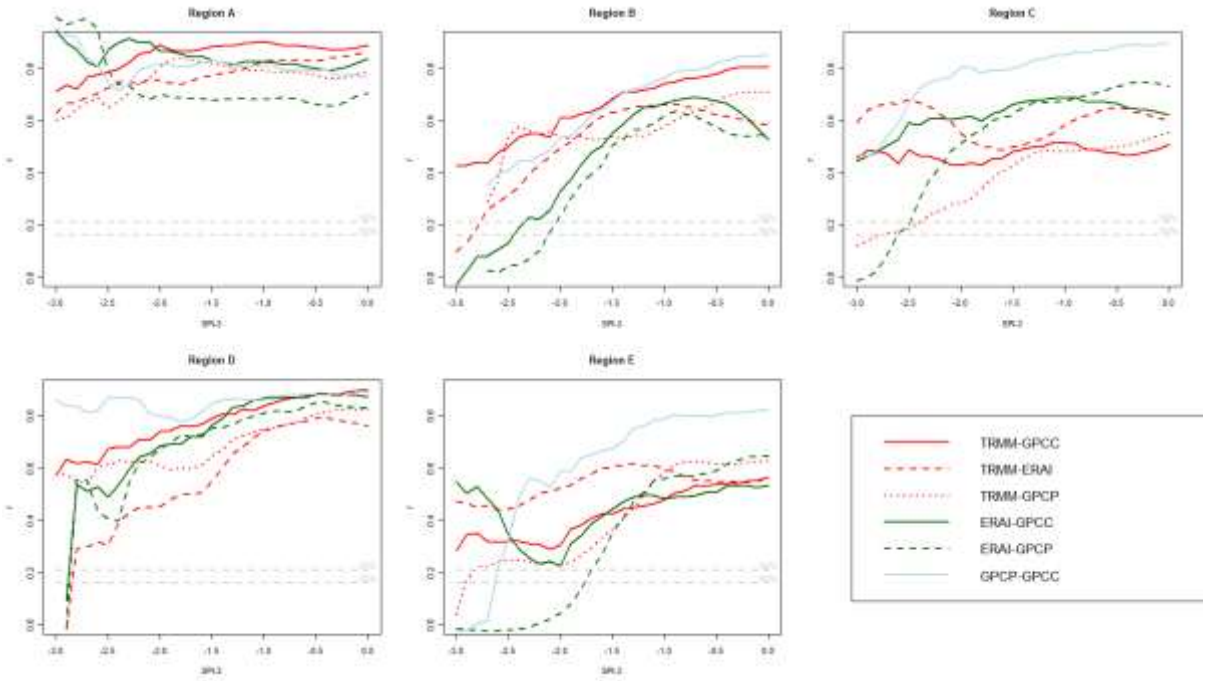

Figure 4-25 Pearson's Correlation coefficient of fractional areas on drought between different datasets and thresholds. The x-axis represents the threshold from which SPI below this value are considered to calculate the areas.

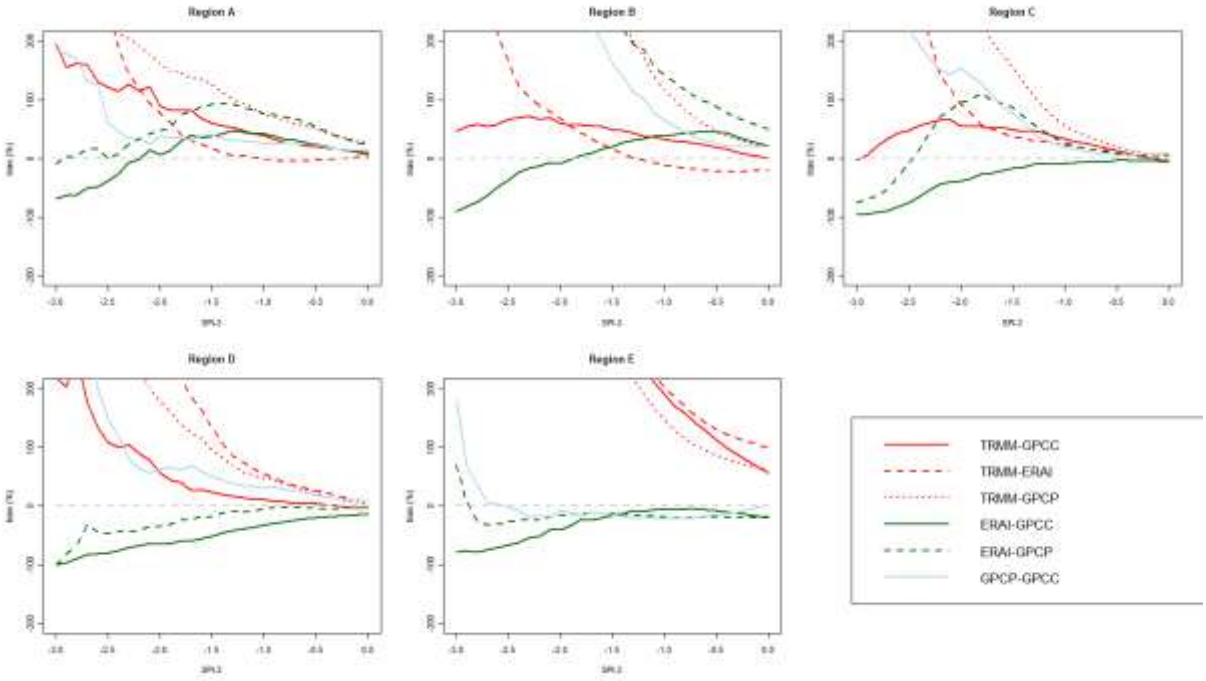

Figure 4-26 Bias between estimation of fractional areas on drought for different datasets and thresholds. The x-axis represents the threshold from which SPI below this value are considered to calculate the areas.

Also, the bias between estimations (Figure 4-26) presents an acceptable departure between estimations from normal conditions until values near -0.5. Then, below these threshold the bias increase exponentially surpassing quickly (around SPI values of -1) a bias of 100%. Again, for Niger and GHA regions for none of the cases a good approximation is observed, only there is a reasonable agreement between ERAI and GPCC estimations.

However, as depicted in Figure 4-26, the position parameter is well represented for all datasets and regions since the bias of consider areas with values below zero are negligible. This result suggests that the main sources of error in the SPI estimation are defined as how well the theoretical distribution represents the tails of the observed distribution.

Figure 4-27 to Figure 4-29 shows the spatial agreement of areas with SPI below 0, -0.5 and -1 using ERAI, GPCP and TRMM datasets estimations. Again in a yearly basis a threshold of -0.5 seems to be a good representation of the areas affected with a good agreement between estimations, while for SPI values below -1 it's difficult to found areas with good agreement.

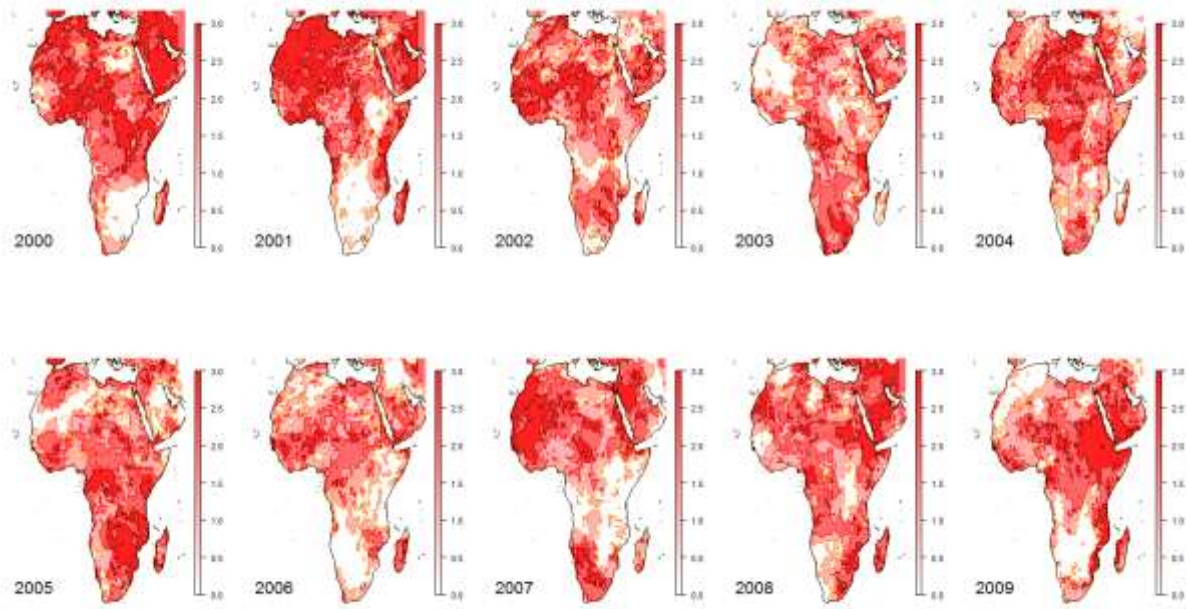

Figure 4-27 Spatial agreement of between ERA-I, GPCP and TRMM SPI-3 estimations. Grid cells with SPI-3 below 0.0 were considered. Values are ranged between 0 (no dataset with SPI below the threshold) and 3 (all datasets below the threshold).

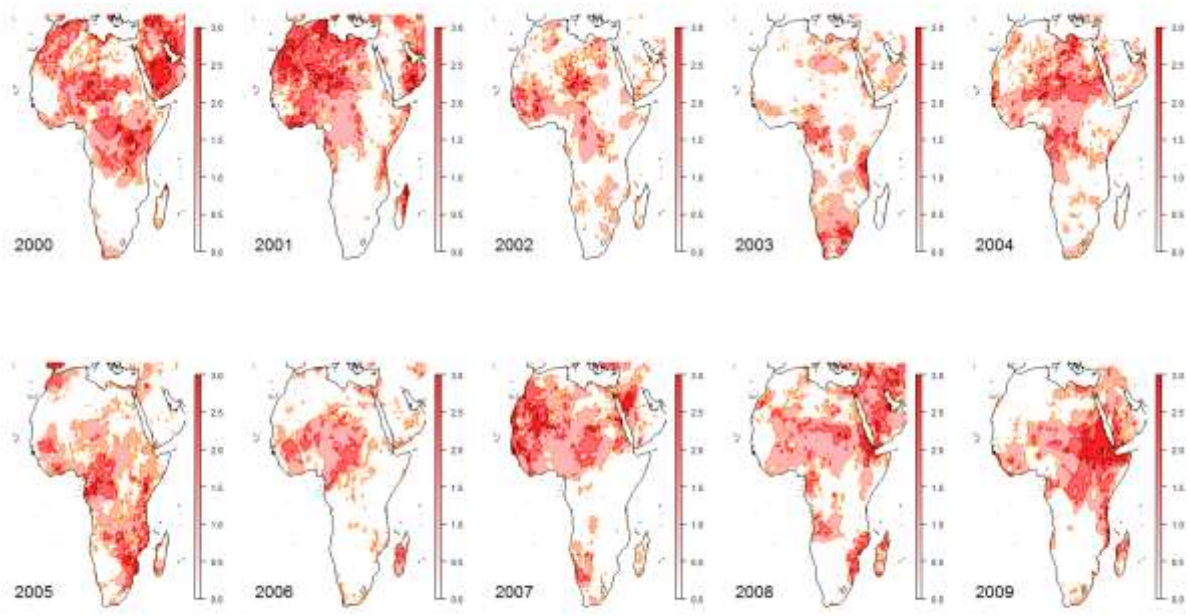

Figure 4-28 Spatial agreement of between ERA-I, GPCP and TRMM SPI-3 estimations. Grid cells with SPI-3 below -0.5 were considered. Values are ranged between 0 (no dataset with SPI below the threshold) and 3 (all datasets below the threshold).

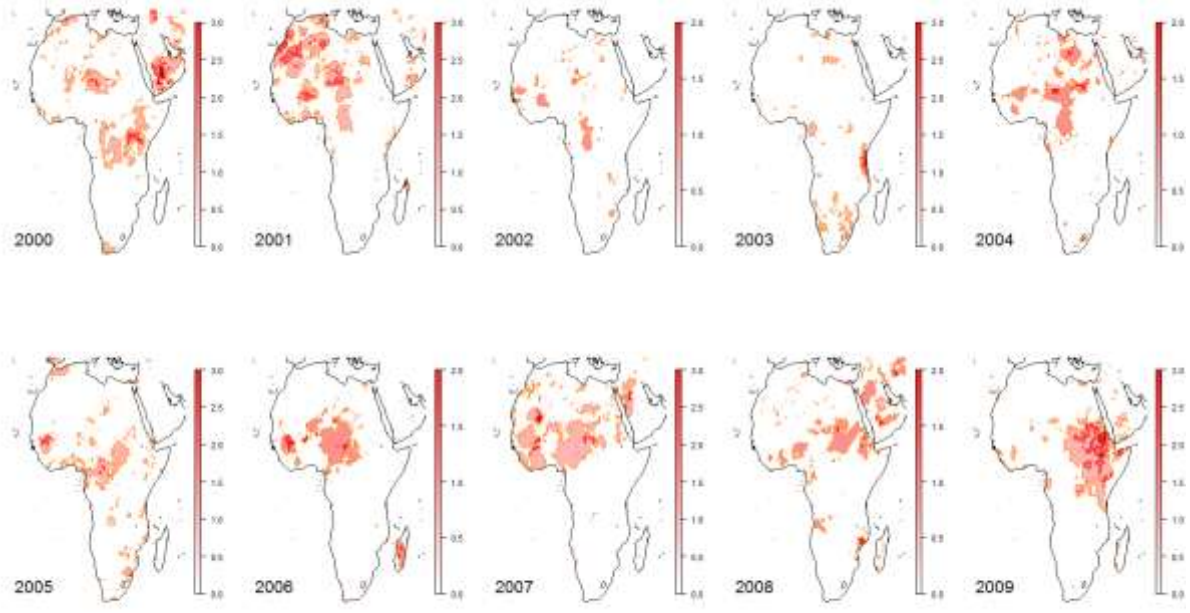

Figure 4-29 Spatial agreement of between ERA-I, GPCP and TRMM SPI-3 estimations. Grid cells with SPI-3 below -1.0 were considered. Values are ranged between 0 (no dataset with SPI below the threshold) and 3 (all datasets below the threshold).

In order to objectively define areas where indicators are in agreement the temporal correlation at grid cell level between indicators were performed during the 1998-2010 common period. Figure 4-30 shows the correlation between SPI-3 TRMM and the other indicators. In order to perform the comparison at grid cell level the TRMM estimation was resized using bilinear weights to interpolate values on 0.25°x0.25° to 0.5°x0.5° grids. Figure 4-31 also shows the correlation maps between SPI-3 ERAI and the others excluding the TRMM estimation.

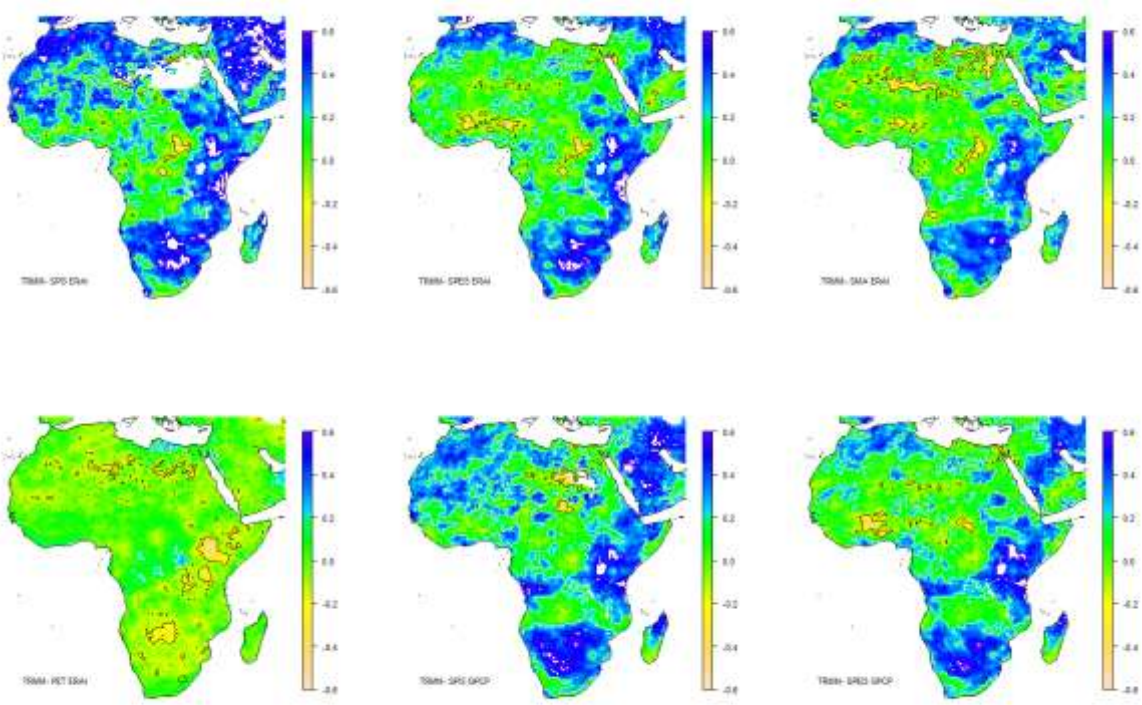

Figure 4-30 Temporal correlation between SPI-3 TRMM and SPI-3 ERAI, SPEI-3 ERAI, SMA, PET, SPI-3 GPCP and SPEI 3 GPCP.

These results confirm and extend the findings in Deliverable D4.2 where SPI computed with ERAI and GPCP was compared. For those datasets a good agreement in the South and North West was observed, while is present a low agreement in Central Africa. However, if SPI-3 TRMM estimation is also compared with ERAI estimation a better agreement is observed. In this comparison not only the North West area and Southern Africa shows a good agreement. Now a good agreement (significant correlations) is also observed in east Africa and the region that includes the Great Horn of Africa (excluding Somalia). Soil moisture anomalies also show a good agreement in those areas.

As the depicted also in the previous analysis, the estimations of the indicators over Central Africa reflect the high uncertainty present in the precipitation datasets. At this region, no significant correlations are observed between SPI estimations using the different datasets.

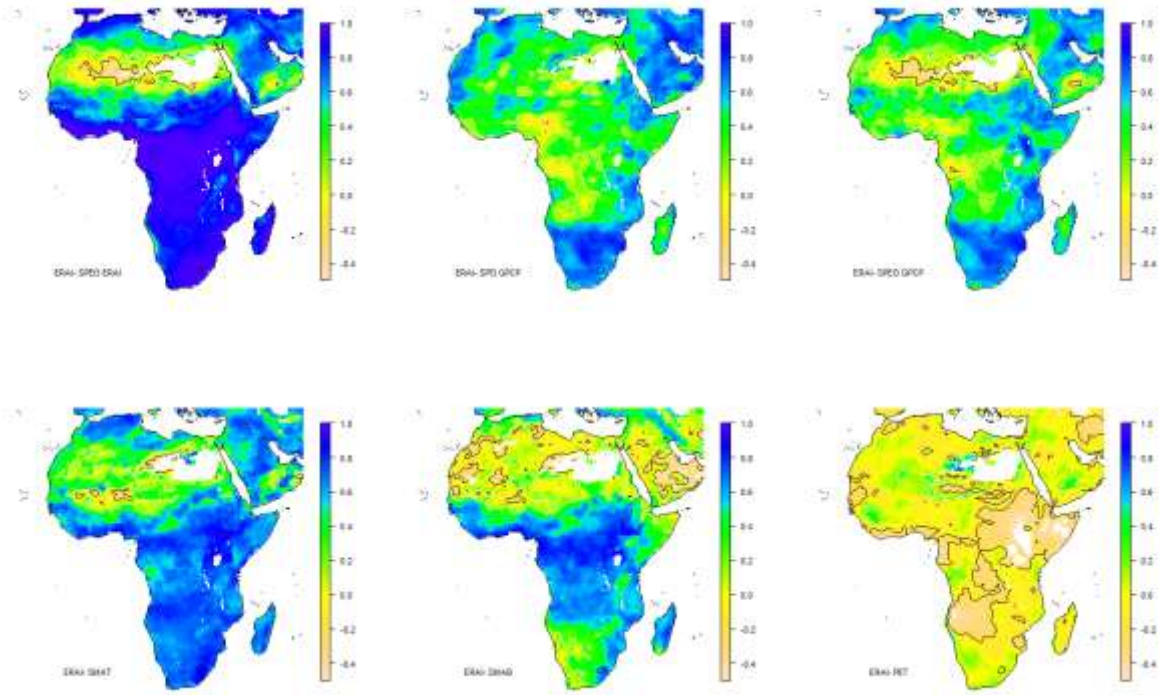

Figure 4-31 Temporal correlation between SPI-3 ERAI and SPEI-3 ERAI, SPI-3 GPCP, SPEI-3 GPCP, SMA at the top meter of the soil (SMAT), SMA at the bottom layer (SMAB), and PET.

4.6 PERSISTENCE ANALYSIS OF DROUGHT CONDITIONS

In addition to the analysis of the areas affected by droughts and in order to characterize drought as a physical processes, it is important to have a detailed knowledge of the temporal behaviour of the temporal parameters that represents its evolution, like the memory or persistence of the process.

According to the selected threshold (namely SPI values below -0.5, -1, etc.), each month is described by only one of the states that describe a drought. $P_i(X_1; \ldots; X_i)$ was defined as the probability of each state sequence of length i (namely, X represent the dry conditions). This probability describes the persistence of dry conditions over i months. The sequence of the probabilities $P_i(x)$ states that x will be

maintained over i months before it switches over to another sequence. This quantity is called the ‘‘exit time distribution’’ (Nicolis et al., 1997).

Figure 4-32 shows the defined exit time distribution to remain in dry conditions for each estimation and region. The result presents a wide range of distributions for each region, and including that at the Great Horn of Africa there are not values below -1 for the GPCC estimation. Again the threshold selected is the parameter that defines the homogeneity or heterogeneity between the estimation of the exit time distributions for the different datasets.

Figure 4-33 shows the probability of remain in dry conditions (parameter that defines the exit time distribution) as function of the spatially averaged SPI are below a certain threshold. This threshold defines which months are considered as dry and which months are considered as normal or wet. This relation also could define the cut-off value that is possible to define the distribution as occurs in the GHA where the exit time distribution cannot be calculated considering a value of -1 since the minimum spatially averaged value was 0.8. As observed in the previous sections, the region around SPI values of -0.5 and -1.0 (except for GHA) intends to be a more coherent behaviour between transition probabilities and datasets.

Moreover, if is considered that the exit time distribution should be the same for all datasets (and also the parameter that defines this distribution) it’s possible to fix the transition probability and then standardize the threshold according to the values of SPI associated with this value. In Table 4-3 the associated spatially averaged SPI thresholds that define a certain exit time distribution at Niger and Nile basins are represented. For instance, in order to have a P value of 0.4 the SPI values ranges according the different datasets between -0.8 and -1.0 at Niger and between -0.6 and -1.2 at Blue Nile basin. As stated previously these differences are due by the difference in the baseline statistics, spatial resolution and intrinsic properties of each dataset. Scaling the values that are defined as dry conditions according to these criteria could allow a better agreement of regions affected between the different datasets.

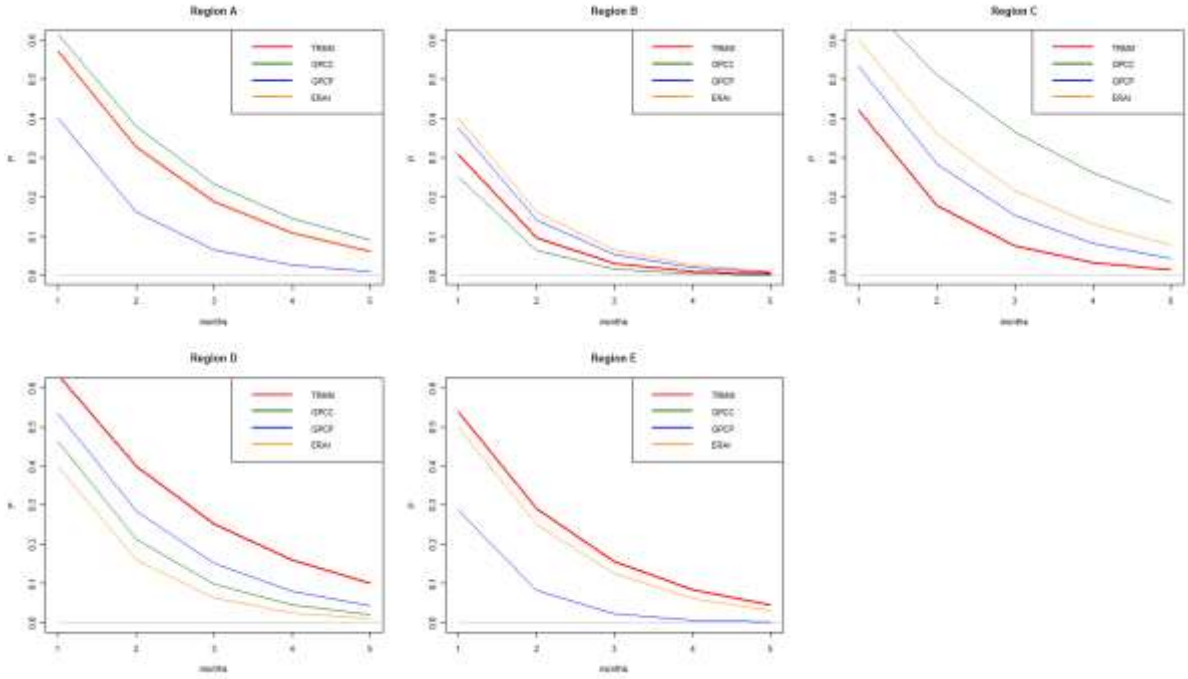

Figure 4-32 Theoretical Exit time distribution for dry conditions (SPI below -1.0) at each region.

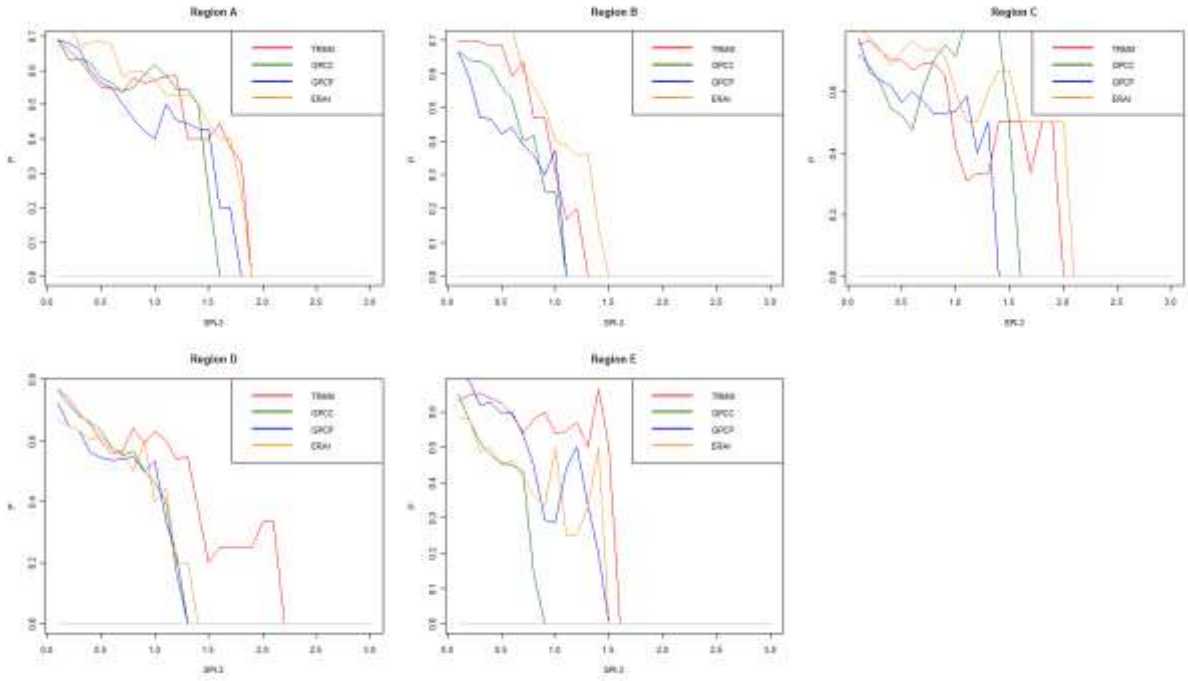

Figure 4-33 Probability of no change of state while the SPI are below certain thereshold (x-axis)

P	Niger basin				Blue Nile basin			
	TRMM	GPCC	GPCP	ERAI	TRMM	GPCC	GPCP	ERAI
0.00	-1.3	-1.1	-1.1	-1.5	-2.0	-1.6	-1.4	-2.1
0.05	-1.3	-1.1	-1.1	-1.5	-2.0	-1.6	-1.4	-2.1
0.10	-1.1	-1.1	-1.1	-1.4	-2.0	-1.6	-1.4	-2.1
0.15	-1.1	-0.9	-0.9	-1.4	-2.0	-1.6	-1.4	-2.1
0.20	-1.2	-0.9	-0.9	-1.4	-1.1	-1.6	-1.2	-2.1
0.25	-1.2	-0.9	-0.9	-1.2	-1.1	-0.6	-1.2	-1.1
0.30	-1.0	-0.9	-0.9	-1.2	-1.1	-0.6	-1.2	-1.1
0.35	-1.0	-0.7	-0.8	-1.2	-1.2	-0.6	-1.2	-1.1
0.40	**-0.8**	**-0.7**	**-0.7**	**-1.0**	**-1.0**	**-0.6**	**-1.2**	**-1.1**
0.45	-0.8	-0.8	-0.6	-0.9	-1.0	-0.6	-1.2	-1.1
0.50	-0.8	-0.6	-0.3	-0.9	-1.4	-1.5	-1.3	-1.1
0.55	-0.6	-0.5	-0.2	-0.8	-1.4	-0.4	-0.5	-1.0
0.60	-0.6	-0.4	-0.2	-0.7	-0.9	-0.7	-0.6	-1.0
0.65	-0.7	-0.2	-0.1	-0.7	-0.9	-0.3	-0.2	-1.4
0.70	-0.1	-0.1	-0.1	-0.6	-0.5	-0.8	-0.2	-0.9
0.75	-0.1	-0.1	-0.1	-0.6	-0.1	-0.9	-0.1	-0.8
0.80	-0.1	-0.1	-0.1	-0.4	-0.2	-1.3	-0.1	-0.1

Table 4-3 spatially averaged SPI thresholds and its associated transition probability (P) at regions Niger and Blue Nile basins.

5. THE GREAT HORN OF AFRICA 2010-2011 DROUGHT

This section illustrates a specific drought event over the Great Hon of Africa using meteorological and remote sensing indicators between 2010 and 2011. Section 5.1 analyses the drought using the SPI indicator and section 5.2 analyses the drought impact on vegetation using the fAPAR and NDWI anomalies.

5.1 EVOLUTION OF PRECIPITATION ANOMALIES

The rainfall conditions were assessed using the Standardized Precipitation Index (SPI). For this analysis we used rainfall data from the Global Precipitation Climatology Centre (GPCC) reanalysis product for the years 1960-2009 to define normal conditions and rainfall data from the GPCC monitoring (up to June 2011) and first guess (July – August 2011) products for the observed rainfall.

The evolution of the SPI for 3-month rainfall accumulations (SPI-3) is shown in Figure 5-1. Severe drought conditions in terms of the SPI-3 began in eastern Kenya in October 2010 and spread eastwards to southern Somalia into the beginning of 2011. In April 2011 extreme drought conditions were evident in the Kenya-Somalia border region becoming more extreme by June 2011. In July and August, although the famine situation in Somalia continued, the extent of the drought affected area was reduced; however we should take in consideration that the rainy season in Somalia should start only in September; at the same time an area on southern Sudan and bordering Ethiopia, previously identified as under threat, as well as northern Tanzania became drought affected. A time series of the spatial average of SPI-3 for the most affected area in June 2011 is shown in Figure 5-2. For the SPI-3 a more severe rainfall deficit was observed for MAM in 2000 than in 2011, although with more spatial variation, as shown by the error bars. This means that although some parts of the region experienced more severe rainfall deficits in MAM 2000, such severe rainfall deficits were not as widespread throughout the region compared to MAM 2011.

The evolution of the SPI for 6-month (SPI-6) rainfall accumulations is shown in Figure 5-3. Severe drought conditions were evident in southern Ethiopia from September 2010 and continued to June 2011 becoming more widespread, with the most extreme

conditions observed in the Somalia-Kenya border area and Uganda. In July and August this indicator also shows southern Sudan and bordering Ethiopia as being drought affected, as well as northern Tanzania. The time series of the mean SPI-6 for the most affected area in June 2011 shows that current conditions are comparable to previous 6-month rainfall deficits (Figure 5-4), although a more extreme SPI-6 was observed in mid-2000, corresponding to the extreme SPI-3 value that was observed around the same time.

The SPI-12 shows a similar evolution (Figure 5-5). In July 2010, extreme 12-month drought conditions were already evident in Sudan and western parts of Ethiopia. Severe 12-month drought conditions began in southern Ethiopia around December 2010 – January 2011 and spread throughout much of the Greater Horn of Africa by April 2011. These conditions remained also throughout the months of July and August confirming the findings of SPI-3 and SPI-6. The persistence of the rain deficit into the wet season for southern Sudan and neighboring areas of western Ethiopia has lead to drought conditions in these areas, as well as in northern Tanzania. The time series for mean SPI-12 for the most affected region until June 2011 shows that current conditions are only comparable with the long-term rainfall deficit observed in 1992, 1994 and 2000/2001 (Figure 5-6).

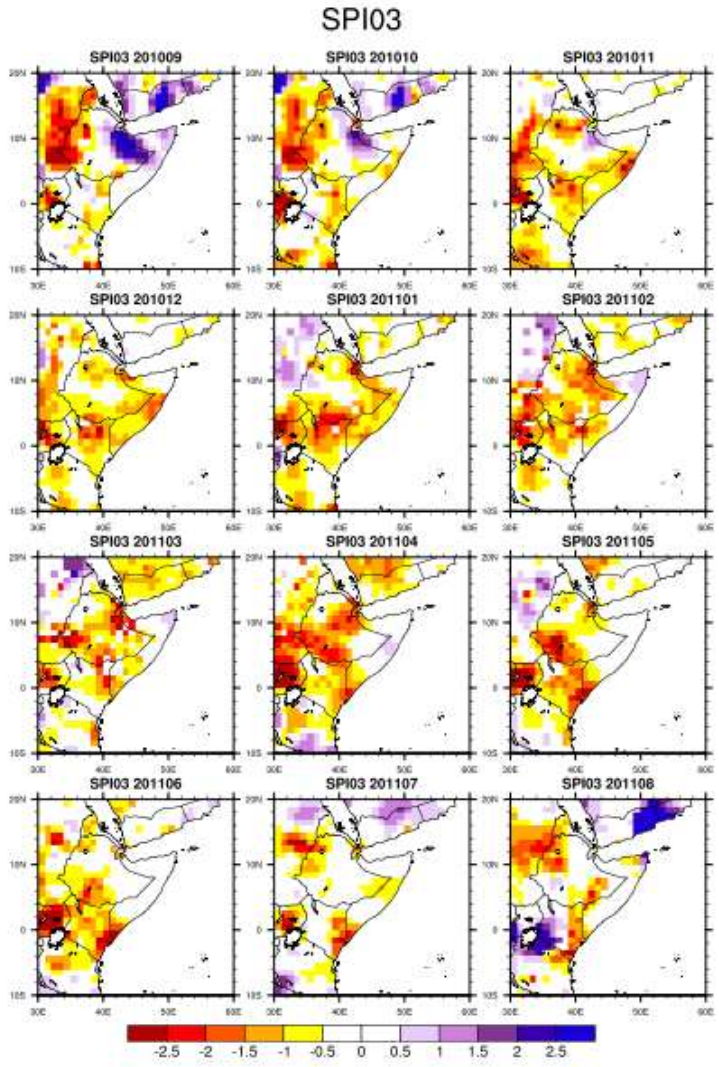

Figure 5-1 Evolution of the SPI for 3-month rainfall accumulations

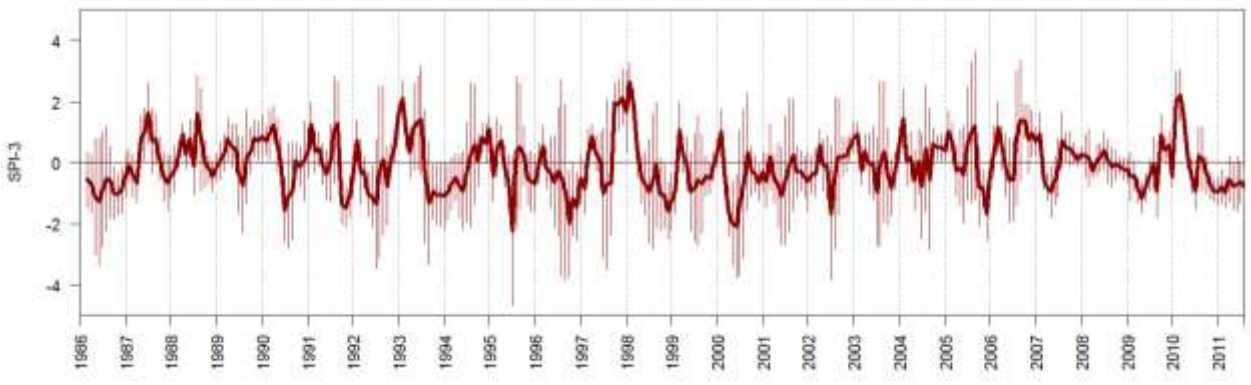

Figure 5-2 Time series of the spatial average of SPI-3 for the most affected area (the vertical lines represent ± 1 standard deviation).

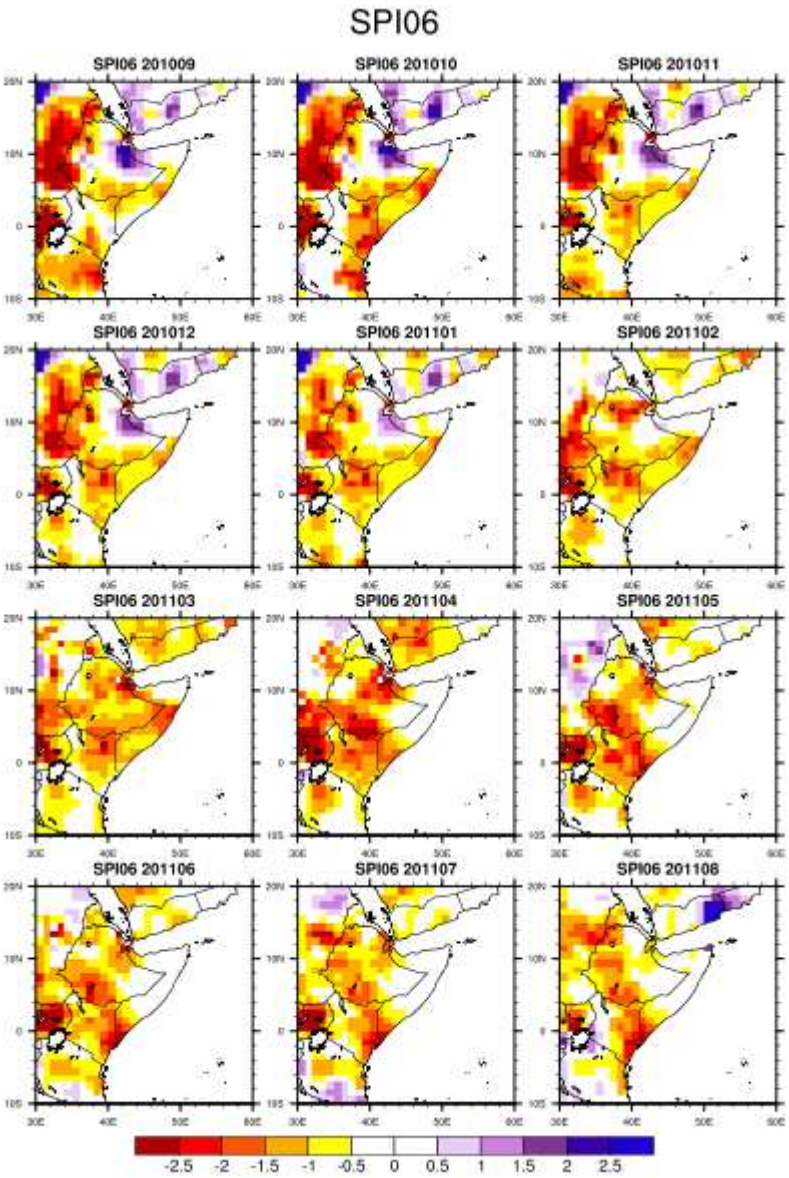

Figure 5-3 Evolution of the SPI for 6-month rainfall accumulations.

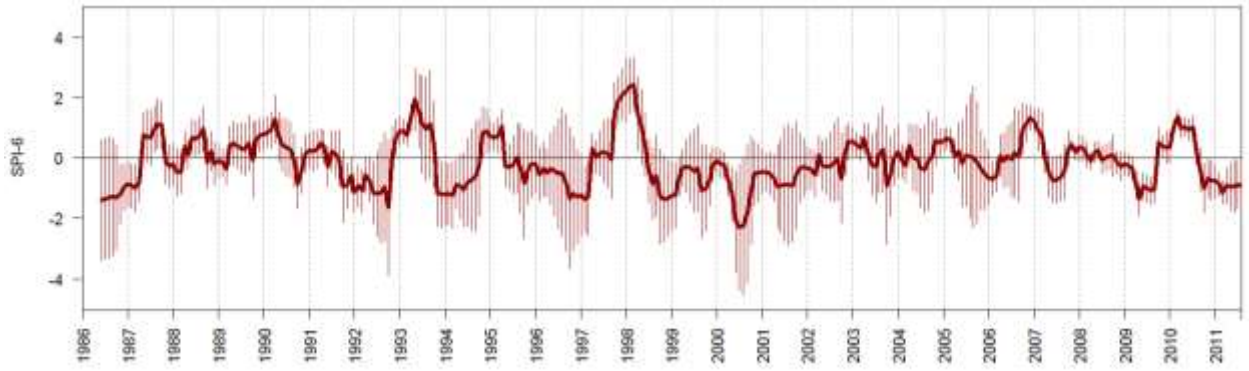

Figure 5-4Time series of the spatial average of SPI-6 for the most affected area (the vertical lines represent ± 1 standard deviation).

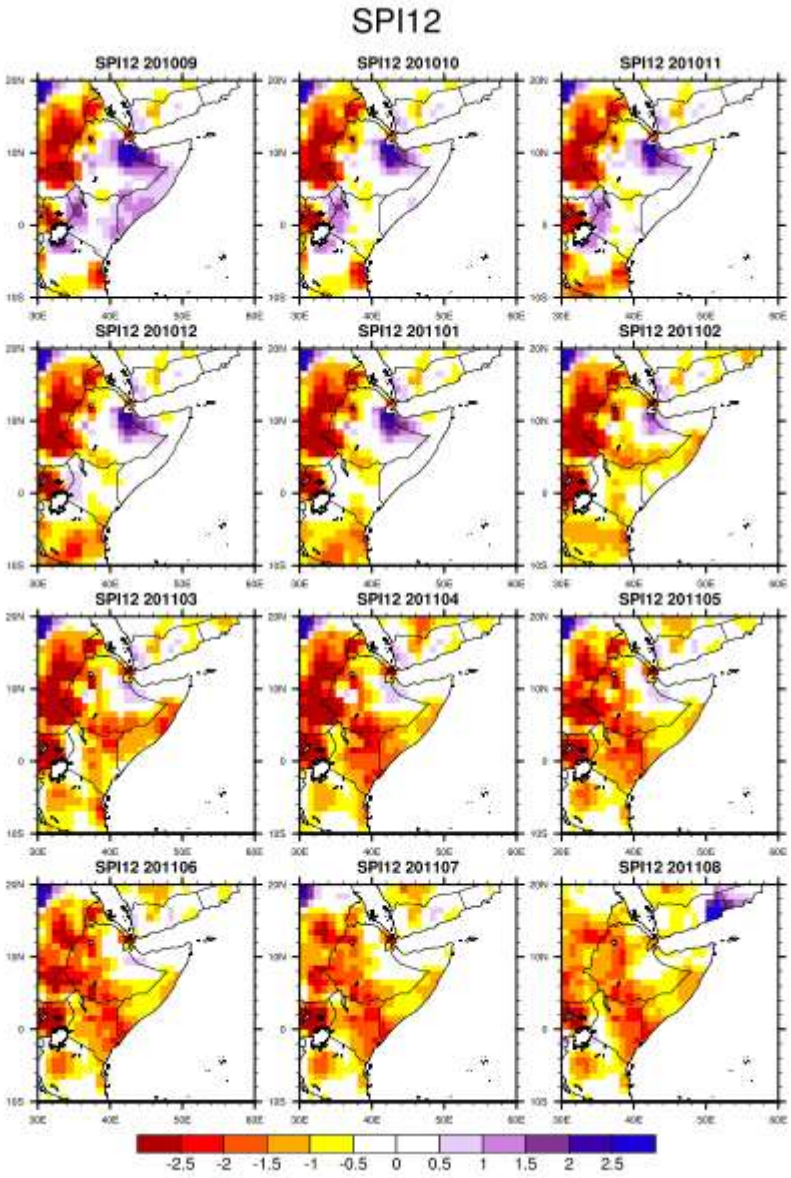

Figure 5-5 Evolution of the SPI for 12-month rainfall accumulations

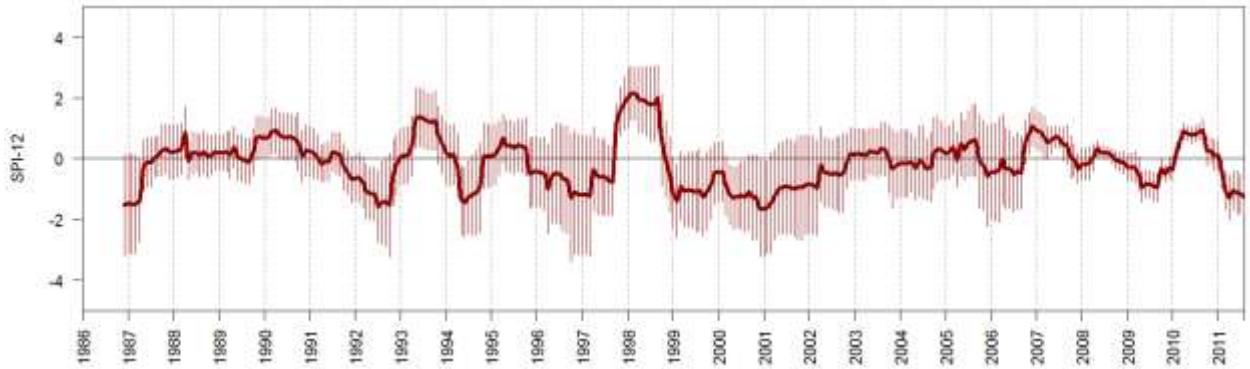

Figure 5-6 Time series of the spatial average of SPI-12 for the most affected area (the vertical lines represent ± 1 standard deviation).

5.2 MONITORING OF THE VEGETATION CONDITIONS

Vegetation conditions in the Greater Horn of Africa were evaluated using two remote sensing derived indices: the fraction of Absorbed Photosynthetic Active Radiation, fAPAR, and the Normalized Difference Water Index, NDWI. fAPAR provides information related to the green biomass, while the NDWI is more related to the water content of the canopy.

At the beginning of October 2010, the vegetation conditions as depicted by the fAPAR anomalies in the Horn of Africa were close to normal (Figure 5-7). In Mid-October and November, negative fAPAR anomalies began to be recorded in Somalia (central and southern parts), Ethiopia (mainly the south-eastern part) and in Kenya (northern and eastern parts). In December, the spatial extension of the drought as recorded by the fAPAR anomalies remained relatively constant, with a very spatially coherent negative signal registered for South Somalia.

From January until the beginning of May 2011, fAPAR anomalies became more negative in the above mentioned regions. In terms of extent and intensity, the peak of the drought was observed between end of April and beginning of May. Additionally, negative fAPAR anomalies also began to be recorded in northern Tanzania. From May onwards, an improvement of the vegetation conditions was observed in Ethiopia while the fAPAR anomalies remained negative in Somalia and Kenya.

The particularly poor vegetation conditions in Somalia and northern Kenya can be seen to be a result of the shortage of rainfall during the rainy season of March to May. Time series of spatially averaged fAPAR and NDWI anomalies were extracted for the most affected area, comprising Somalia, Ethiopia and Kenya. For both vegetation indices, the current drought is the most severe recorded during the available time series (largest negative anomalies). Although the archives of the vegetation indexes are relatively short (NDWI, from 04/1998-06/2011; fAPAR, from 06/2002-06/2011), it can be seen that the current drought is quite exceptional in terms of impact on the vegetation in this area (Figure 5-8).

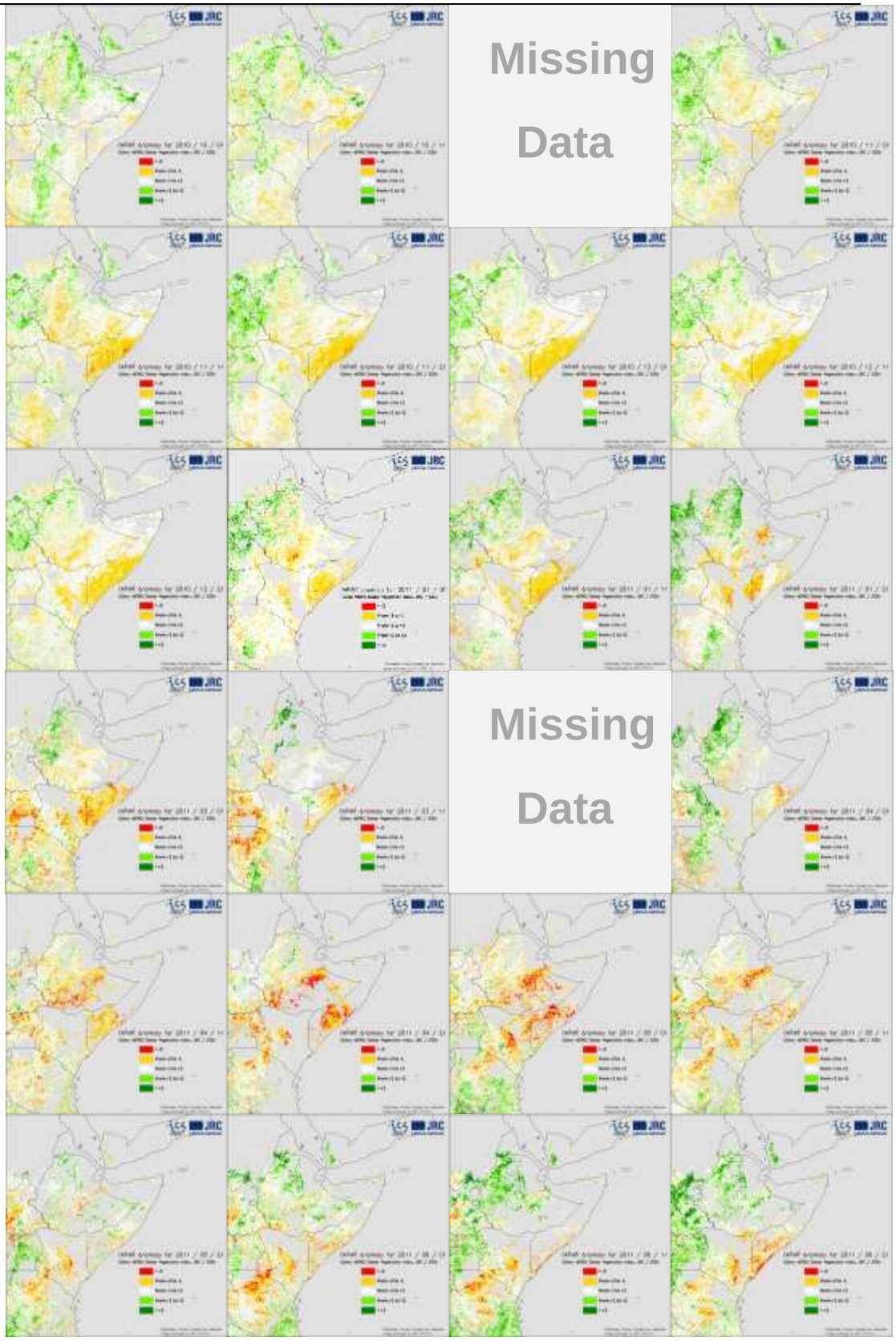

Figure 5-7 fAPAR 10-day anomaly from October 2010 to June 2011. Green colours correspond to positive anomalies (vegetation greener than normal), white to near-normal vegetation conditions and yellow and red to negative anomalies (vegetation less green than normal). Grey colour corresponds to "no data". The images from the 3rd 10-day period of October 2010 and 3rd 10-day period of March 2011 are missing.

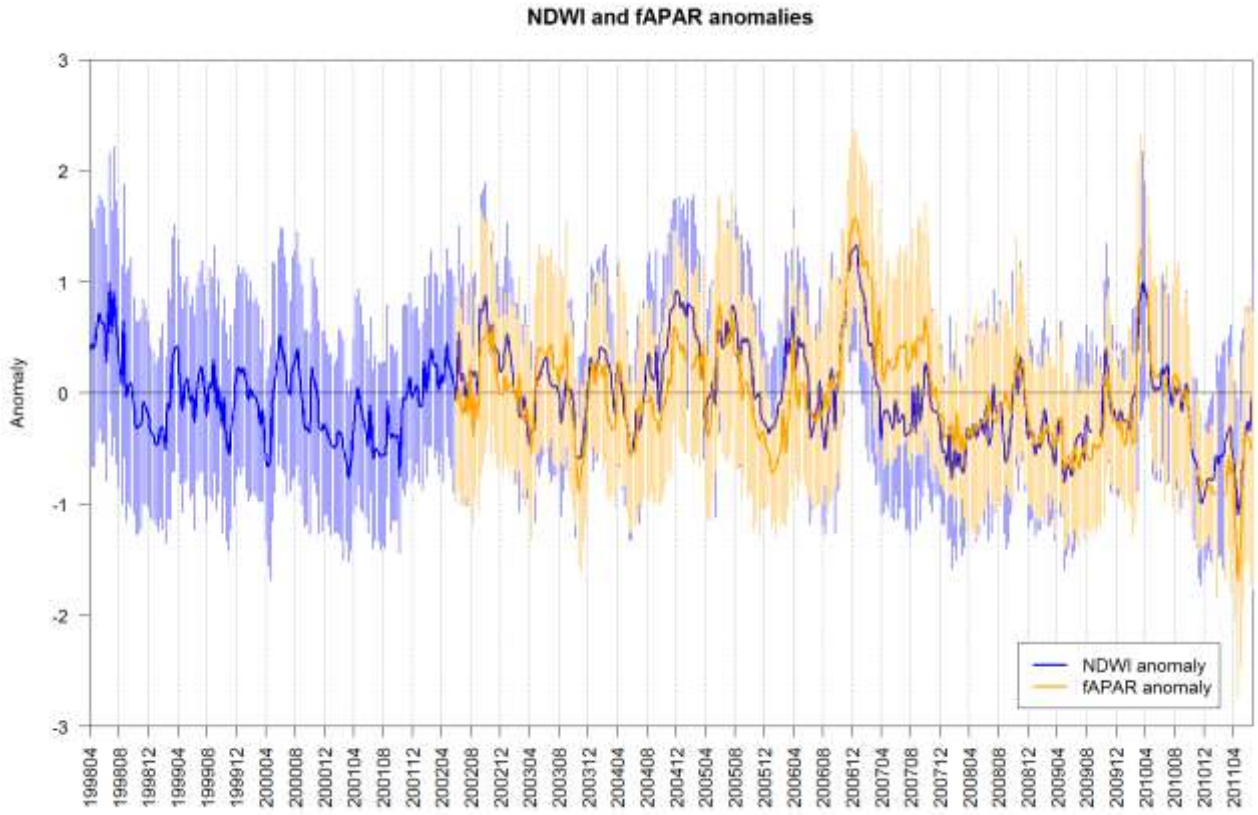

Figure 5-8 Time series of the spatial average of fAPAR and NDWI anomalies for the most affected area (the vertical lines represent ± 1 standard deviation).

The analyses of different meteorological and remote sensing indicators show that the territories most affected by drought are located between southern Somalia, southern Ethiopia, eastern Kenya, and north-eastern Tanzania. This area was delimited considering the failure of the 2 previous rainy seasons (October-December 2010 and March-May 2011), which was reflected in severe anomalies in both meteorological and remote sensing indicators, implying a significant drought impact on vegetation, including crops.

Over the south-east of the Horn of Africa, roughly coinciding with the area most affected by the drought so far, the annual rainfalls are almost totally concentrated in two main rainy periods (Figure 2-1): between September and November and between mid-March and mid-May. No irrigation is available in this area and therefore local food production is completely dependent on the rainfall. Due to the relatively short rainy periods the cultivated crops are mainly cereals characterized by fast growth (maize, millets, sorghum, etc.). The shortage of rain during this two crop growing seasons contributed to the complete failure of the seasonal food production.

The analysis of the SPI (Standardized Precipitation Index) over the last 25 years clearly shows the exceptionality of the current rain shortage which is only comparable to the 2000/2001 season.

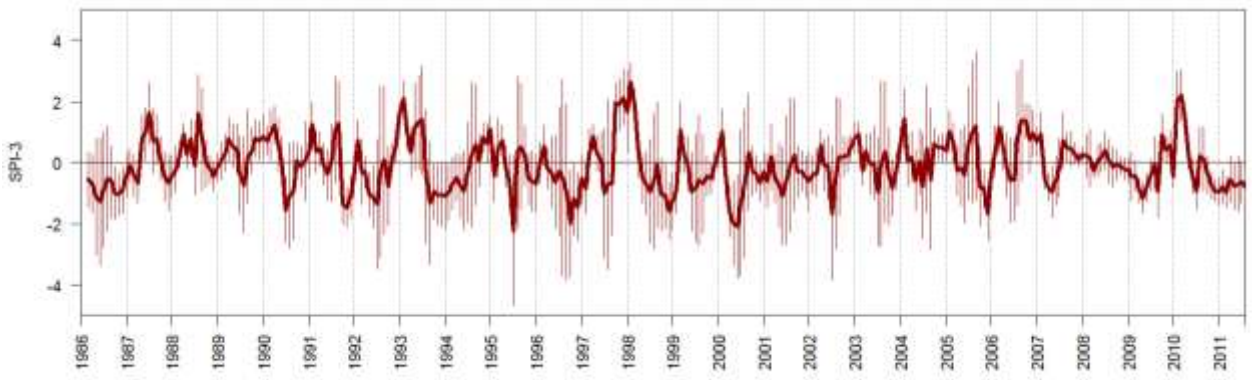

Figure 5-2 Time series of the spatial average of SPI-3 for the most affected area (the vertical lines represent ± 1 standard deviation).

,

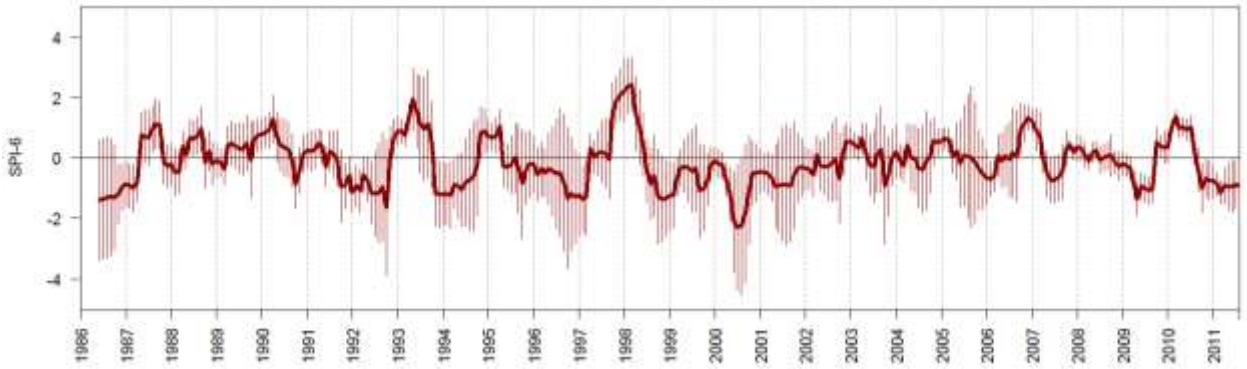

Figure 5-4Time series of the spatial average of SPI-6 for the most affected area (the vertical lines represent ± 1 standard deviation).

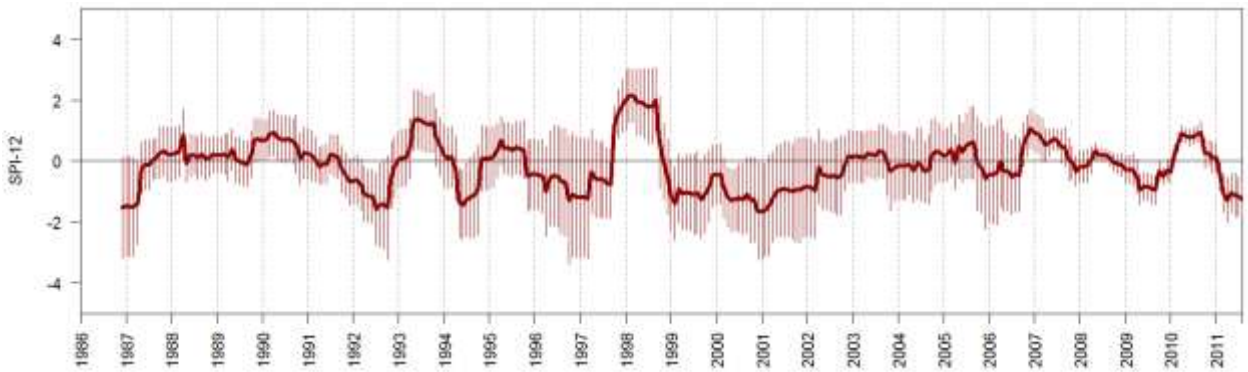

Figure 5-6 Time series of the spatial average of SPI-12 for the most affected area (the vertical lines represent ± 1 standard deviation).

The effect of drought on the vegetation, including agricultural areas, is clearly shown on the analysis of the anomalies of two vegetation indicators, the fAPAR (fraction of Active Photosynthetic Active Radiation) and the NDWI (Normalized Difference Water Index). In this case, the analyses of the vegetation indicators show a higher impact on vegetation than in any of the previous years starting in 1989.

5.3 GHA 2010-2011 DROUGHT: THE KENYA EXPERIENCE

5.3.1 Drought characterization at Kenya country level

Droughts have been occurring more frequently over the Greater Horn of Africa (GHA) region. This is evidenced by the recent droughts (1999 – 2001, 2005 – 2006, 2009 and 2010-2011). The 2010/2011 was termed as the worst drought the region has faced in 60 years. The drought caused severe food crises across Somalia, Ethiopia and Kenya that threatened the livelihood of more than 13.3 million people. The drought was associated with La Niña condition that developed over the Eastern Pacific in July 2010 and persisted till May 2011. This La Niña event affected the October-December (OND) rainfall season in 2010 and the March-May (MAM) rainfall in 2011. Having in mind that the MAM and OND seasons are the major growing seasons in the region, having two consecutive seasons failing had major implications.

The term La Niña is used to describe the periodic building up of unusually cold waters in the eastern and central equatorial Pacific Ocean. It has been observed that during La Niña, world-wide weather and climate extremes such as droughts, floods, cold/hot spells and tropical cyclones tend to be more common at specific locations, even for some regions that are very far away from the Equatorial Pacific Ocean (Glantz, 2002). Such weather and climate extremes are often associated with far reaching socio-economic impacts including loss of lives and property; mass migration of people and animals; and lack of water, energy, food and other basic needs of human kind. Over the eastern equatorial sector of the GHA region the cold episodes (La Niña) are largely associated with suppressed October to December rainfall (Nicholson and Selato, 2000), as was evident during the prolonged droughts of 1988/89, 1999/2000 and most recently 2010/2011.

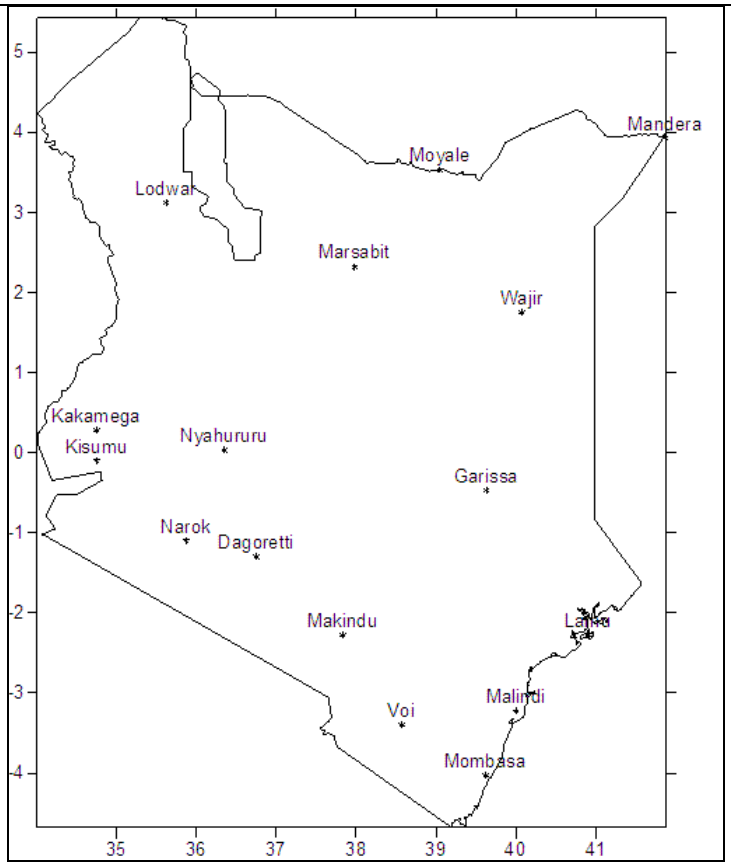

Figure 5-9 Spatial distribution of stations used.

The 2010/2011 drought over the GHA region was observed to be the worst that the region has experienced during the last 60 years (Trócaire, 2011). It is for this reason that this drought was considered for this case study. Kenya, Ethiopia and Somalia were the countries most affected. In particular, the drought monitoring and mitigation experience at country level in Kenya during this drought were the center of focus in the study.

The data used in the study included station daily rainfall data for the period 1961 to 2011 for all stations. The distribution of the stations used is shown in Figure 5-9. These stations were selected due to the availability of daily data for the period.

The Percent of Normal (PN), cumulative rainfall at daily and monthly time scale and Standardized Precipitation Index (SPI) were used in this section to describe the drought conditions. PN is expressed as the actual rainfall compared to the normal rainfall in percentage. Usually, the long term mean rainfall value is considered as the normal. PN can be calculated in a variety of time scales ranging from a single month to a group of months representing a particular season, calendar year or water year. PN in this study was calculated using seasonal time steps. Usually, lower PN (PN<100%) values indicate dry circumstances.

First, monthly rainfall cumulative for the two years, 2010 and 2011, were compared with the monthly Long Term Means (LTMs). Figure 5-10 show that Lodwar received rainfall below its LTM for most of 2010 and up to September in 2011. Figure 5-11 show that Voi received rainfall almost equal to and below the LTM for most of 2010 and 2011, except after October 2011. Figure 5-12 show that Narok received rainfall below the LTM for most of 2010 while in 2011, the station received rainfall below the LTM until October when it started receiving above the LTM. Figure 5-13, shows that Kisumu received rainfall above the LTM in 2010 and in 2011 the station received rainfall below the LTM until August. Figure 5-14 show that Dagoretti received rainfall above the LTM in 2010, while in 2011 the station received rainfall below the LTM all year. Figure 5-15, shows that Malindi received rainfall below the LTM from September 2010 and this continued throughout 2011. Figure 5-16, shows that Mandera received rainfall above the LTM in 2010 and in 2011 the station received rainfall below the LTM until October when it started receiving rainfall above the LTM.

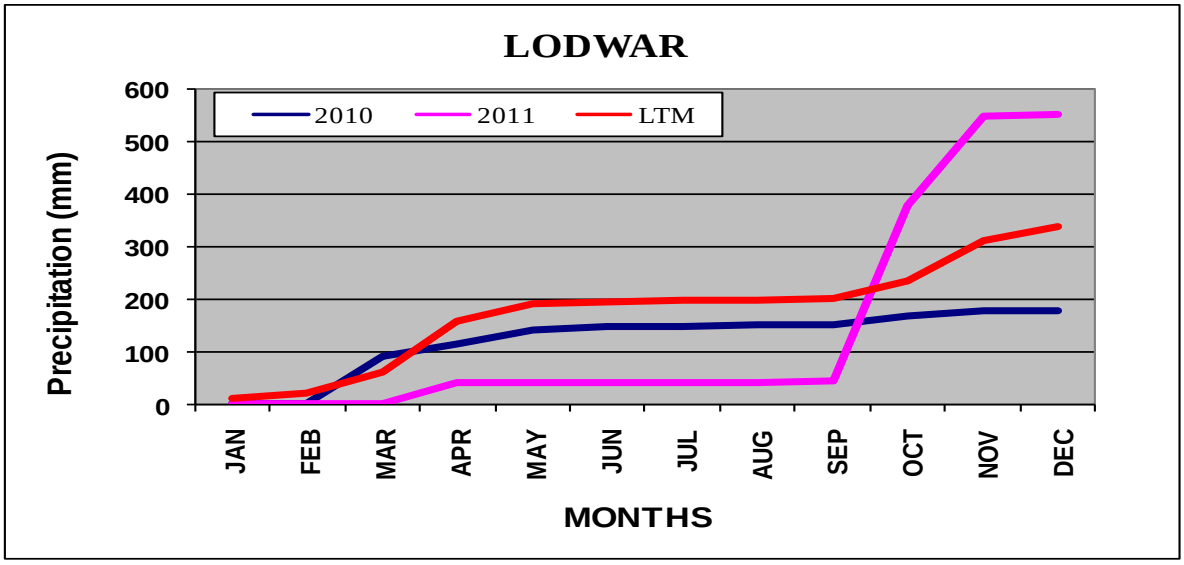

Figure 5-10 ***Time series of monthly cumulative rainfall for Lodwar***

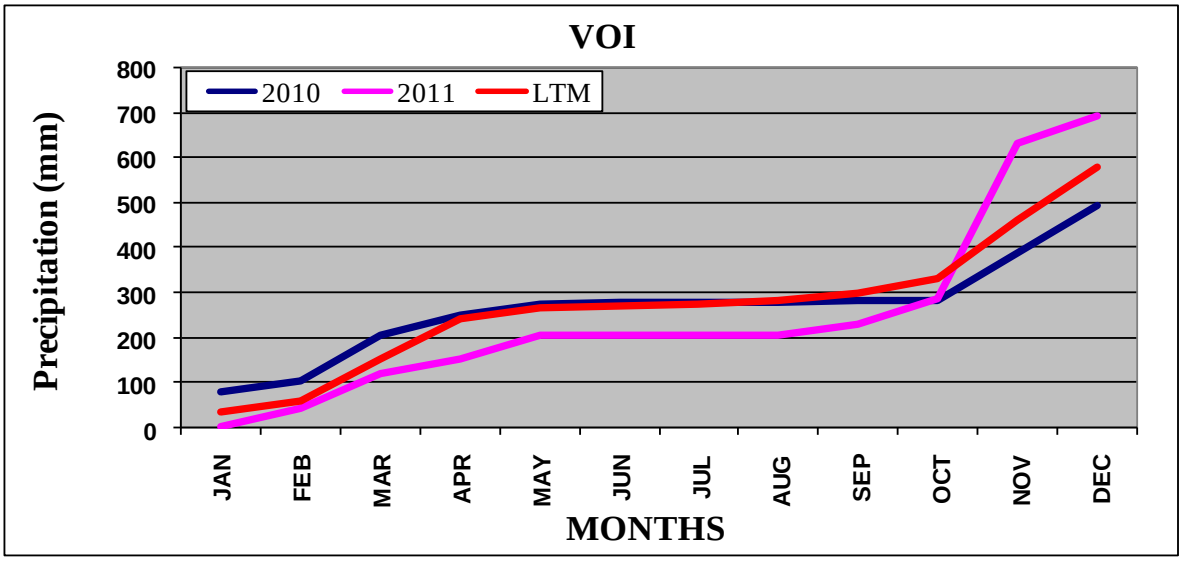

Figure 5-11 ***Time series of monthly cumulative rainfall for Voi.***

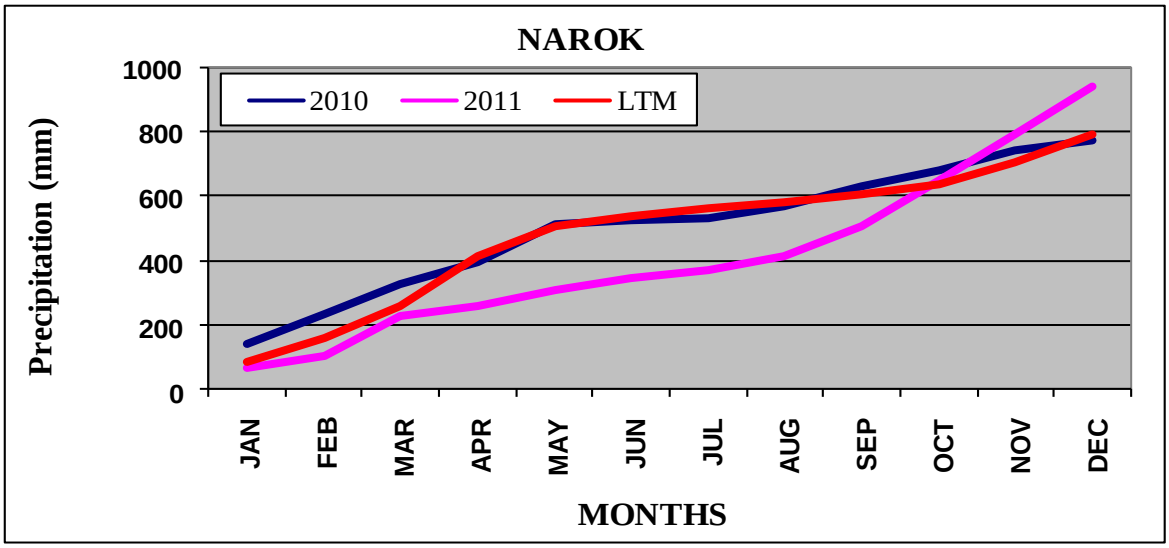

Figure 5-12 ***Time series of monthly cumulative rainfall for Narok.***

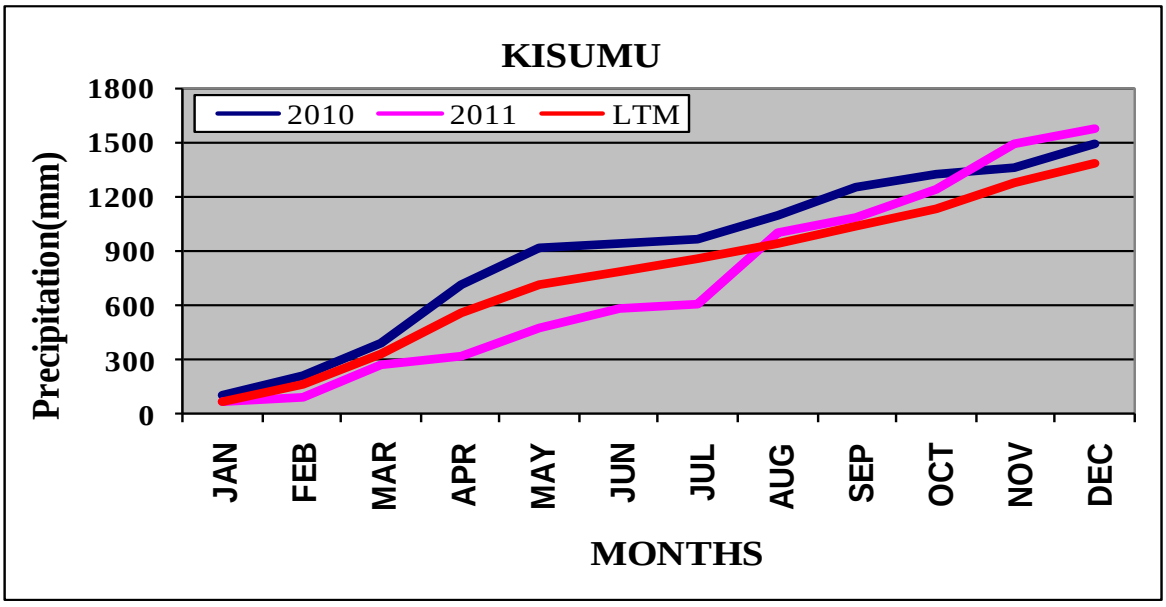

Figure 5-13 Time series of monthly cumulative rainfall for Kisumu

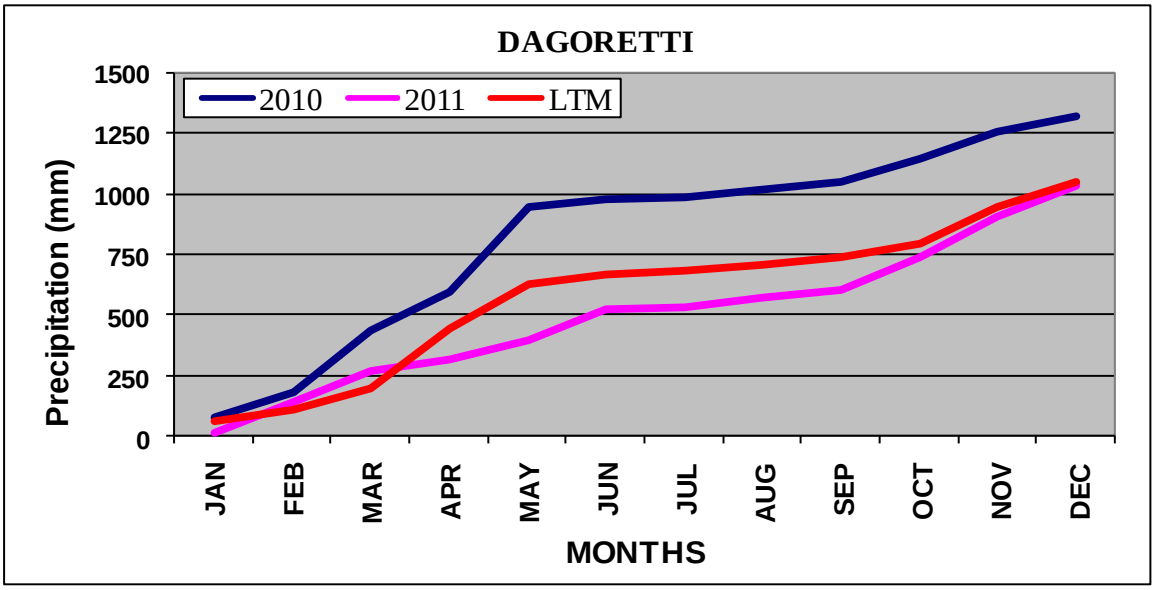

Figure 5-14 *Time series of monthly cumulative rainfall for Dagoretti.*

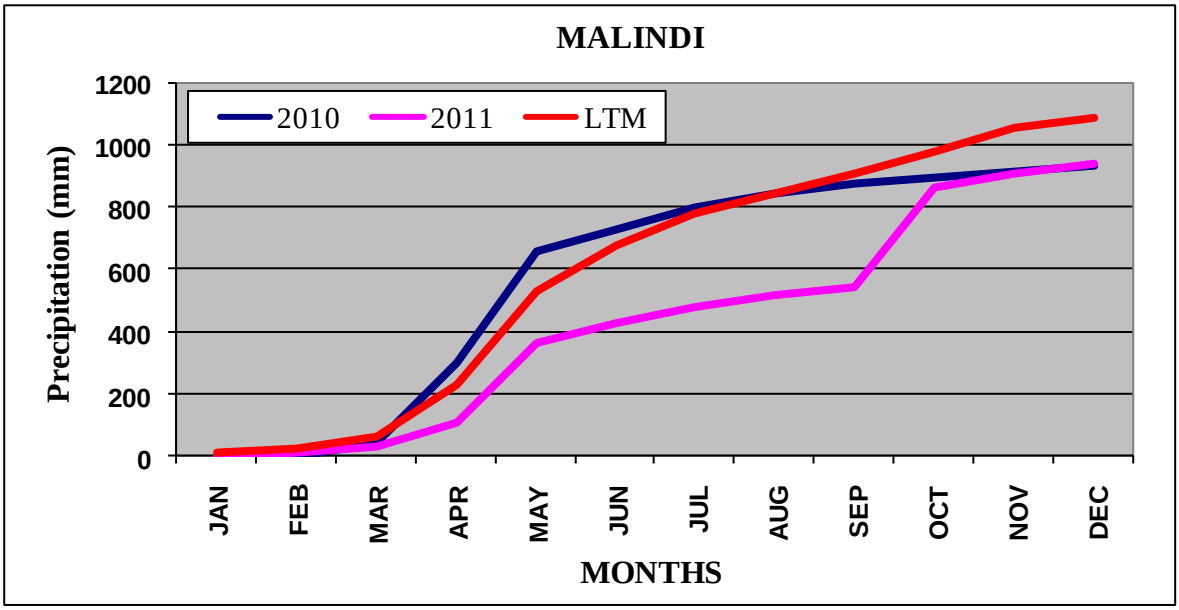

Figure 5-15 ***Time series of monthly cumulative rainfall for Malindi.***

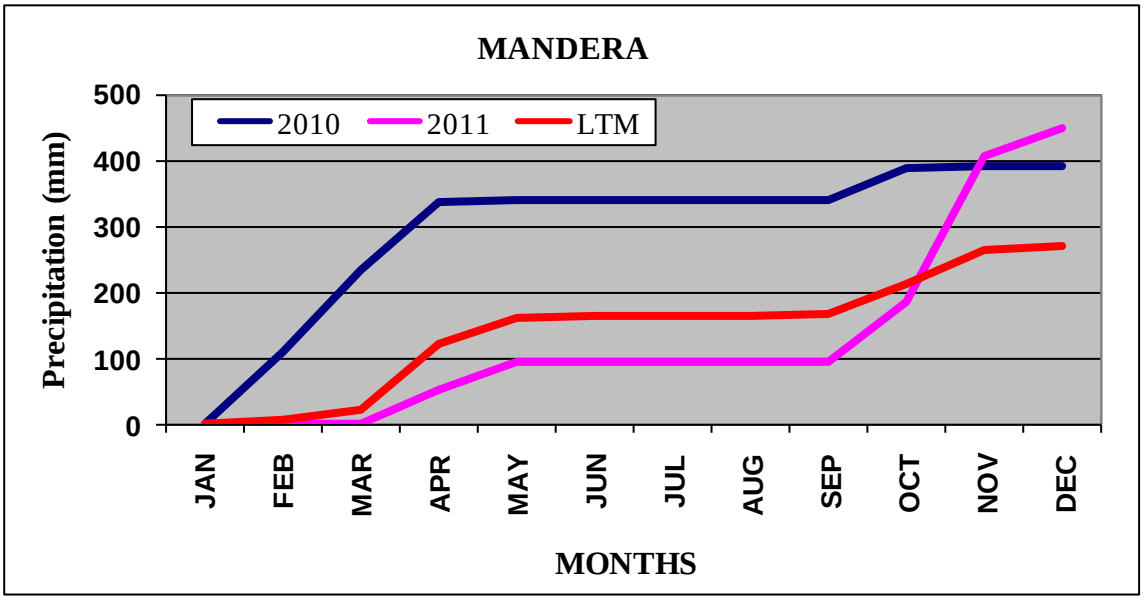

Figure 5-16 ***Time series of monthly cumulative rainfall for Mandera.***

In order to assess regions affected by drought conditions, spatial composites of Percent normal was calculated for the two rain seasons; i.e. October-November-December (OND) and March-April-May (MAM) for the years 2010 and 2011. Figure 5-17 shows that some stations in the Northwestern and southern parts of the country started experiencing dry conditions (PN< 100%) as early as MAM 2010. In OND

2010 all stations in the country had PN < 100%. This OND season marked the beginning of the 2010/2011 drought for most parts of the country except in North and Southwest Kenya (Marsabit, Lodwar, Voi and Narok) where it started earlier in MAM.

For MAM 2011 (Figure 5-18) all the stations in the country experienced dry conditions, with most stations having PN<60%. This confirms that the drought which started in OND 2010 continued and affected the following wet season (MAM 2011). In OND 2011 all stations shows wet conditions (PN>100%), this was an indication that it was a normal or above normal wet season, marking the end of the 2010/2011 drought.

Daily rainfall cumulatives for the two rain seasons in 2010 and 2011 were compared with the daily Long Term Means (LTMs) for these seasons. The results paint the same picture as the seasonal Percent Normal, where some stations started experiencing dry conditions as early as March 2010. The results however, offer more details, when during the season the stations started experiencing drought conditions.

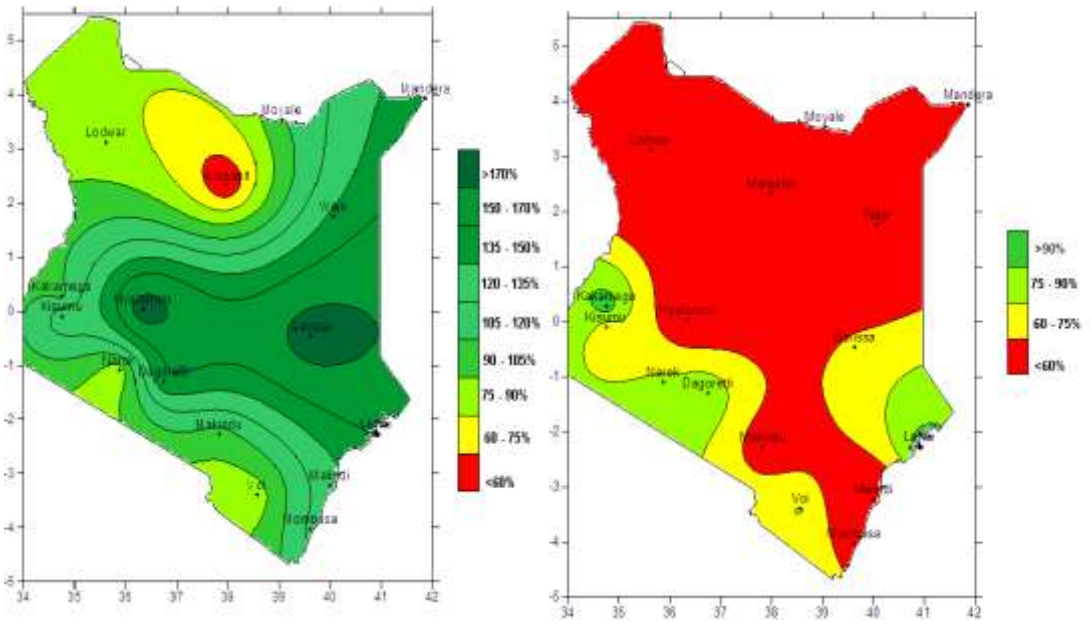

Figure 5-17 Spatial *distribution of Percent Normal for MAM 2010 (left panel) and OND 2010 (right panel) over the Kenya.*

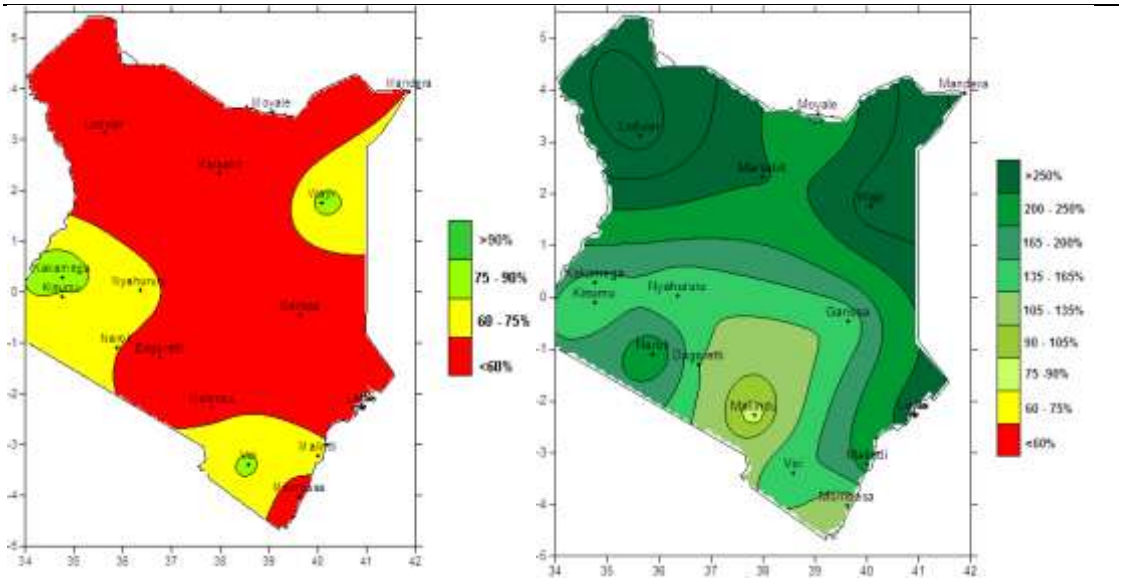

Figure 5-18 ***Spatial distribution of Percent Normal for MAM 2011 (left panel) and OND 2011 (right panel) over the Kenya.***

Figure 5-19 show that Lodwar started receiving less than 100% of its LTM at the end on March 2010 and this progressed till the end of October 2011. Figure 5-20, shows that Voi started receiving less than 100% of its LTM in mid April 2010 and this progressed till mid October 2011. Figure 5-21, shows that Narok started receiving less than 100% of its LTM in early April 2010 and this progressed till the end of October 2011.

Figure 5-22, shows that Kisumu started receiving less than 100% of its LTM in October 2010 and this progressed till the end of May 2011. Figure 5-23, shows that Dagoretti started receiving less than 100% of its LTM in mid-December 2010 and this progressed till the end of May 2011. Figure 5-24, shows that Malindi started receiving less than 100% of its LTM in October 2010 and this progressed till the end of May 2011. Figure 5-25 below, shows that Mandera started receiving less than 100% of its LTM at the end of October 2010 and this progressed till the end of May 2011.

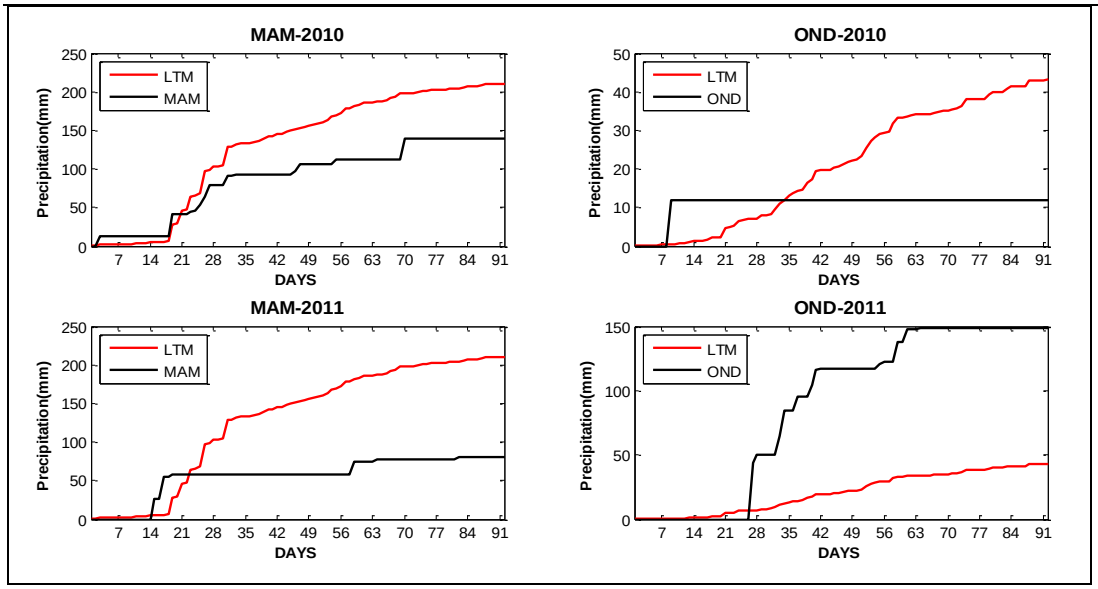

Figure 5-19 ***Lodwar time series of daily cumulative rainfall MAM 2010 (left upper panel), OND 2010 (right upper panel), MAM 2011 (left lower panel) and OND 2011 (right lower panel).***

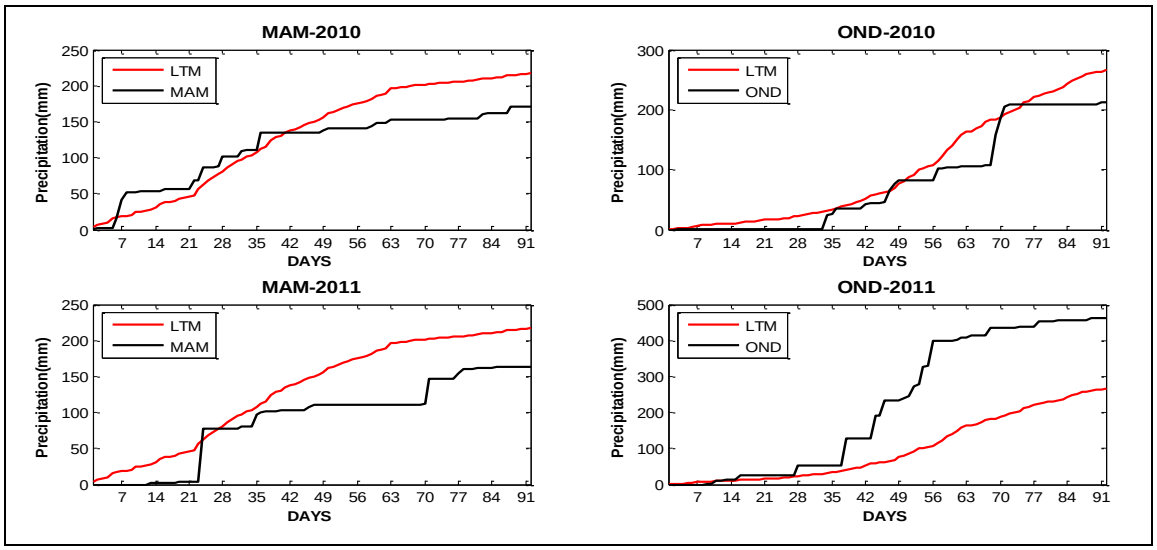

Figure 5-20 ***Voi time series of daily cumulatives MAM 2010 (left upper panel), OND 2010 (right upper panel), MAM 2011 (left lower panel) and OND 2011 (right lower panel).***

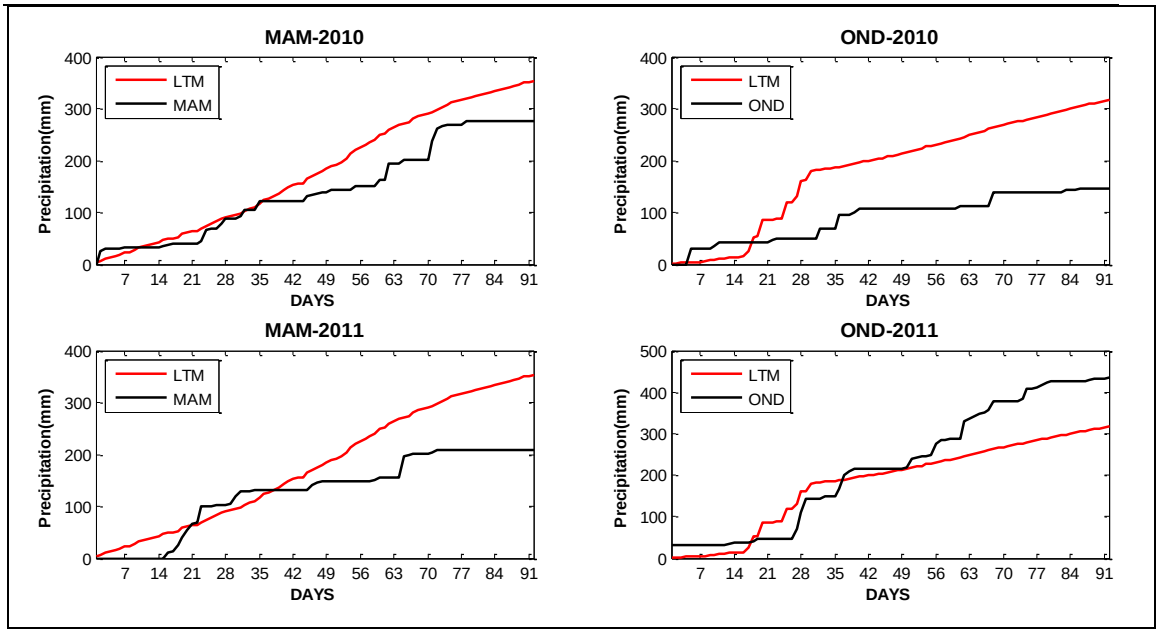

Figure 5-21 ***Naroktime series of daily cumulatives MAM 2010 (left upper panel), OND 2010 (right upper panel), MAM 2011 (left lower panel) and OND 2011 (right lower panel).***

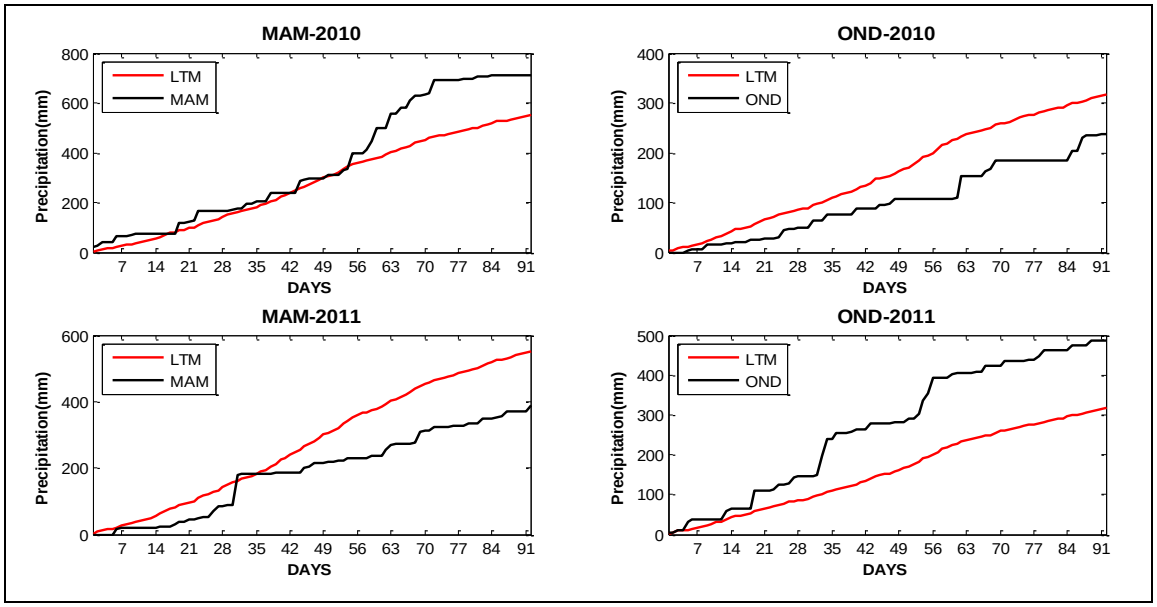

Figure 5-22 Kisumu ***time series of daily cumulatives MAM 2010 (left upper panel), OND 2010 (right upper panel), MAM 2011 (left lower panel) and OND 2011 (right lower panel).***

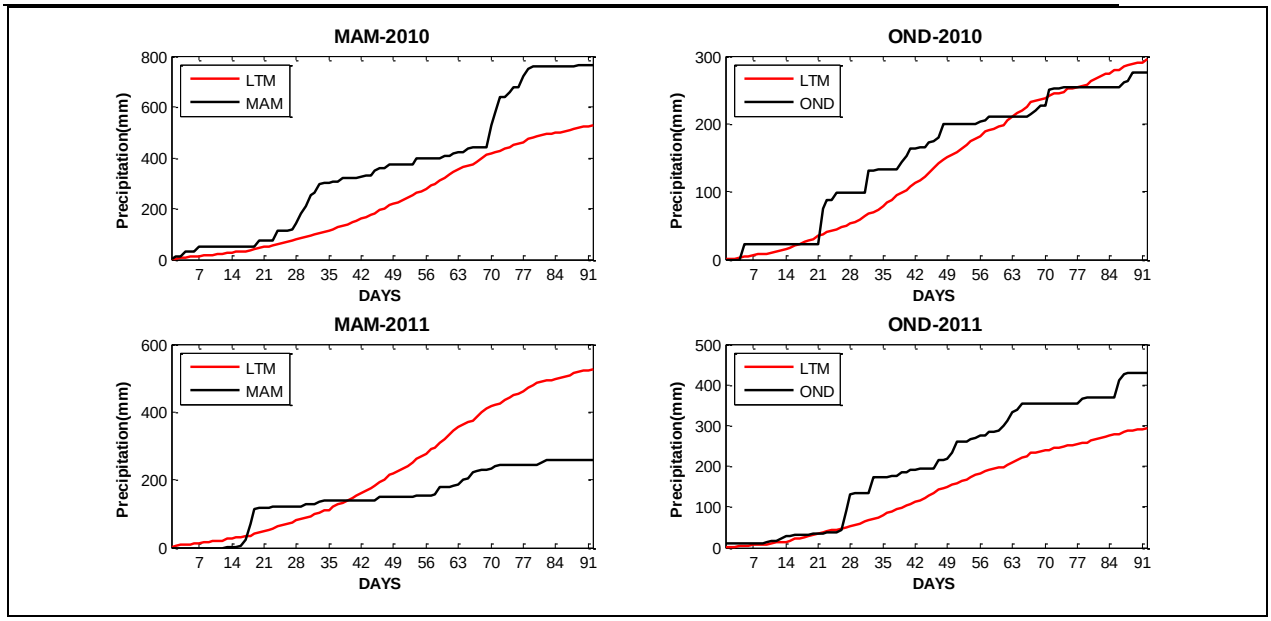

Figure 5-23 ***Dagorettitime series of daily cumulatives MAM 2010 (left upper panel), OND 2010 (right upper panel), MAM 2011 (left lower panel) and OND 2011 (right lower panel).***

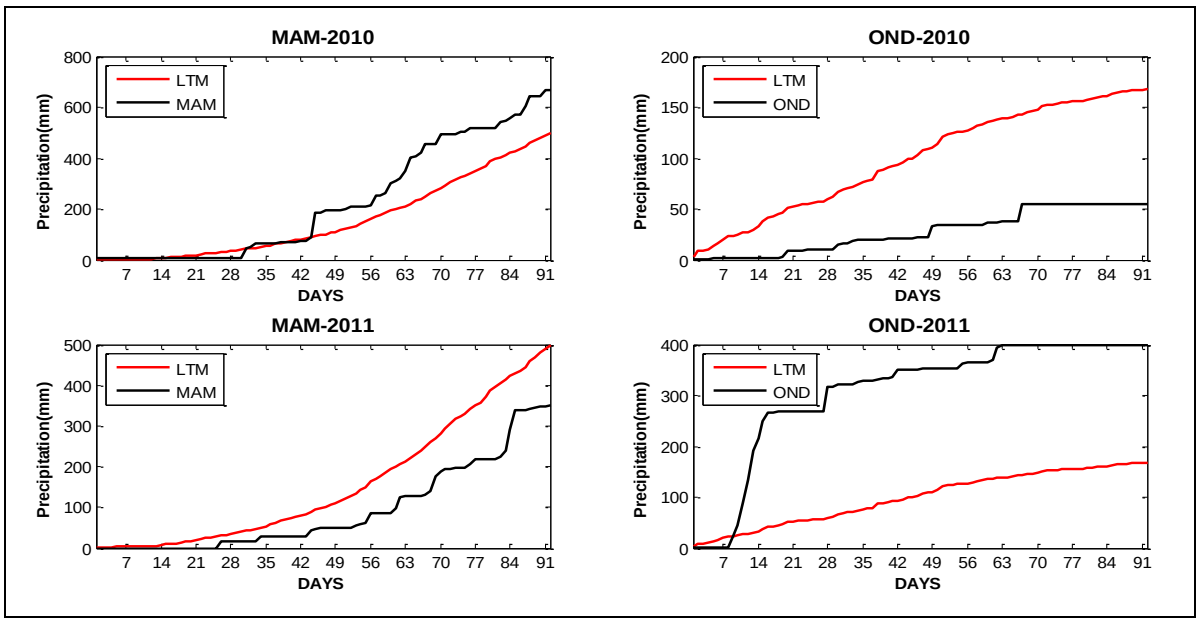

Figure 5-24 ***Malinditime series of daily cumulatives MAM 2010 (left upper panel), OND 2010 (right upper panel), MAM 2011 (left lower panel) and OND 2011 (right lower panel).***

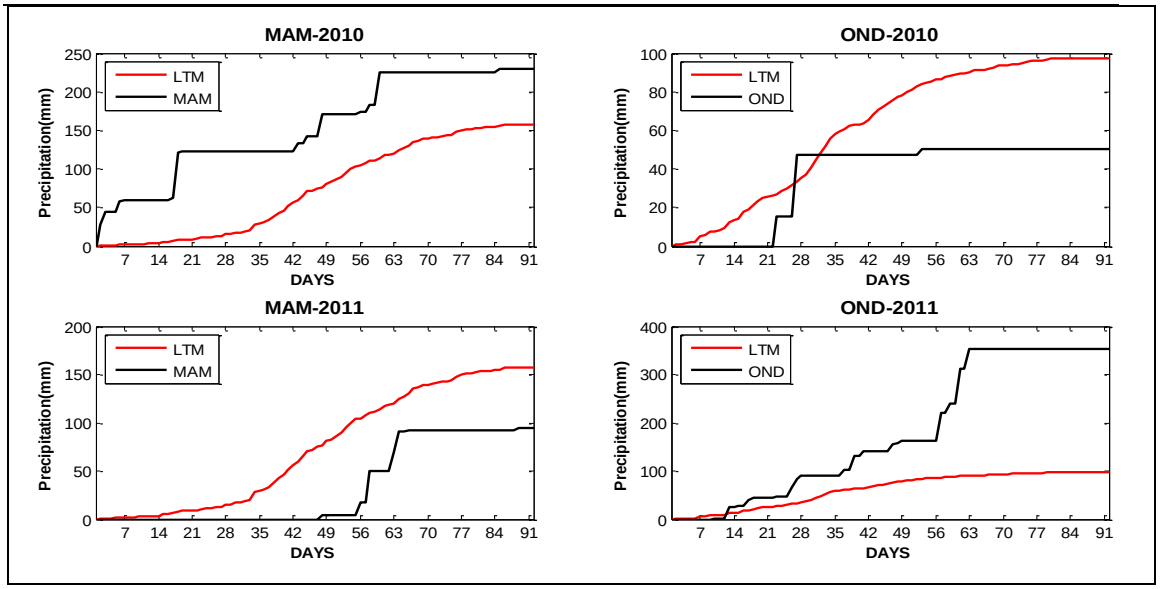

Figure 5-25 ***Manderatime series of daily cumulatives MAM 2010 (left upper panel), OND 2010 (right upper panel), MAM 2011 (left lower panel) and OND 2011 (right lower panel).***

Observed station monthly rainfall data for the stations used above, were also used to calculate three-month time scale Standardized Precipitation Index (SPI) for the OND 2010 and MAM 2011 seasons.

Figure 5-26 show that by October 2010 only the Eastern parts of the country were experiencing moderate drought conditions and a small section at the Southeastern part was experiencing severe drought. The rest of the country experienced moderately wet to near normal conditions. As the season progressed more parts of the country started experiencing moderate drought conditions and by December 2010 most of the country had SPI values below -0.5 with the Northeastern part of the country experiencing severe drought conditions with SPI values being as low as -1.6.

Figure 5-27 show that the SPI values continued dropping. By March 2011 the Eastern part of the country had values below -2, which is an indication of extreme drought conditions. The western part of the country had values which indicated near normal to moderate drought conditions. However, during May most of the country had values that indicated moderate to severe drought conditions.

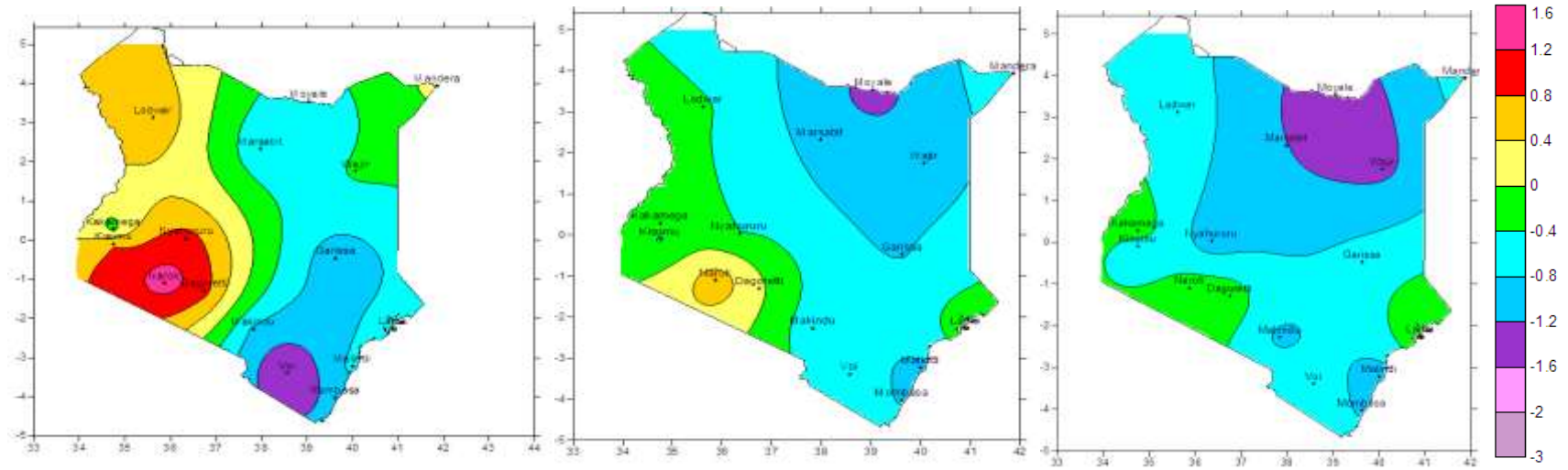

Figure 5-26 *Spatial distribution of Standardized precipitation index for October 2010 (left panel), November 2010 (middle panel) and December 2010 (right panel) over Kenya.*

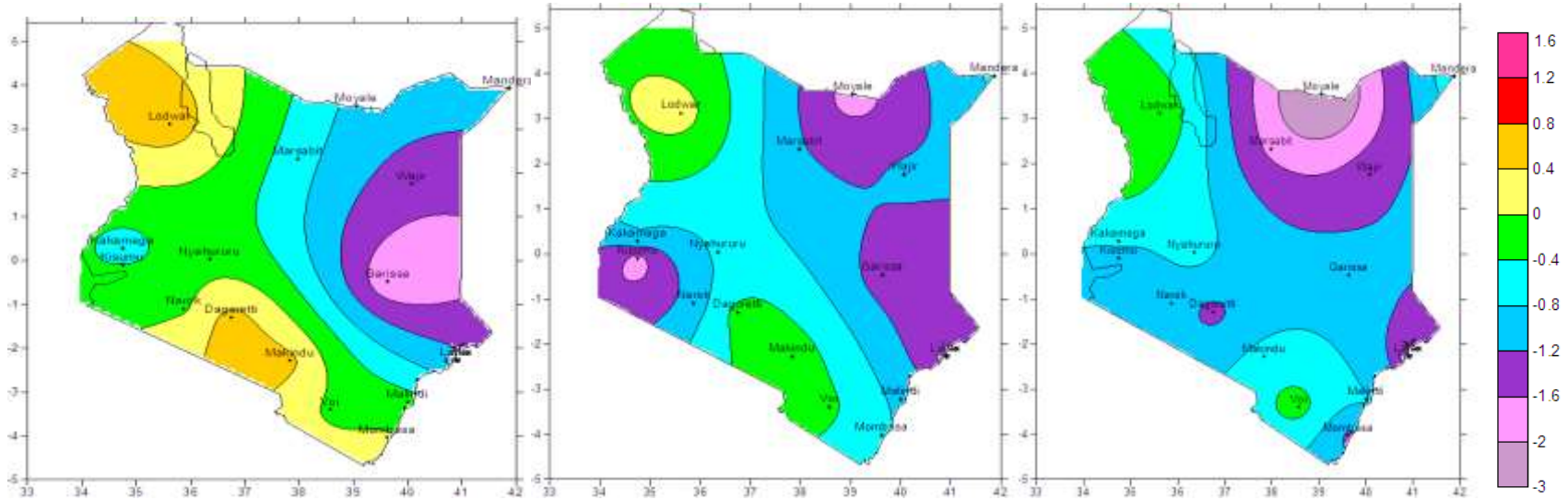

Figure 5-27 ***Spatial distribution of Standardized precipitation index for March 2011 (left panel), April 2011 (middle panel) and May 2011 (right panel) over Kenya.***

Monthly rainfall data at each station was used to calculate 3 month time scale Standardized Precipitation Index for 2010 and 2011. This time series gives a clearer picture of the value of SPI month to month in the two years.

From Figure 5-28, the SPI values show that Lodwar experienced near normal conditions from October to December 2010. In January and February 2011 it experienced moderate drought conditions, and from March 2011 the conditions reverted to near normal. From Figure 5-29, the SPI values show that Voi experienced moderate drought from August 2010 to November 2010 and near normal conditions from December 2010 to June 2011. From Figure 5-30 the SPI values show that Narok experienced near normal conditions from October 2010 to May 2011 but in June 2011 it experienced moderate drought conditions. From Figure 5-31, the SPI values show that Kisumu experienced near normal conditions from October 2010 to March 2011, in April 2011 moderate conditions. From Figure 5-32, the SPI values show that Dagoretti experienced near normal conditions from October 2010 to April 2011 and in May experienced moderate drought conditions. From Figure 5-33, the SPI values show that Malindi experienced near normal conditions from October 2010 to May 2011 except in February 2011 when moderate drought conditions were experienced. From Figure 5-34, the SPI values show that Mandera experienced near normal conditions in October and November 2010, in December 2010 moderate drought conditions started being experienced and these went on till February 2011 and from March 2011 near normal conditions started being experienced.

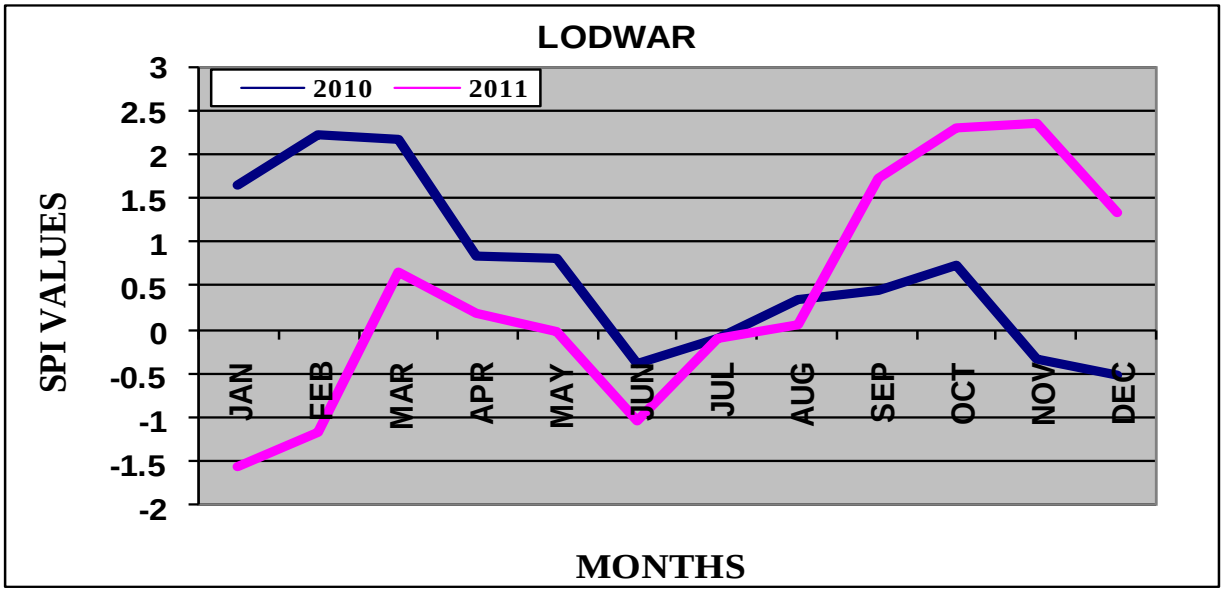

Figure 5-28 Time series of Standardized Precipitation Index for 2010 and 2011 over Lodwar.

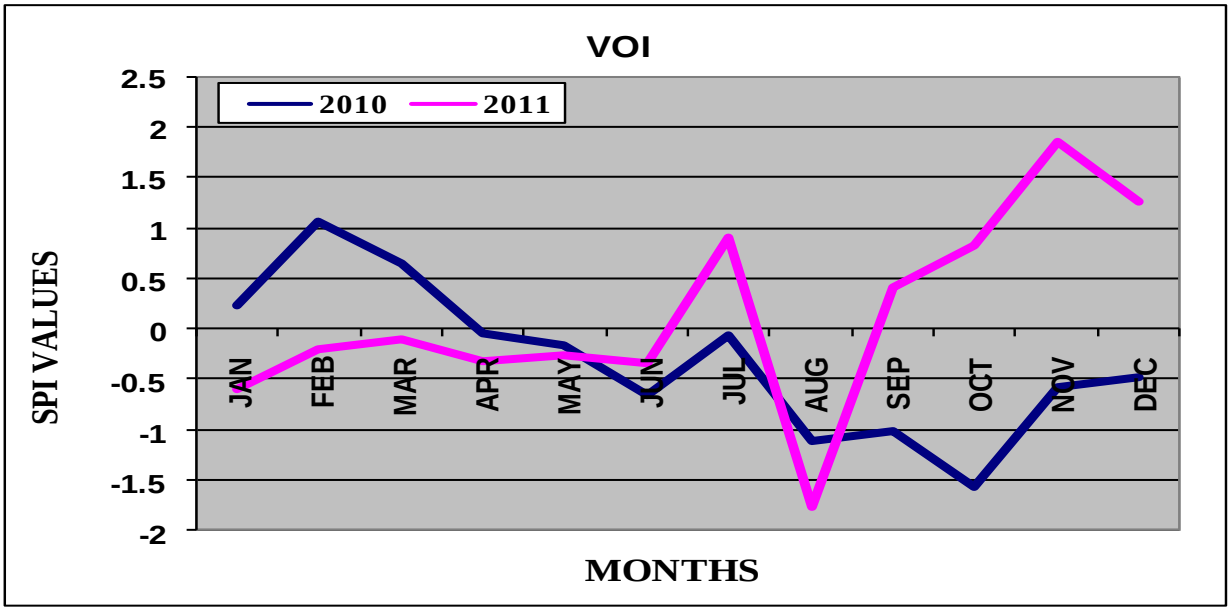

Figure 5-29 ***Time series of Standardized Precipitation Index for 2010 and 2011 over Voi.***

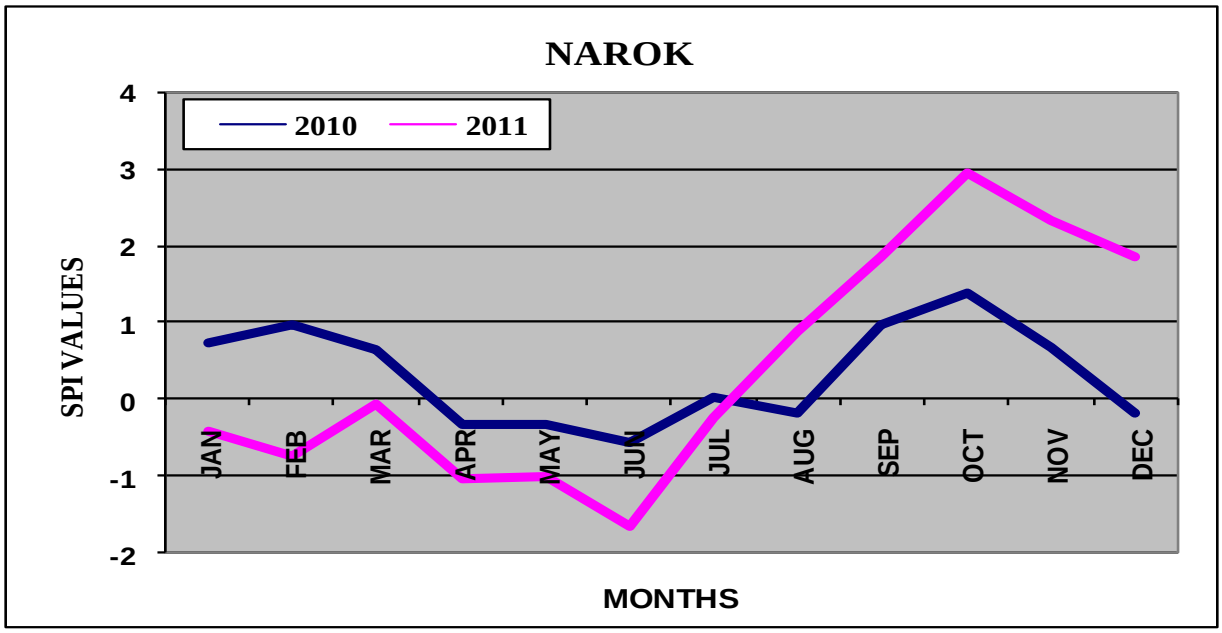

Figure 5-30 ***Time series of Standardized Precipitation Index for 2010 and 2011 over Narok.***

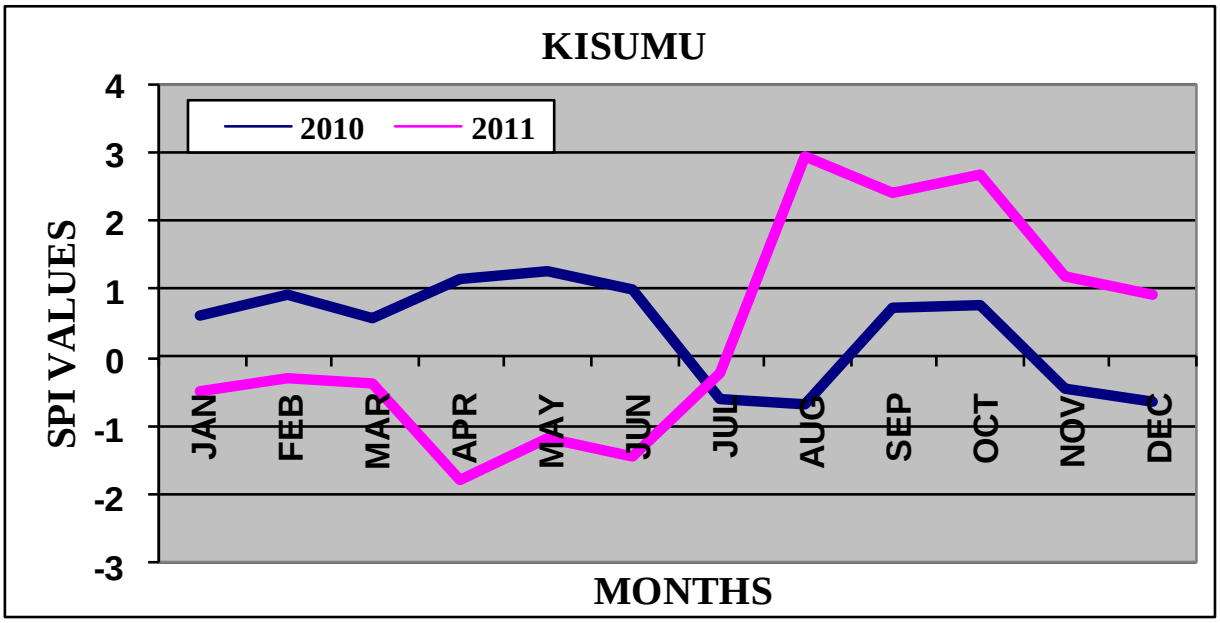

Figure 5-31 ***Time series of Standardized Precipitation Index for 2010 and 2011 over Kisumu.***

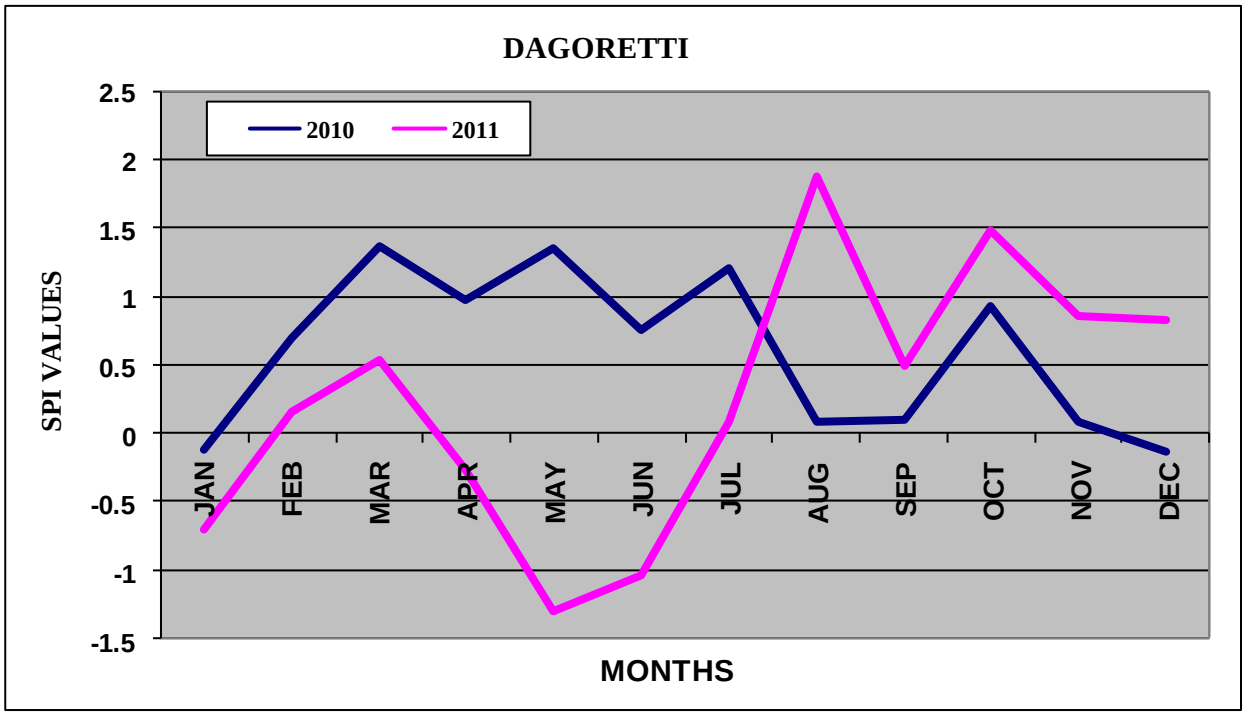

Figure 5-32 Time series of Standardized Precipitation Index for 2010 and 2011 over Dagoretti.

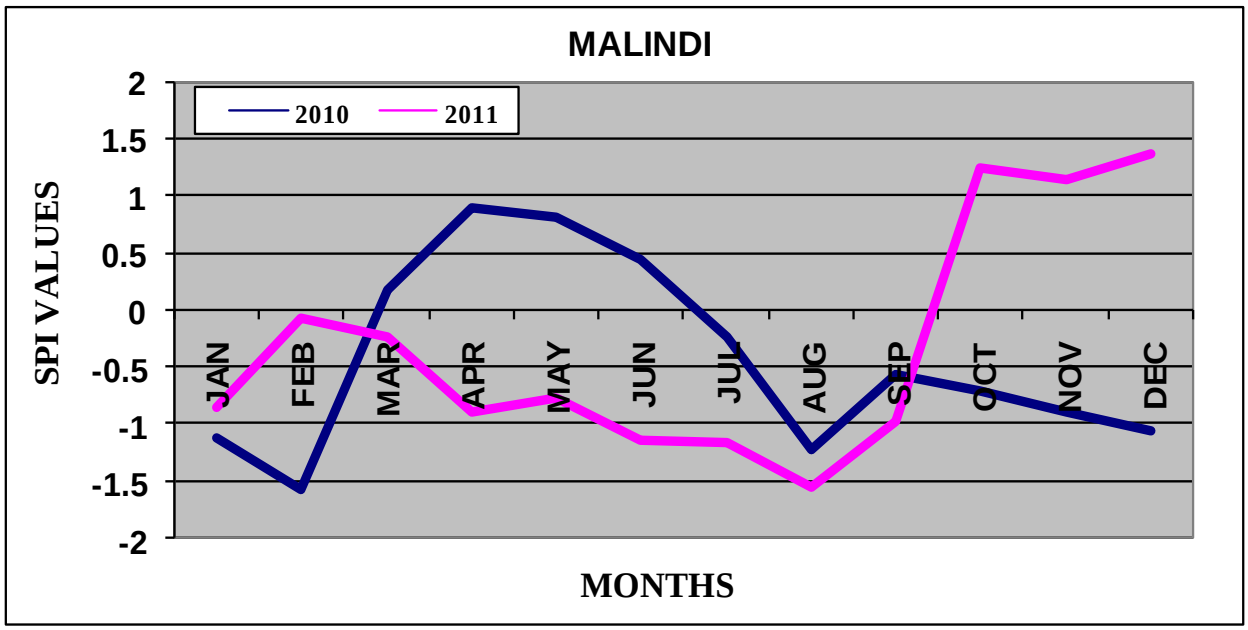

Figure 5-33 Time series of Standardized Precipitation Index for 2010 and 2011 over Malindi.

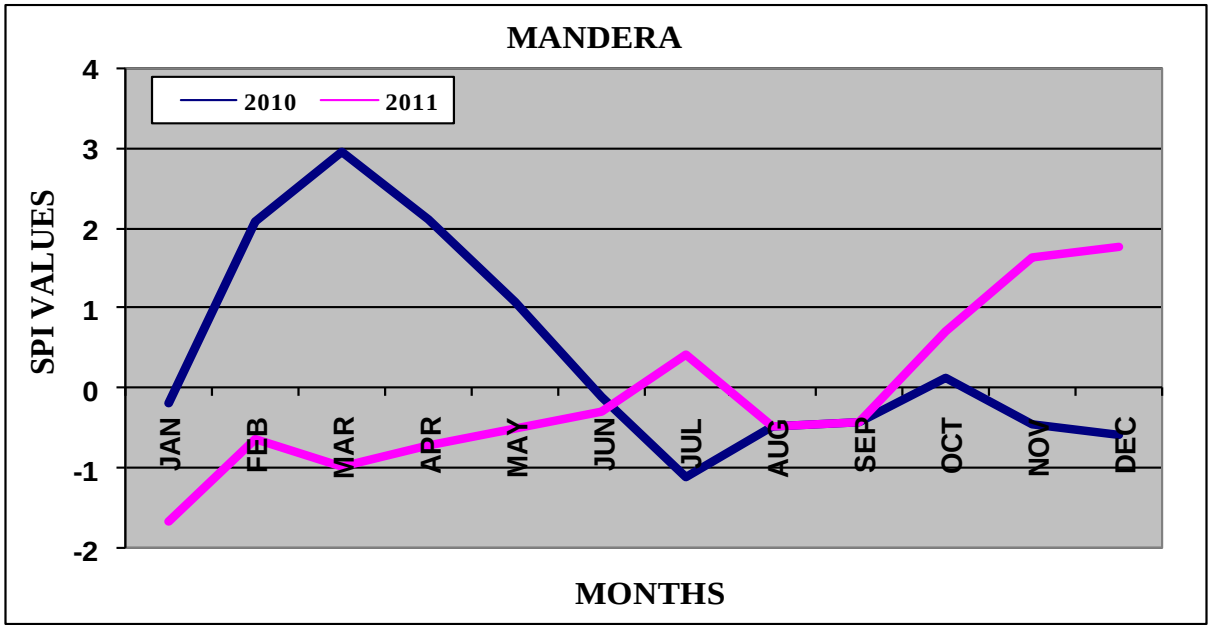

Figure 5-34 Time series of Standardized Precipitation Index for 2010 and 2011 over Mandera.

This section compares the drought indicators calculated from the observed station data set and the ERA-I dataset generated by ECMWF for DEWFORA Project from models data. The period October-December 2010 will be considered in the comparison.

Model and station observed datasets were used to calculate three month timescale SPIs. The results indicated that for the period October- December 2010 the model gave drought conditions for the whole country while the observed data showed near normal to moderately wet conditions for the western parts of the country.

From Figure 5-35, the SPI generated from observed data indicate that most of Kenya had near normal conditions and even moderately wet conditions for the western part of the country; it's only in the extreme southeastern where moderate conditions were observed. However, the SPI from the model data show that only the north coast and a small section of the eastern part experienced near normal conditions, while the rest of the country experienced moderate drought to severe drought in the northwestern part.

Figure 5-36 shows the SPI generated from observed data in November 2010. For this month most of the country experienced near normal conditions, while the SPI generated from model data show that most of the country experienced moderate to extreme drought conditions.

From Figure 5-37, the SPI generated from observed data indicate most of the country had near normal conditions in December. In the other hand, the SPI generated from model data show that most of the country experienced moderate to extreme drought conditions.

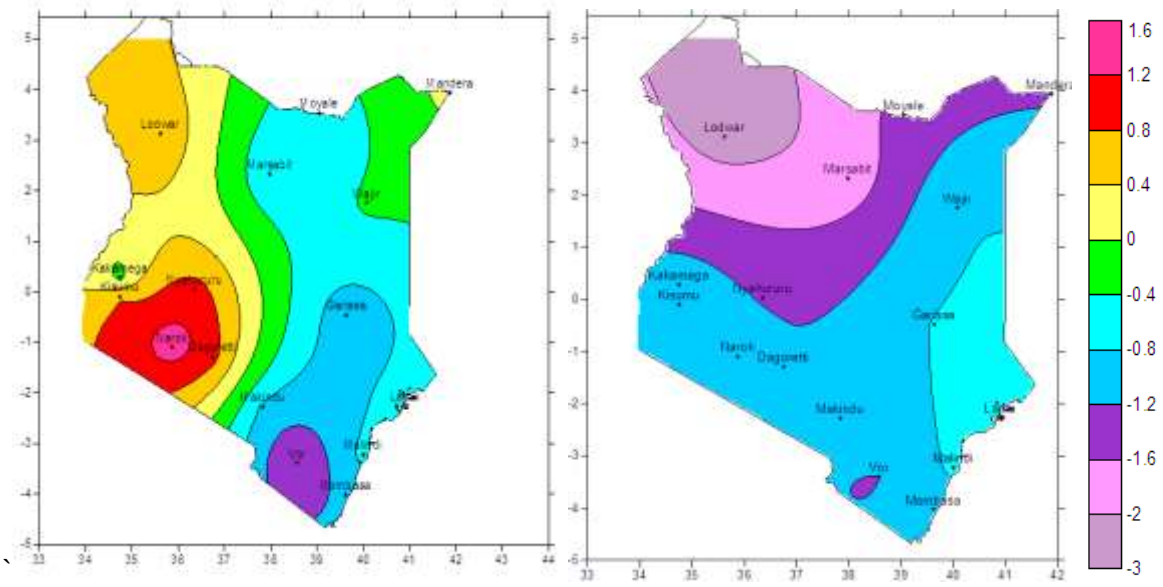

Figure 5-35 ***Spatial distribution of Standardized precipitation index for October 2010 over Kenya, calculated from observed data (left panel) and calculated from model data (right panel).***

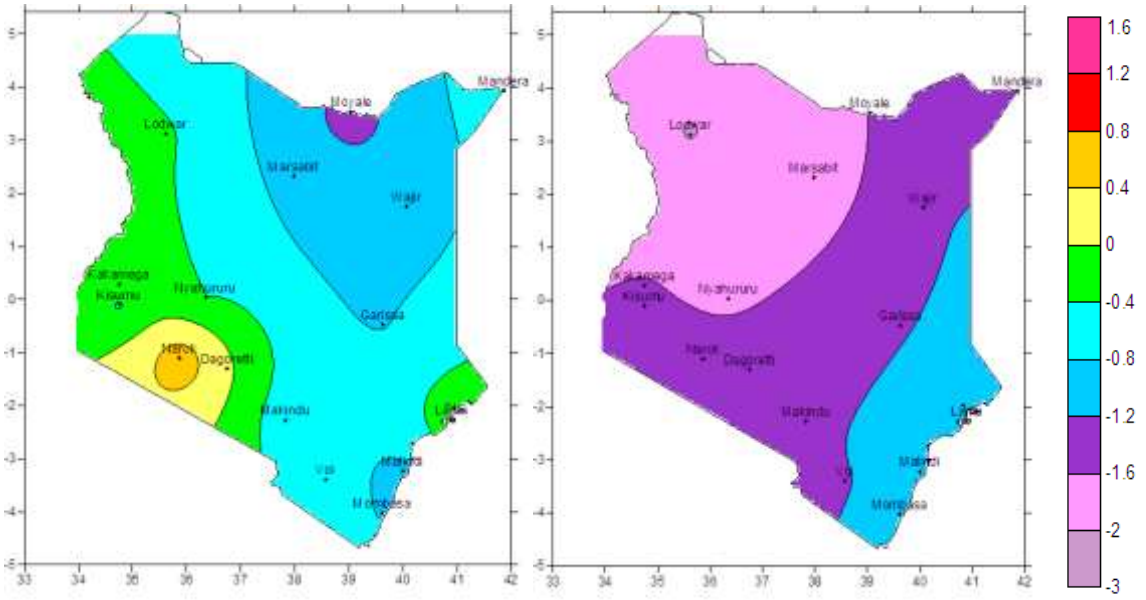

Figure 5-36 Spatial *distribution of Standardized precipitation index for November 2010 over Kenya, calculated from observed data (left panel) and calculated from model data (right panel).*

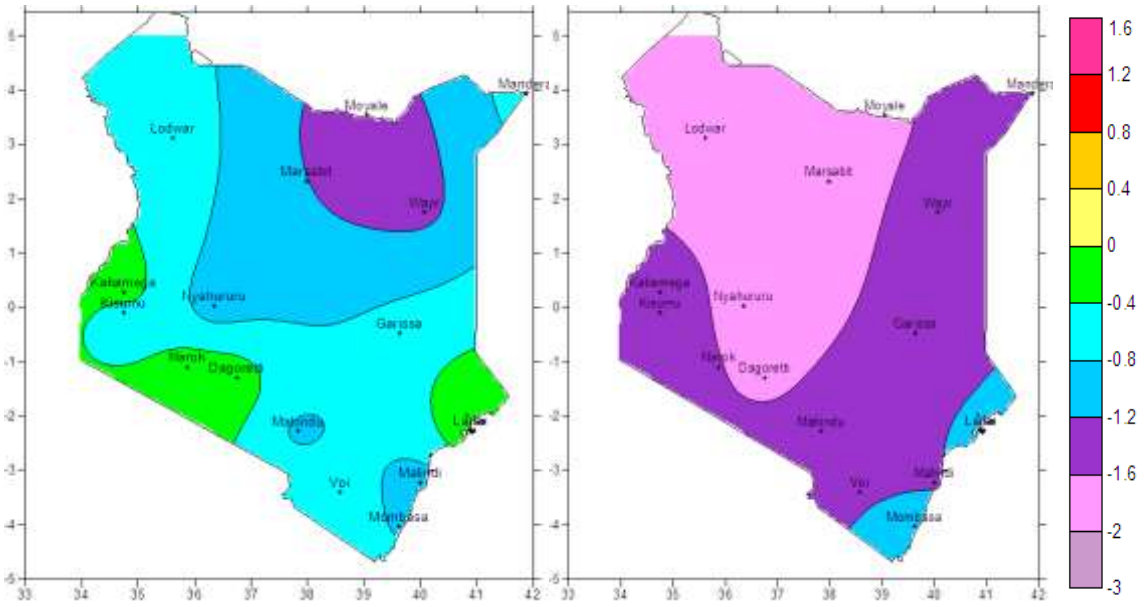

Figure 5-37 *Spatial distribution of Standardized precipitation index for December 2010 over Kenya, calculated from observed data (left panel) and calculated from model data (right panel).*

The analysis of the time series of SPI's in the year 2010 shows some differences between the values generated from the model data and those developed from observed model data. For most stations the model SPIs indicate moderate to extreme drought from June 2010, while this is captured from October in most stations for the observed data SPIs.

From Figure 5-38, the model data SPI indicate extreme to severe drought was experienced in Lodwar from June to December 2010, but the SPI computed with observed data show

near normal conditions were experienced throughout this period. From Figure 5-39, the model data SPI indicate extreme to severe drought was experienced in Voi from July to December 2010, the observed data SPIs indicate the same conditions were experienced from August to November 2010.

From Figure 5-40, the observed data SPI don't indicate any drought conditions were experienced during 2010 in Narok. However, the model data SPIs indicated moderate drought conditions were experienced in July and October-December. The same behavior is observed in Figure 5-41 and Figure 5-42.

At Malindi (Figure 5-43) the model SPIs are almost similar to the observed SPIs both indicating moderate drought in November and December. Similarly in Mandera (Figure 5-44) shows a good agreement in the observed and model data SPIs.

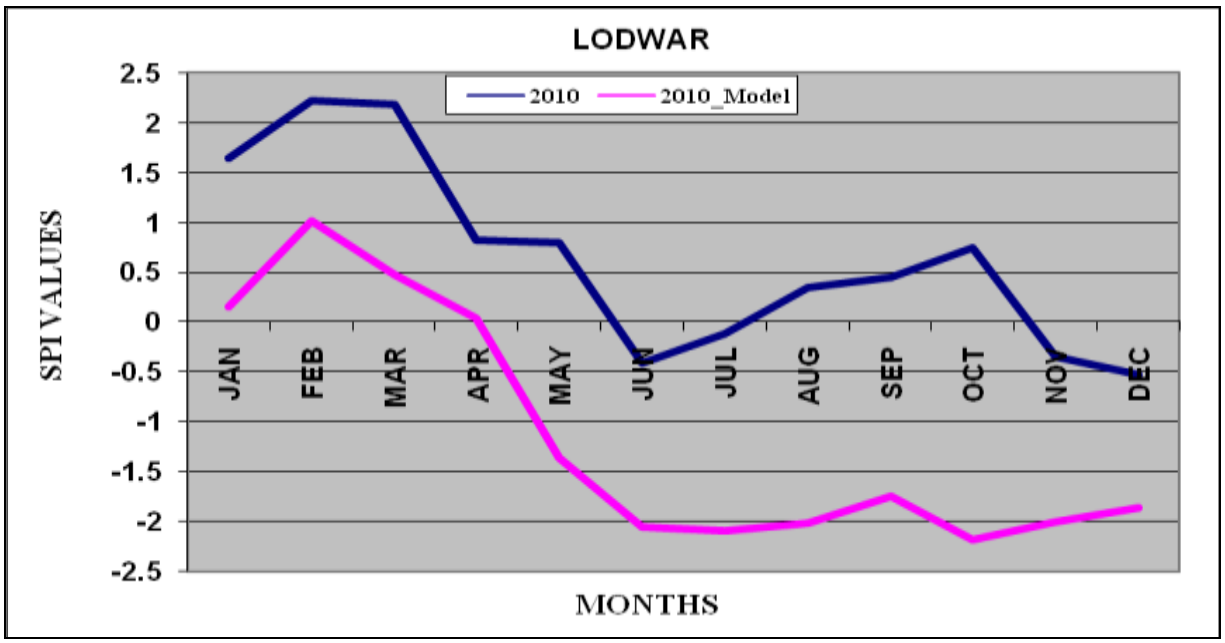

Figure 5-38 ***Time series of Standardized Precipitation Index, calculated from model (pink) and calculated form observed station data (dark blue) over Lodwar***

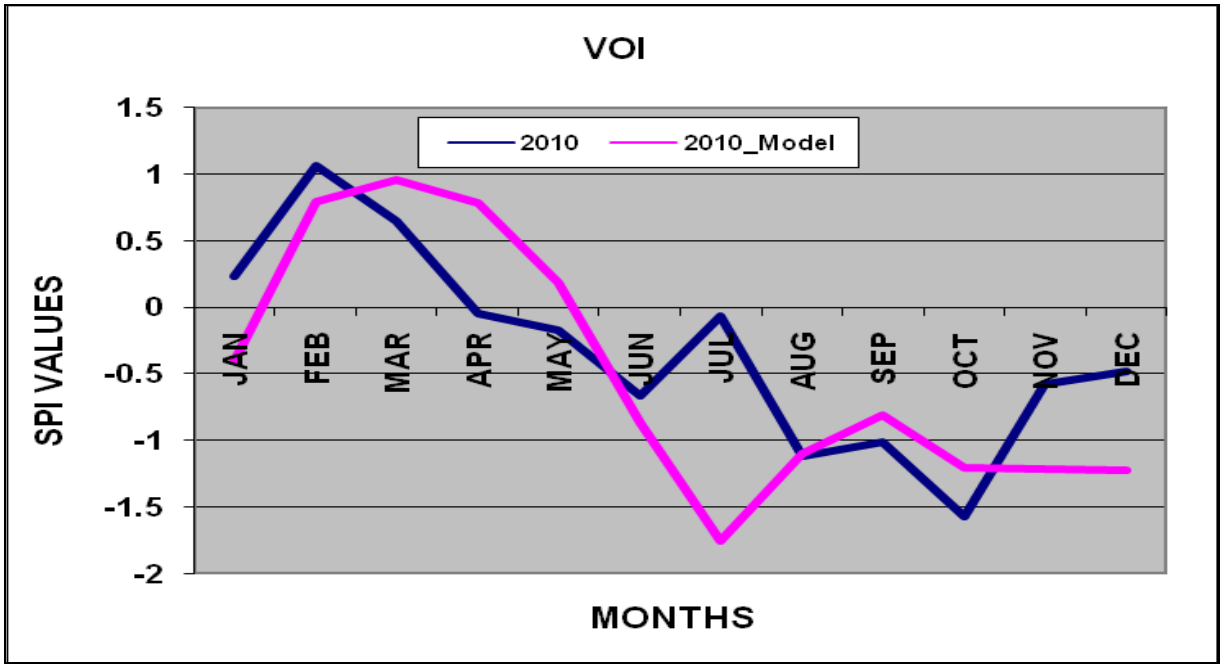

Figure 5-39 ***Time series of Standardized Precipitation Index, calculated from model (pink) and calculated form observed station data (dark blue) over Voi***

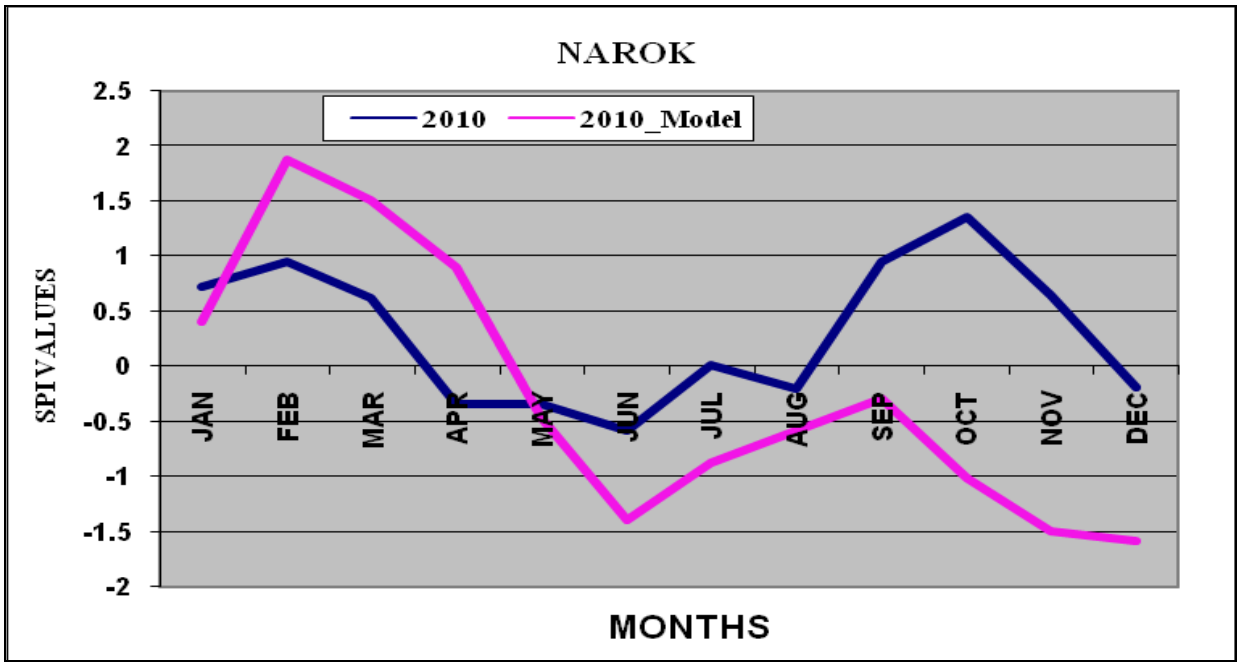

Figure 5-40 ***Time series of Standardized Precipitation Index, calculated from model (pink) and calculated form observed station data (dark blue) over Narok***

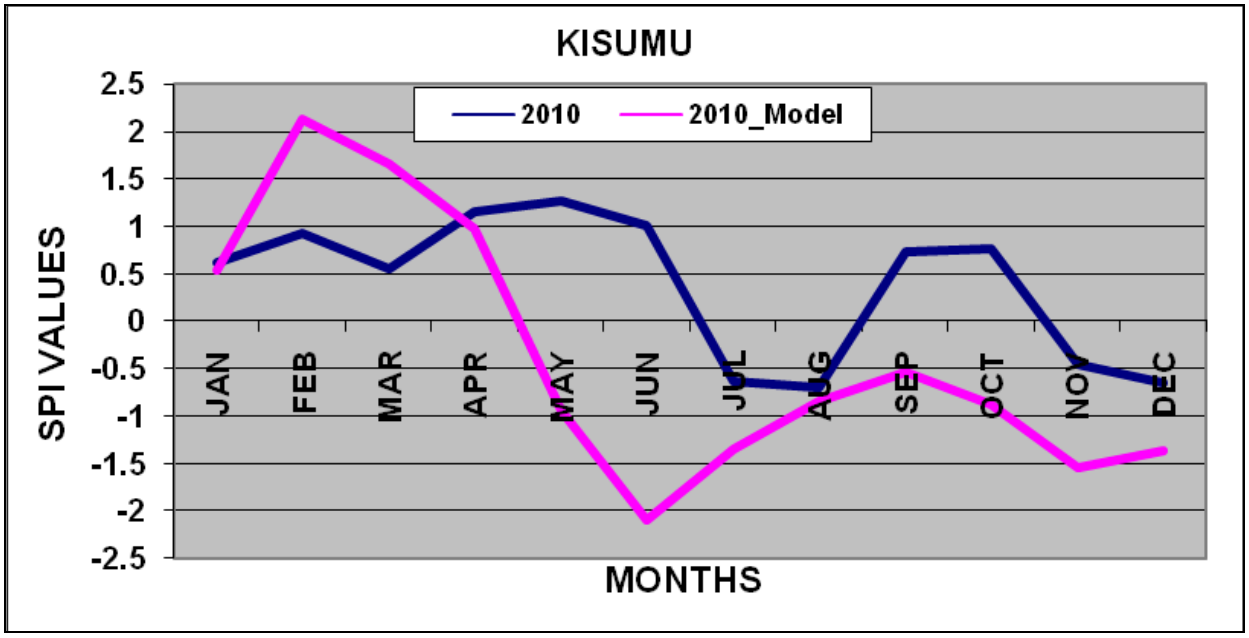

Figure 5-41 ***Time series of Standardized Precipitation Index, calculated from model (pink) and calculated form observed station data (dark blue) over Kisumu.***

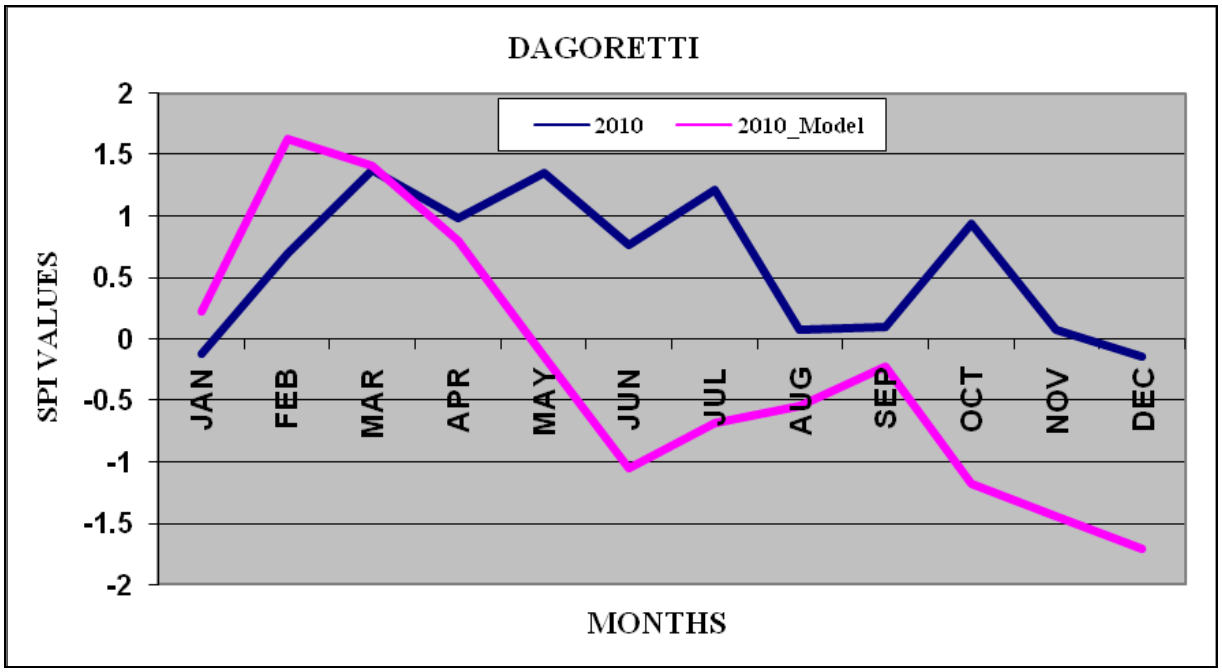

Figure 5-42 Time ***series of Standardized Precipitation Index, calculated from model (pink) and calculated form observed station data (dark blue) over Dagoretti.***

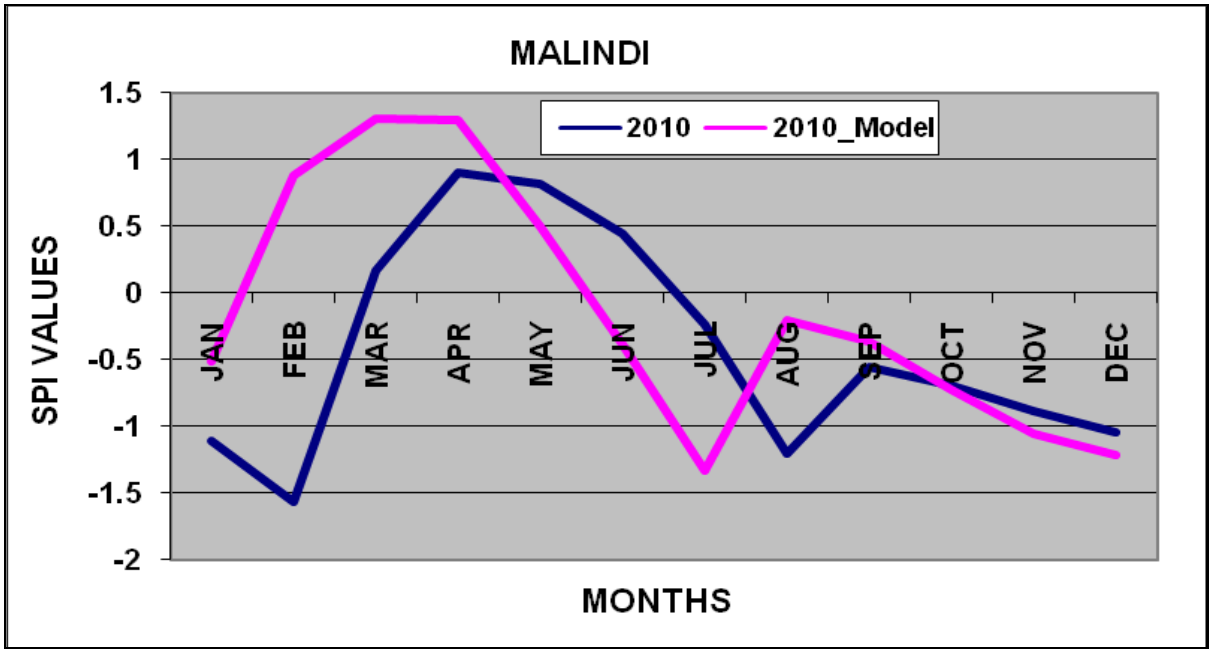

Figure 5-43 ***Time series of Standardized Precipitation Index, calculated from model (pink) and calculated form observed station data (dark blue) over Malindi.***

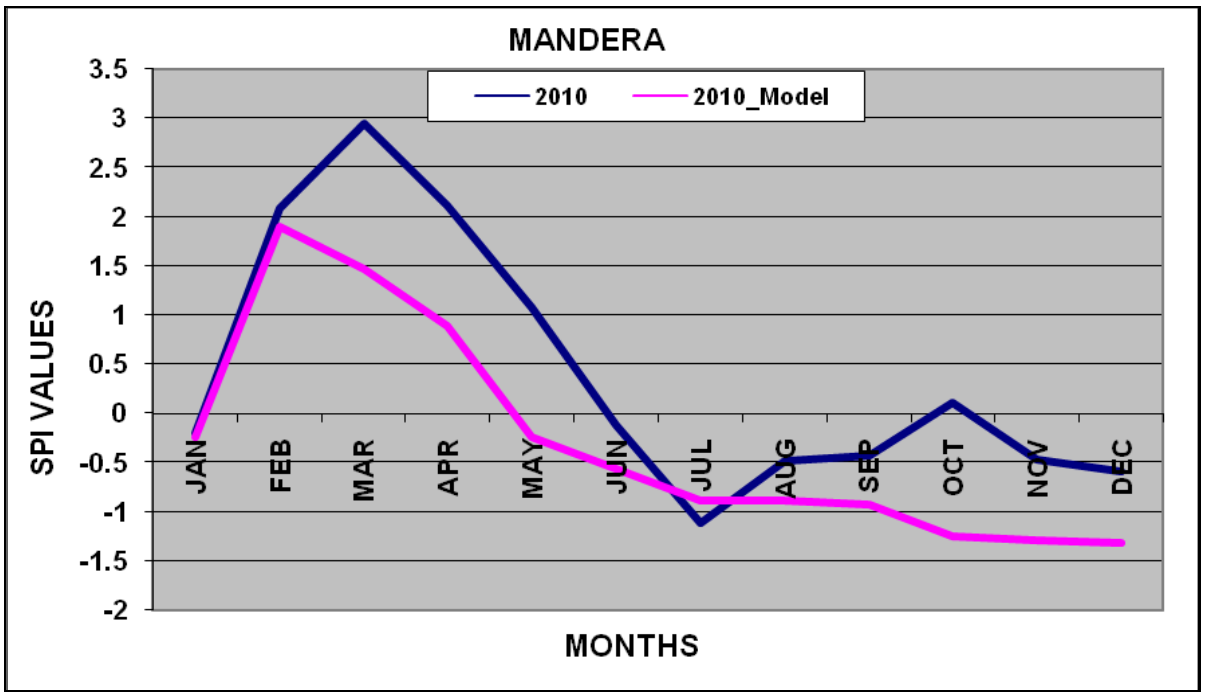

Figure 5-44 ***Time series of Standardized Precipitation Index, calculated from model (pink) and calculated form observed station data (dark blue) over Mandera.***

5.3.2 Drought management in Kenya during 2010/2011 drought

This section looks at the structures that the Kenyan government has place for drought management. It will also look in depth at the measures government agencies put in place prior to the 2010/2011 drought. The section will also examine the level of implementation of the measures and the challenges they faced during implementation.

Rapid developments have taken place within Kenya in the field of food security and drought management. Significant changes in the institutional and operational framework of food security structures within Kenya began in early 1999. These developments included a revised direction for the Kenya Food Security Meeting, the formation of Geographical Review Teams and the establishment of the Kenya Food Security Information Steering Group.

As the country moved into a period of drought stress and potential emergency, these developments were seen to have a positive impact. Equally important to the system was the establishment in June 1999 of the Inter Ministerial Committee on Drought and Food Security (IMCDFS).

The strengthening of the food security and drought management structure was instrumental in mounting a coordinated effort to assess drought stress conditions during the third quarter of 1999.

Running alongside the developments was a period of research by the USAID/FEWS project on Food Aid. The findings of this research in addition to the evolutionary process leading to greater collaboration and joint activity signaled a need to strengthen and indeed redefine the role of the Kenya Food Security Information Steering Group (KFSSG). In essence this was in recognition of the central role the steering group was playing to the Kenya Food Security Meeting (KSFM) and the Inter Ministerial Committee on Drought and Food Security and in recognition of the need to coordinate response activities during transition into alarm phase of the drought cycle in many districts.

The KFSSG meets every month to look at the food security situation in the country. Their decisions are guided by assessments done at district levels. However, the most crucial role of KFSSG is to do Long Rain Assessment (LRA) and Short Rain Assessment (SRA) reports and give recommendations of the action to be taken based on what has happened in the current season and what is forecasted to happen in the next season.

5.3.3 Drought adaptation and mitigation interventions

While compiling the LRA report in 2010 the KFSSG noted that the performance of the 2010 long rains was more favorable in the western half of the country than in the eastern pastoral

and marginal agricultural areas. Rains had also begun earlier-than-usual, in February, in the eastern half of the country but ended early in April or early May. Subsequently, parts of the northeastern pastoral districts of Mandera, Marsabit and Isiolo experienced overall below normal long rains. The southern pastoral Maasai rangelands also received fairly poor rains, especially Kajiado district. However, the 2010 long rains were favorable and above normal in key growing areas in the Western, Nyanza, Rift Valley and parts of the Central and Eastern highlands. Rains continued beyond the normal long rains period particularly in the western and Rift Valley.

The KFSSG also looked at the consensus climate outlook for the Greater Horn of Africa for the September through December 2010 short rains that had been released in early September by the IGAD Climate Prediction Applications Center (ICPAC). The forecast suggested the expectation of a moderate to strong La Niña episode. La Niña is associated with drier-than normal conditions in the eastern sector of the country including the northern and northeastern pastoral areas, as well as the drought-prone southeastern and coastal marginal agricultural lowlands. However, the outlook indicated that the western sector, including the northwestern pastoral districts and the high potential cropping highlands in the Rift Valley and western Kenya, were likely to receive above-normal short rains.

The major point of concern was the likelihood that La Niña conditions could persist through the March to May 2011 period, because the eastern sector of the country would experience two consecutive drought seasons, in effect reversing the recovery process and likely reverting to the heightened food insecurity that prevailed prior to October 2009.

With the above in mind the KFSSG made the following intervention recommendations:

Table 5-1 ***Summary of Priority Interventions by Sector – June - December 2010***

	SECTOR	**INTERVENTION**
1.	**AGRICULTURE SECTOR**	Provision of drought-tolerant seeds and seed bulking; post-harvest management and aflatoxin campaigns and surveillance; promotion of value addition of agricultural produce; water harvesting and irrigation; soil conservation and conservation agriculture; value addition though processing; establishment of cereal banks; and promotion of greenhouse technology.
2.	**LIVESTOCK SECTOR**	Livestock vaccinations and disease surveillance; re-stocking of small stocks; fodder conservation; re-seeding pastures and rangeland rehabilitation; promotion of alternative livelihoods; and streamlining livestock marketing chain.

3.	**HEALTH AND NUTRITION SECTOR**	Integrated Management of Acute Malnutrition; emergency polio immunization; public health surveillance of food and water; provision of effective insecticide-treated nets; micronutrient supplementation and de-worming; health and nutrition education; support to infant and young child feeding; water treatment chemicals; integrated outreach programs and medical supplies; nutrition surveys; supplementary feeding program and disease surveillance.
4.	**WATER SECTOR**	Drilling and equipping of boreholes; construction and de-silting of water sources; construction and rehabilitation of water sources; provision of storage tanks; protection of open water wells; promotion of rain/water harvesting technologies; repair of four water bowsers; capacity strengthening for rapid response teams.
5.	**EDUCATION SECTOR**	Provision of water tanks for roof catchment and rain water harvesting; advocacy campaigns against child labor and early marriages; Provision of water trucking and shallow well rehabilitation; expansion of home grown school meals programme; Infrastructure improvement programme (construction of toilets/ renovation of existing ones); health education campaigns for de-worming.
6.	**FOOD SECTOR**	Food and associated costs for 1.2 million people affected by drought for the next six months (September 2010-February 2011). An estimated 96,310 MT of food commodities will be required from September 2010 to February 2011.

While compiling the SRA report the KFSSG noted that the short rains began about two to three weeks later than expected in most of the assessment districts. The rains were low and characterized by poor spatial and temporal distribution throughout the season. In addition, rains ended after six weeks to one month, in most areas. The regions in the northern, northwestern and northeastern pastoral areas are some of the areas that received less than 20 percent of normal and were the key areas of concern. The rest of the pastoral, agro-pastoral and marginal agricultural and coastal lowlands had areas that received between 20-50 percent of normal rains. The poor rain was the key factor that accelerated depletion of resources and livelihood productivities, precipitating a marked decline in household food security.

The short rains having failed in most parts of the country and with the forecast of continuing La Nina condition into March-May 2011, the KFSSSG recommended the following interventions:

Table 5-2 ***Summary of Priority Interventions by Sector – March to August 2011***

	SECTOR	INTERVENTION
1.	**AGRICULTURE SECTOR**	Promote water harvesting, soil conservation and agro-forestry; timely provision of drought tolerant certified seeds and fertilizer; capacity building on Good Agricultural Practices (GAP) and post-harvest management; construction of community based storage facilities; provision of green house and micro-irrigation kits; promote fruits processing and value addition; construction and expansion of irrigation infrastructure; and promotion of conservation agriculture.
2.	**LIVESTOCK SECTOR**	Disease surveillance and vaccinations; livestock treatments; hay and feeds supplements; livestock off-take; and Kenya Meat Commission (KMC) meat processing.
3.	**HEALTH AND NUTRITION SECTOR**	Scale-up integrated management of acute malnutrition through provision of therapeutic feeds; accelerated integrated mobile outreach services in hard to reach areas to increase access to health and nutrition services; promotion and protection of infant and young child feeding practices including health education; blanket supplementary feeding to all children under two years and pregnant and lactating women; procurement of additional drugs, long lasting insecticide treated nets (LLITNs); micronutrient supplementation for children and mothers at community and facility level and de-worming; and accelerated disease, water safety and nutrition surveillance.
4.	**WATER SECTOR**	Rehabilitation of boreholes, dams and pans, repair of water supplies; water trucking; purchase and distribution of plastic tanks; water quality surveillance and treatment chemical; drilling of emergency boreholes and fuel subsidy.
5.	**EDUCATION**	Expansion of home grown school meals programme; water

	SECTOR	trucking to schools; advocacy; campaigns against child labor and early marriages; provision of water tanks for rain water harvesting; health education campaign and de-worming.
6.	**FOOD SECTOR**	Food and associated costs for 2.4 million people affected by drought, for the next six months (March - August 2011). An estimated 96,310 MT of food commodities will be required.

The drought management system in Kenya is in place at the district level. The government receives the drought early warning reports and the proposed interventions before the drought starts. However, the government's reaction time is normally slow and the disbursement of funds needed for the interventions is not enough and not provided in due time. Most of the resources are used for the emergency stage of the drought and little is left for the recovery stage.

There are also other underlying challenges when it comes to drought management. For example, pastoral communities which are often affected by drought because they live in arid areas, have cultures that will not have them embrace the government's animal off-take program easily. Similarly people don't want to change their traditional crops and seeding methods.

The drought management staff at the district level also recommend for aid most of the time instead of recommending lasting solutions. There is also need to have emergency guidelines for all sectors, which would go a long way in helping coordinate the Non-Governmental Organizations (NGOs) actions.

6. CONCLUSIONS

This study evaluated the capabilities of different drought indicators (including precipitation, runoff, soil moisture and vegetation) in detect the timing and extension of drought across Africa, using four different precipitation datasets. The analysis was performed on a Pan-African scale and on a regional scale focused on the case studies areas and also the Great Horn of Africa. This report presents a global overview of available drought indicators on a pan-Africa scale, their main characteristics and limitations and their performance over the cases studies areas.

A comparison of the annual cycle and monthly precipitation time series shows a general agreement in the timing of the peaks including the Great Horn of Africa were there are two rainy seasons. The main differences are observed thus in the ability to represent the magnitude of the wet seasons and extremes.
For the monthly mean the precipitation datasets fit each other well over all regions with the only exception of CMAP dataset that shows in general lower agreement. At Oum er-Rbia, Niger and Limpopo basins there exists a lower disagreement between datasets with mean absolute errors below 10 mm/month. The bias in those two regions is below 20 %. The worst performance of ERAI is observed at Blue Nile and GHA regions with overestimations of monthly precipitation could be around 40 mm/month and the bias are around 50% in the second.

The comparative analysis between TRMM, ERAI, GPCP and GPCC datasets suggests that is feasible to use TRMM time series with high spatial resolution for reliable drought monitoring over Africa. It's possible to take advantage of this dataset mainly at regional level by taking advantage of their high spatial resolution. However, higher discrepancies in SPI estimations are shown in mountainous areas and areas with sparse in situ station density. In the other hand, drought monitoring at continental level with ERA-Interim is mainly possible outside the areas influenced by the ITCZ.

A non-parametric resampling bootstrap approach was used to compute the confidence bands of the sampling uncertainties associated with the SPI estimation. The proposed approach for drought monitoring has the potential to be used in support of decision making at continental and sub-continental scales over Africa or other regions that have a sparse distribution of rainfall measurement instruments.
This kind of approach could be used to improve the monitoring of rainfall conditions in two ways. Firstly, to obtain an unbiased estimation of the Gamma parameters with short precipitation time series. This could allow the development of a Pan-African SPI using near

real-time rainfall estimates. The second is to estimate the confidence bands of SPI. This can prepare decision makers, through the measurement of uncertainties associated with the datasets, to better understand in which situations this tool is more reliable than others. Moreover, this type of approach could enable some forecast applications. For instance, it is possible to use the distribution information for each member of the bootstrap as initial conditions to develop drought scenarios. These types of scenarios could prepare decision makers and local stakeholders to take the appropriate action needed in the cases of high and low risks situations.

In order to objectively define areas where indicators are in agreement the temporal correlation at grid cell level between indicators were performed during the 1998-2010 common period. At continental level is shown a good agreement between drought indicators in North West and Southern Africa, while a low agreement in Central Africa was observed. However, if SPI-3 TRMM estimation is also compared a good agreement is also observed in east Africa and the region that includes the Great Horn of Africa. The estimations of the indicators over Central Africa reflect the high uncertainty present in the precipitation datasets. At this region, no significative correlations are observed between indicators. These results confirm and extend the findings in Deliverable D4.2.

The comparison between SPI estimations suggest that the main sources of error are the uncertainties (due by lack of ground information, estimation algorithms, parameterization of the convection, etc.) in the datasets rather than the estimation of the distribution parameters.

In fact, Oum er-Rbia and Limpopo regions are those that exhibit a better agreement between estimations with correlation coefficient mostly greater than 0.8. The mean absolute error is usually around 0.3 at these locations but could reach 0.5 at Oum er-Rbia between ERAI and GPCP estimations and 0.46 between TRMM and ERAI at the Limpopo basin.

While for the other regions the discrepancies between datasets are also acceptable with MAE's around 0.3 and 0.5 and correlation coefficient 0.7 and 0.9. The greater discrepancies are observed at Niger basin, where the mean absolute error between the datasets and ERAI estimation are greater than 0.46, reaching 0.65 if ERAI and GPCP are compared. Also, is observed that ERAI underestimates SPI compared with the other datasets mainly during the second half of the period analysed.

Regarding the areas that are under drought, all the datasets agrees with the certain time of onset and recovery but there are sometimes disagreements on the area affected and also this agreement tends to be dependent on the threshold selected.

The integrated use of two different sources of information, meteorological and remote sensing data, shows great potential to synergistically monitor drought events in the Horn of Africa.

7. REFERENCES

Adeyewa, Z. D., and K. Nakamura, 2003: Validation of TRMM radar rainfall data over major climatic regions in Africa. J. Appl. Meteor., 42, 331–347

Adler, R.F., G.J. Huffman, A. Chang, R. Ferraro, P. Xie, J. Janowiak, B. Rudolf, U. Schneider, S. Curtis, D. Bolvin, A. Gruber, J. Susskind, P. Arkin, E. Nelkin 2003: The Version 2 Global Precipitation Climatology Project (GPCP) Monthly Precipitation Analysis (1979-Present). J. Hydrometeor., 4, 1147-1167.

Camberlin P, Philippon N, 2002: The east African March–May rainy season: associated atmospheric dynamics and predictability over the 1968–97 period. J. Climatol. 15, 1002–1018.

Ceccato, P., Flasse, S., Tarantola, S., Jacquemond, S., and Gregoire, J.M. 2001: Detecting vegetation water content using reflectance in the optical domain. Remote Sensing of Environment 77: 22–33.

Ceccato, P., Flasse, S., and Gregoire, J.M. 2002: Designing a spectral index to estimate vegetation water content from remote sensing data: Part 2. Validation and applications. Remote Sensing of Environment 82: 198-207.

Climate Change Climate Action Climate Justice, 2011, Trócaire Policy Report

Dee, D., and Coauthors, 2011: The ERA-Interim reanalysis: Configuration and performance of the data assimilation system. Quart. J. Roy. Meteor. Soc., 137, 553–597

DEWFORA D2.1, 2011: inventory of drought monitoring and forecasting systems in Africa. http://www.dewfora.net/Publications

DEWFORA D2.2, 2011: Inventory of institutional frameworks and drought mitigation and adaptation practices in Africa. http://www.dewfora.net/Publications

DEWFORA D4.1, 2011: Meteorological drought forecasting at regional and continental scale. http://www.dewfora.net/Publications

DEWFORA D4.2, 2011: Skill of the multi-model forecasting system in predicting variables and drought indicators. http://www.dewfora.net/Publications

DEWFORA D4.3, 2012 Potential to supplementing drought early warning systems with new meteorological information. http://www.dewfora.net/Publications

DEWFORA D6.1, 2012: Implementation of improved methodologies in comparative case studies. Inception report for each case study. http://www.dewfora.net/Publications

Dinku T., P. Ceccato, E. Grover-Kopec, M. Lemma, S. J. Connor & C. F. Ropelewski, 2007: Validation of satellite rainfall products over East Africa's complex topography, International Journal of Remote Sensing, 28:7, 1503-1526

Dutra, E., P. Viterbo, and P. M. A. Miranda, 2008: ERA-40 reanalysis hydrological applications in the characterization of regional drought, Geophys. Res. Lett., 35, L19402, doi:19410.11029/12008GL035381.

Efron B, Tibshirani RJ., 1993: An Introduction to the Bootstrap. Chapman & Hall: New York, NY.

Gao, B.-C. 1996: NDWI - A normalized difference water index for remote sensing of vegetation liquid water from space. Remote Sensing of Environment 58: 257-266.

Glantz, M., 2002, La Niña and its Impacts: Facts and Speculation, United Nations University Press, New York.

Gobron N., Aussedat O., Pinty B., Taberner M., and Verstraete M. M., 2004: Medium Resolution Imaging Spectrometer (MERIS) - An optimized FAPAR Algorithm - Theoretical Basis Document. Revision 3.0. Institute for Environment and Sustainability, EUR Report No. 21386 EN, 20 p. http://fapar.jrc.ec.europa.eu/WWW/Data/Pages/FAPAR_Home/FAPAR_Home_Publications/atbd_meris_v4_gen.pdf

Gobron N., Pinty B., Mélin F., Taberner M., Verstraete M.M., Belward A., Lavergne T., and Widlowski J.-L., 2005: The state vegetation in Europe following the 2003 drought. International Journal Remote Sensing Letters, 26 (9): 2013-2020.

Gobron, N., Pinty, B., Mélin, F., Taberner, M., Verstraete, M.M., Robustelli, M., Widlowski, J.-L., 2007: Evaluation of the MERIS/ENVISAT fAPAR Product. Advances in Space Research 39: 105-115.

Gu, Y., Brown, J.F., Verdin, J.P., and Wardlow, B. 2007: A five-year analysis of MODIS NDVI and NDWI for grassland drought assessment over the central Great Plains of the United States. Geophysical Research Letters 34.

Huffman, G. J., R. F. Adler, B. Rudolf, U. Schneider, and P. R. Keehn 1995: Global precipitation estimates based on a technique for combining satellite-based estimates, rain gauge analysis, and NWP model precipitation information. J. Climate, 8, 1285-1295.

Huffman, G.J, R.F. Adler, D.T. Bolvin, G. Gu 2009: Improving the Global Precipitation Record: GPCP Version 2.1. Geophys. Res. Lett., 36,L17808, doi:10.1029/2009GL040000.

Huffman and Coauthors, 2007: The TRMM Multi-satellite Precipitation Analysis (TMPA): Quasi-global, multiyear, combined sensor precipitation estimates at fine scales. J. Hydrometeor., 8, 38–55.

Husak, G. J., Michaelsen, J. and Funk, C. 2007: Use of the gamma distribution to represent monthly rainfall in Africa for drought monitoring applications. International Journal of Climatology, 27: 935–944. doi: 10.1002/joc.1441

IGAD Climate Prediction and Applications Centre (ICPAC) updates on La Niña event and its impact on the Greater Horn of Africa climate: November 2010.

IGAD Climate Prediction and Applications Centre (ICPAC), Climate Watch for the Period March-May 2011: REF: ICPAC/CW/NO.24, May 2011.

IGAD Climate Prediction and Applications Centre (ICPAC), Update of the ICPAC Climate Watch: REF: ICPAC/CW/NO.24, August 2011.

Ivits, E. M. Cherlet, G. Tóth, S. Sommer, W. Mehl, J. Vogt, F. Micale, 2012: Combining satellite derived phenology with climate data for climate change impact assessment, Global and Planetary Change, Volumes 88–89, Pages 85-97, ISSN 0921-8181, 10.1016/j.gloplacha.2012.03.010.

Jenkins, G. S., 2000: TRMM satellite estimates of convective processes in Central Africa during September, October, November 1998: Implications for elevated Atlantic tropospheric ozone, Geophys. Res. Lett., 27, 1711 –1714.

Legates, D. R., and G. J. McCabe Jr. 1999: Evaluating the Use of "Goodness-of-Fit" Measures in Hydrologic and Hydroclimatic Model Validation, Water Resour. Res., 35(1), 233–241

Lélé MI, Lamb PJ. 2010: Variability of the Intertropical Front (ITF) and rainfall over the West African Sudan–Sahel zone. J. Climate 23: 3984–4004.

Linderholm, H.W., Walther, A., Chen, D., 2005: Growing Season Trends in the Greater Baltic Area. University of Goteborg, C69 Rapport, Göteborg. ISSN 1400-383X.

Lloyd-Hughes, B., and M. A. Saunders, 2002: A drought climatology for Europe. Int. J. Climatol., 22, 1571–1592.

Love D. Twomlow S. Mupangwa W. van der Zaag P. Gumbo B. 2006: Implementing the millennium development food security goals - challenges of the southern African context. Physics and Chemistry of the Earth31, 731-737.

McKee T.B., Doesken N.J., Kleist J., 1993: The Relationship of Drought Frequency and Duration to Time Scales. Proc. 8th Conf. on Appl. Clim., 17-22 Jan. 1993, Anaheim, CA, 179-184.

McKee, T. B., N. J. Doesken, and J. Kleist, 1995: Drought monitoring with multiple time scales. Proc. Ninth Conf. on Applied Climatology, Dallas, TX, Amer. Meteor. Soc. 233-236.

Menzel, A., 2002: Phenology, its importance to the global change community. Editorial comment. Climatic Change 54, 379–385.

Nicolis, C., W. Ebeling, and C. Baraldi 1997: Markov processes, dynamic entropies and the statistical prediction of mesoscale weather regimes, Tellus, Ser. A, 49, 108– 118.

Nicholson, S. E. and Selato, J. C., 2000: The influence of La Nina on African rainfall, International Journal of Climatology, vol. 20, pp.1761-1776

Nicholson, S.E., Some, B., Mccollum, J., Nelkin, E., Klotter, D., Berte, Y., Diallo, B.M., Gaye, I., Kpabeba, G., Ndiaye, O., Noukpozounkou, J.N., Tanu, M.M., Thiam, A., Toure, A.A. And Traore, A.K., 2003: Validation of TRMM and other rainfall estimates with a high-density gauge dataset for West Africa. Part II: Validation of TRMM rainfall products. Journal of Applied Meteorology, 42, pp. 1355–1367.

Pinty B., Gobron N., Mélin F., and Verstraete M.M. 2002: Time Composite Algorithm Theoretical Basis Document. Institute for Environment and Sustainability, EUR Report No. 20150 EN, 8 pp.
http://fapar.jrc.ec.europa.eu/WWW/Data/Pages/FAPAR_Home/FAPAR_Home_Publications/pinty_etal_ies_2002.pdf

Reed, B.C., Brown, J.F., VanderZee, D., Loveland, T.R., Merchant, J.W., Ohlen, D.O., 1994: Measuring phenological variability from satellite imagery. Journal of Vegetation Science 5, 703–714.

Rhee, J., G.J. Carbone, 2011: Estimating Drought Conditions for Regions with Limited Precipitation Data. J. Appl. Meteor. Climatol., 50, 548–559.

Rudolf, B.,W. Rueth, and U. Schneider, 1994: Terrestrial precipitation analysis: Operational method and required density of point measurements. Global Precipitation and Climate Change, M. Desbois and F. Desahmond, Eds., Springler-Verlag, 173–186.

Shukla S., A.W. Wood, 2008: Use of a standardized runoff index for characterizing hydrologic drought Geophys. Res. Lett., 35, L02405.

Sheffield, J., G. Goteti, F. H. Wen, and E. F. Wood, 2004: A simulated soil moisture based drought analysis for the United States, J. Geophys. Res., 109(D24).

Silverman, B.W., 1986: Density Estimation for Statistic and Data Analysis. Chapman and Hall, New York.

The 2010 Long Rains Season Assessment Report, Kenya Food Security Steering Group (KFSSG)

The 2010 Short Rains Season Assessment Report, Kenya Food Security Steering Group (KFSSG)

Thom H.C., 1958: A note on the gamma distribution. Monthly Weather Review 86: 117–122.

Thornthwaite, C. W., 1948: An approach toward a rational classification of climate. Geogr. Rev., 38, 55–94.

Tucker, C. J. 1980: Remote sensing of leaf water content in the near infrared. Remote Sensing of Environment 10: 23-32.

Tucker, C.J., Pinzon, J.E., Brown, M.E., Slayback, D., Pak, E.W., ahoney, R., Vermote, E., Saleous, N., Saleous, N., 2005: An extended AVHRR 8-km NDVI data set compatible withMODIS and SPOT vegetation NDVI data. International Journal of Remote Sensing 26, 4485–4498.

Vicente-Serrano, S. M., S. Begueria, and J. I. Lopez-Moreno, 2010: A Multiscalar Drought Index Sensitive to Global Warming: The Standardized Precipitation Evapotranspiration Index, J. Climate, 23(7), 1696-1718, doi: Doi 10.1175/2009jcli2909.1.

Wilks D.S. 2002: Statistical Methods in the Atmospheric Sciences. Elsevier Academic Press Publications: pp. 467.

Willmott, C. J. 1981: On the validation of models. Physical Geography, 2, 184–194

Willmott, C. J., S. M. Robeson, and M. J. Janis, 1996: Comparison of approaches for estimating time-averaged precipitation using data from the USA. Int. J. Climatol., 16, 1103–1115.

World Meteorological Organization (WMO), 2011: Guide to climatological practices. WMO/TN 100, Geneva: WMO, 117 pp.

Xie, P., and P.A. Arkin, 1997: Global precipitation: A 17-year monthly analysis based on gauge observations, satellite estimates, and numerical model outputs. Bull. Amer. Meteor. Soc., 78, 2539 - 2558.

8. APPENDICES

8.1 MAPS OF SPATIAL AGREEMENT BETWEEN INDICATORS IN A MONTHLY BASIS FOR THE PERIOD 2000-2009

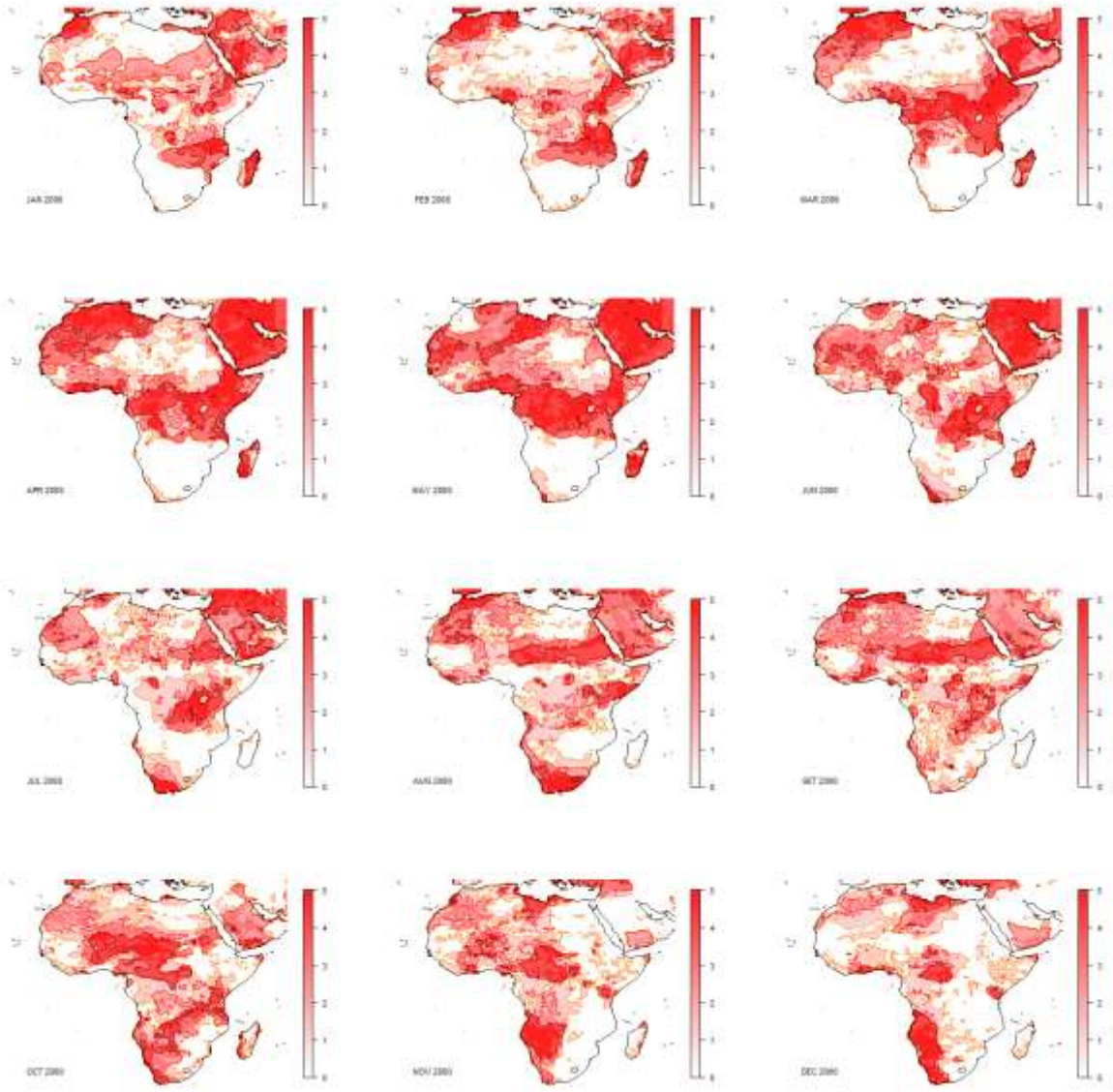

Figure 8-1 Spatial agreement between ERA-I, GPCP and TRMM SPI-3 and ERIA, GPCP SPEI-3 estimations for 2000. Grid cells with SPI-3 below -0.5 were considered. Values are ranged between 0 (no dataset with SPI below the threshold) and 5 (all datasets below the threshold).

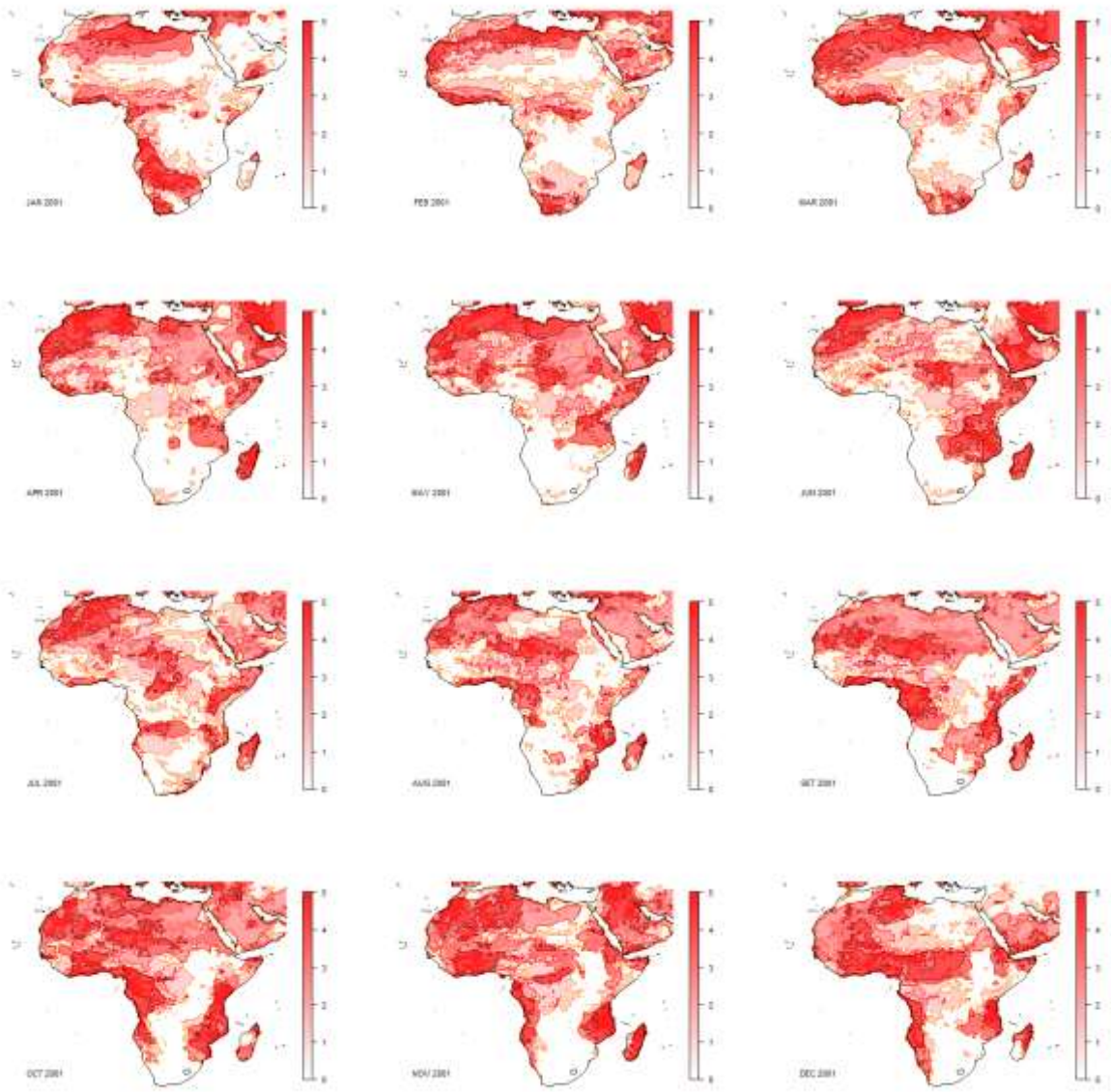

Figure 8-2 Same as Figure 8-1 but for 2001.

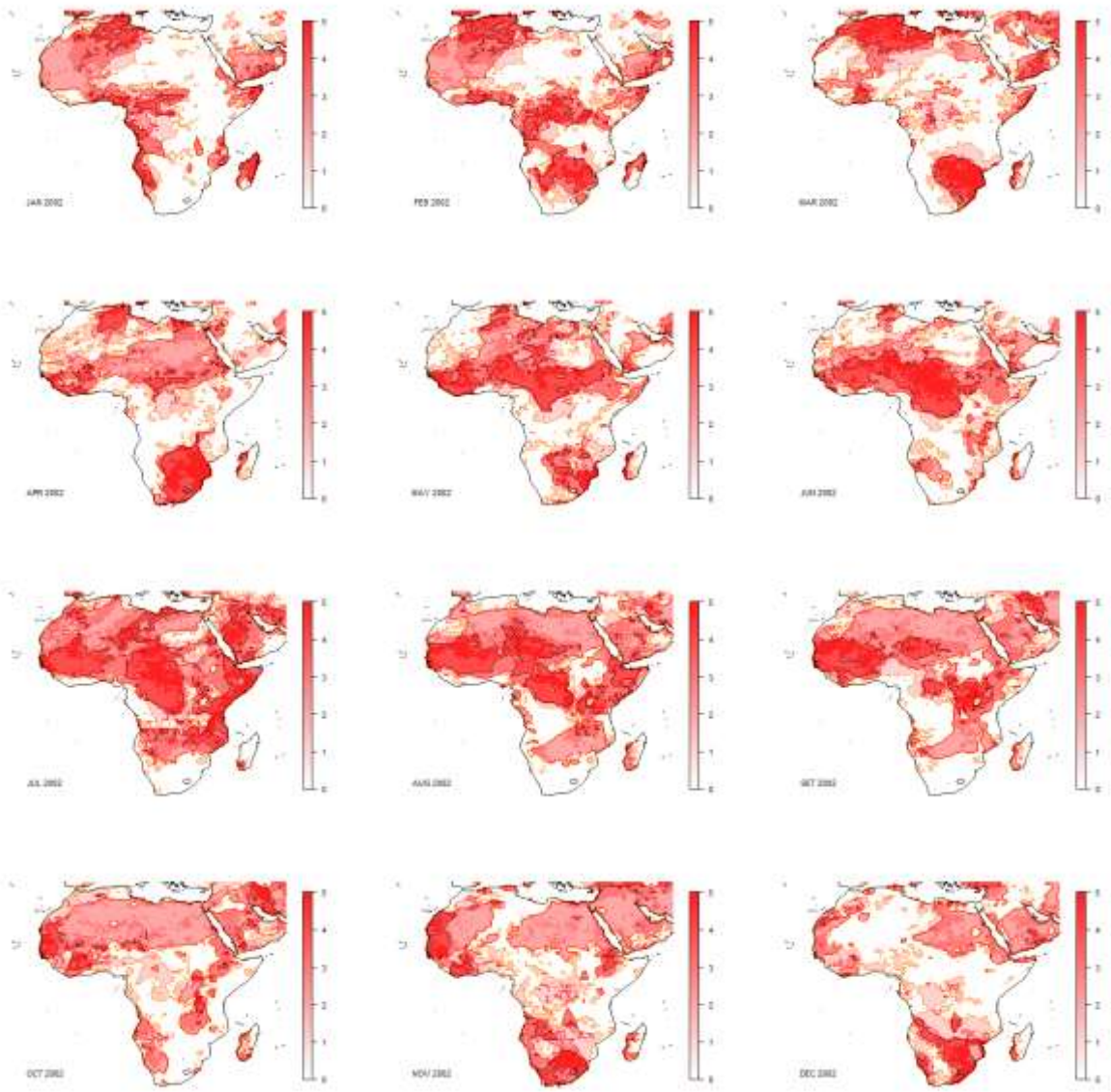

Figure 8-3 Same as Figure 8-1 but for 2002.

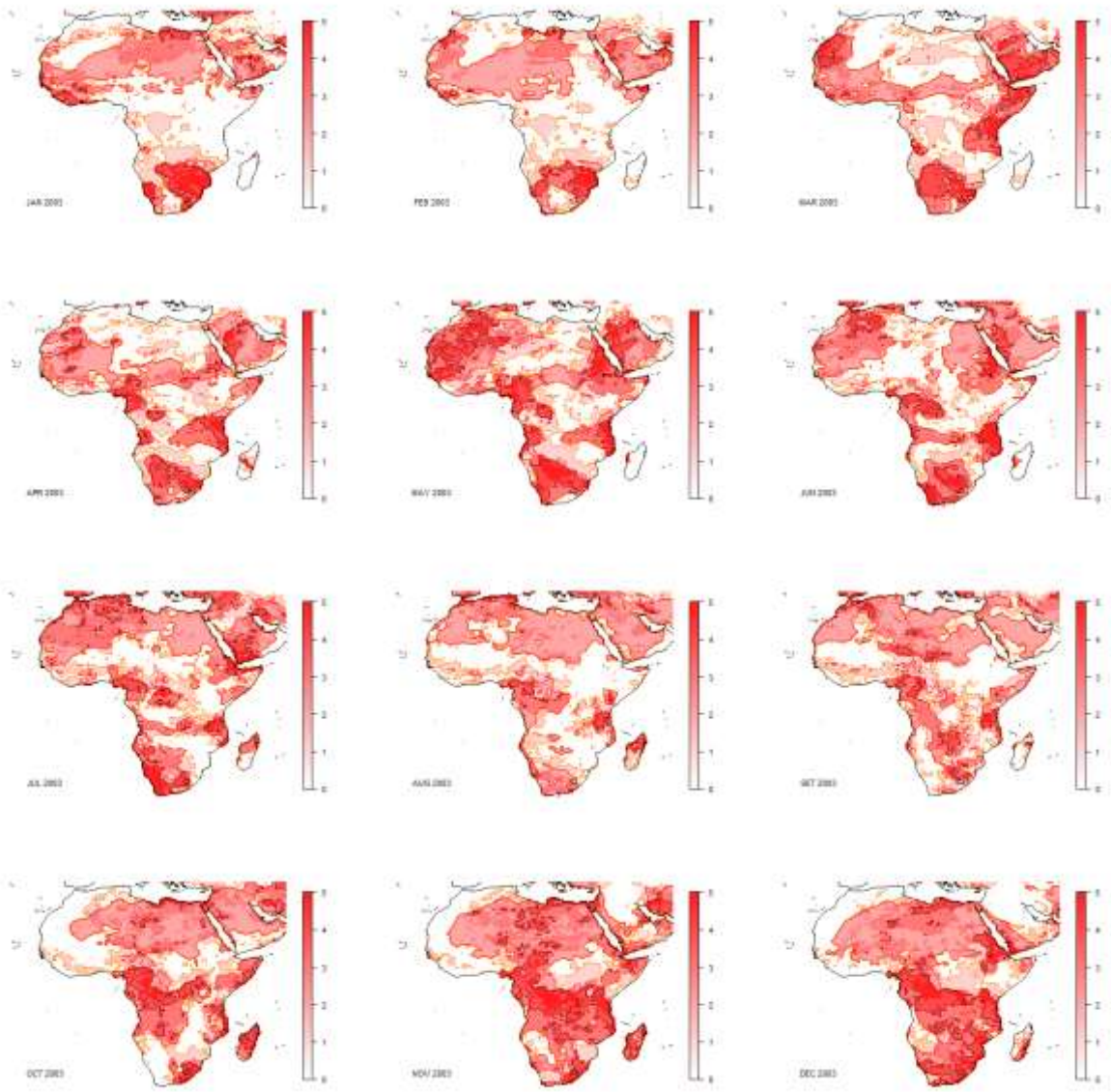

Figure 8-4 Same as Figure 8-1 but for 2003.

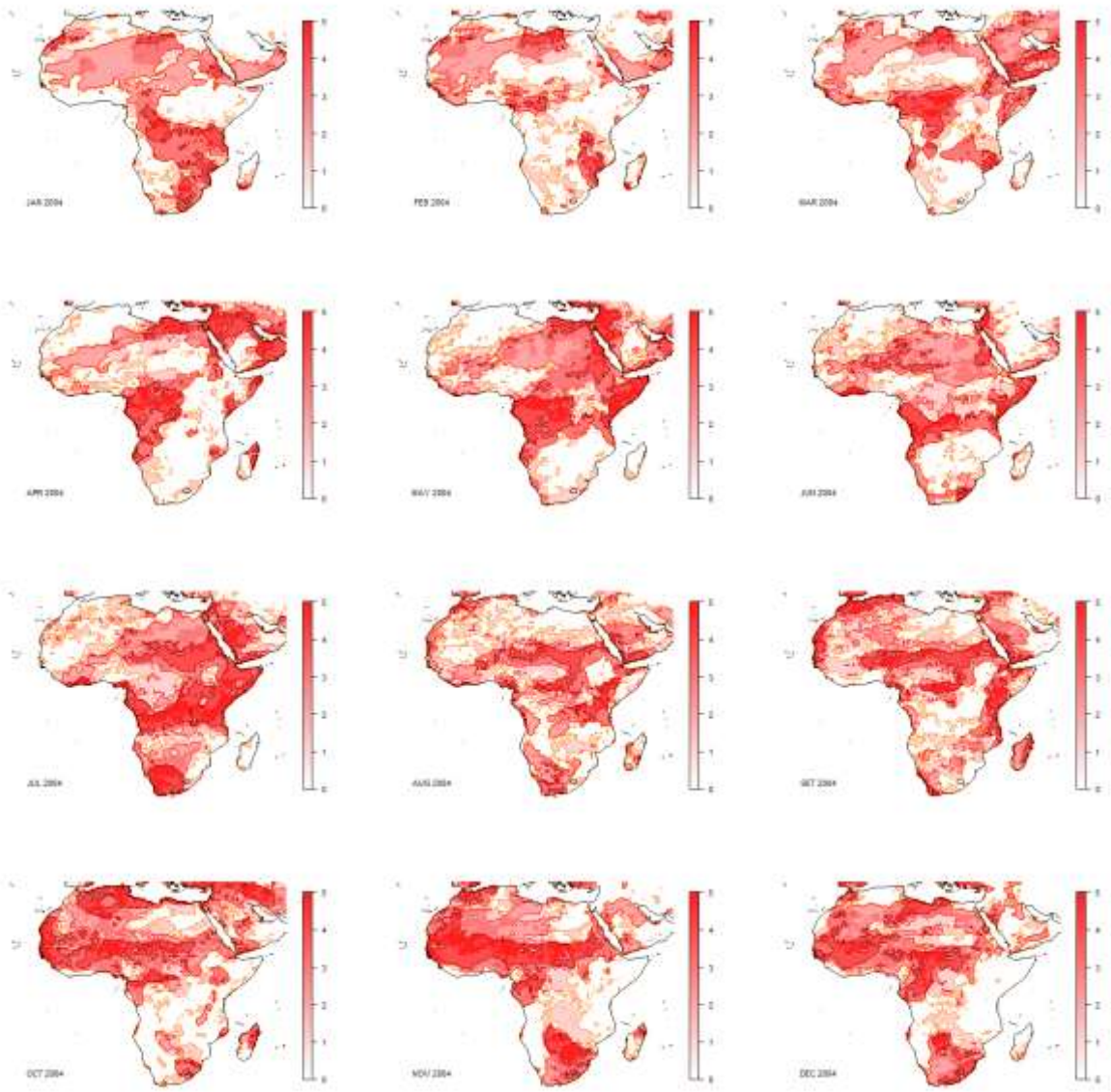

Figure 8-5 Same as Figure 8-1 but for 2004.

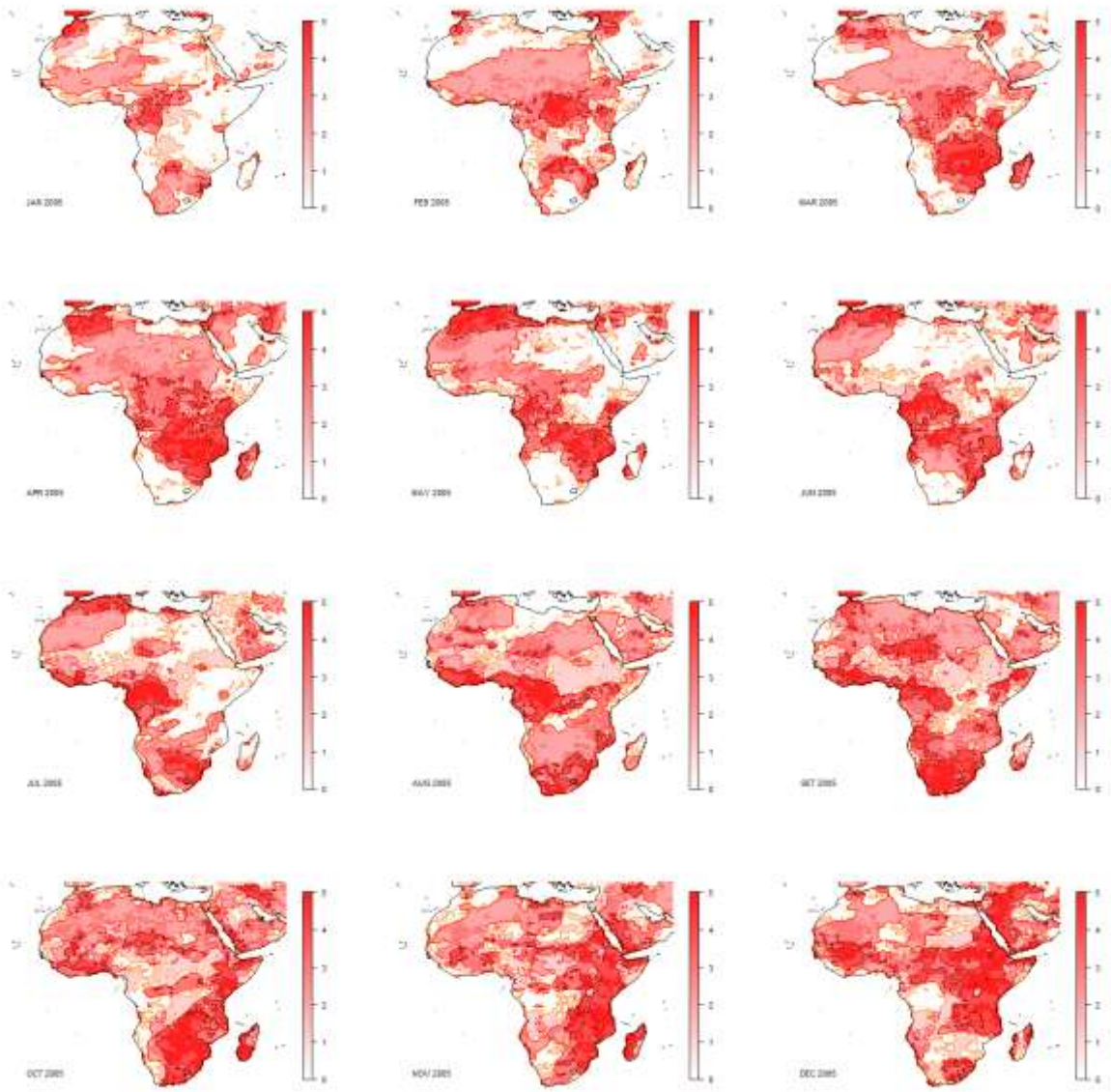

Figure 8-6 Same as Figure 8-1 but for 2005.

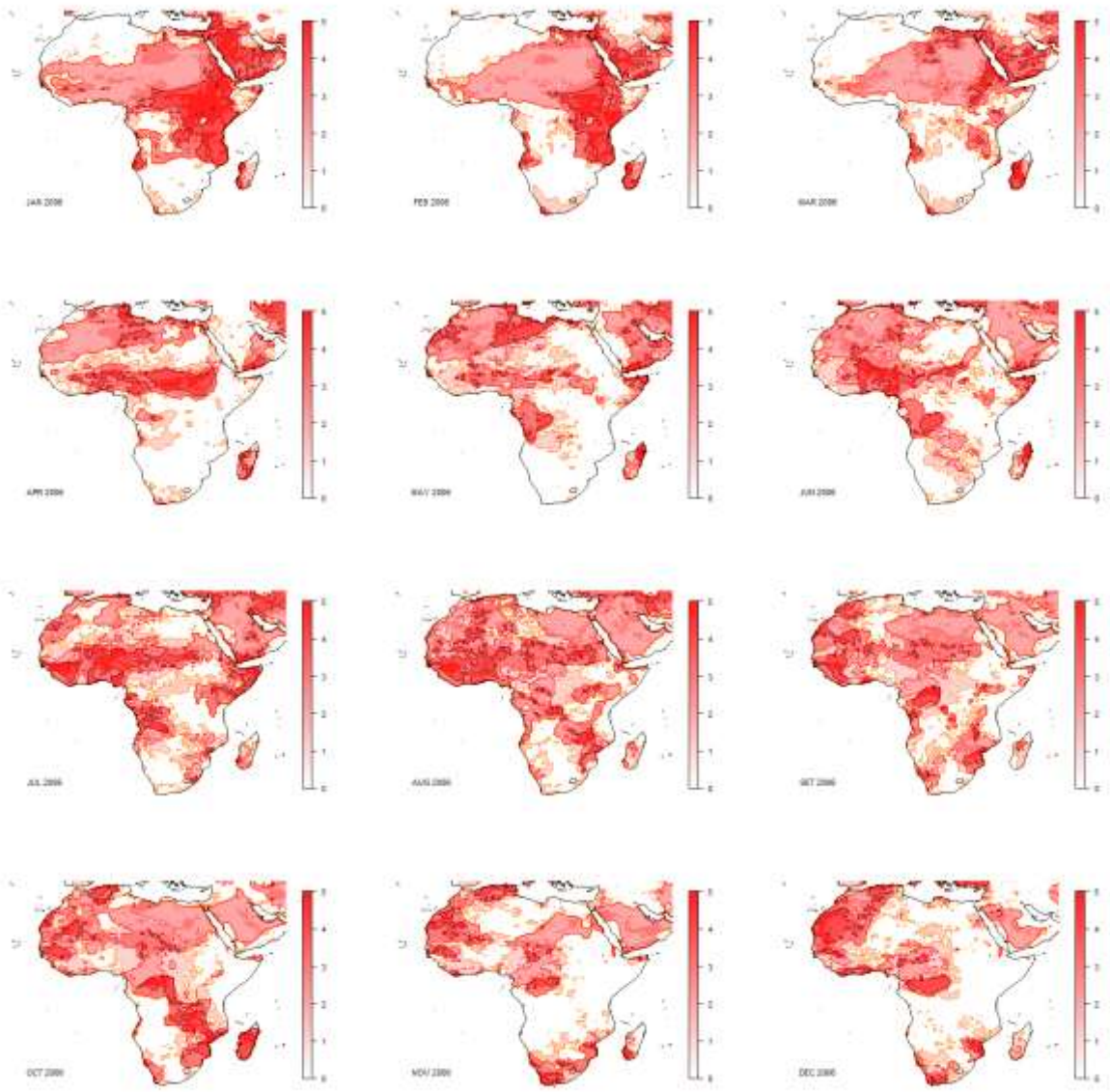

Figure 8-7 Same as Figure 8-1 but for 2006.

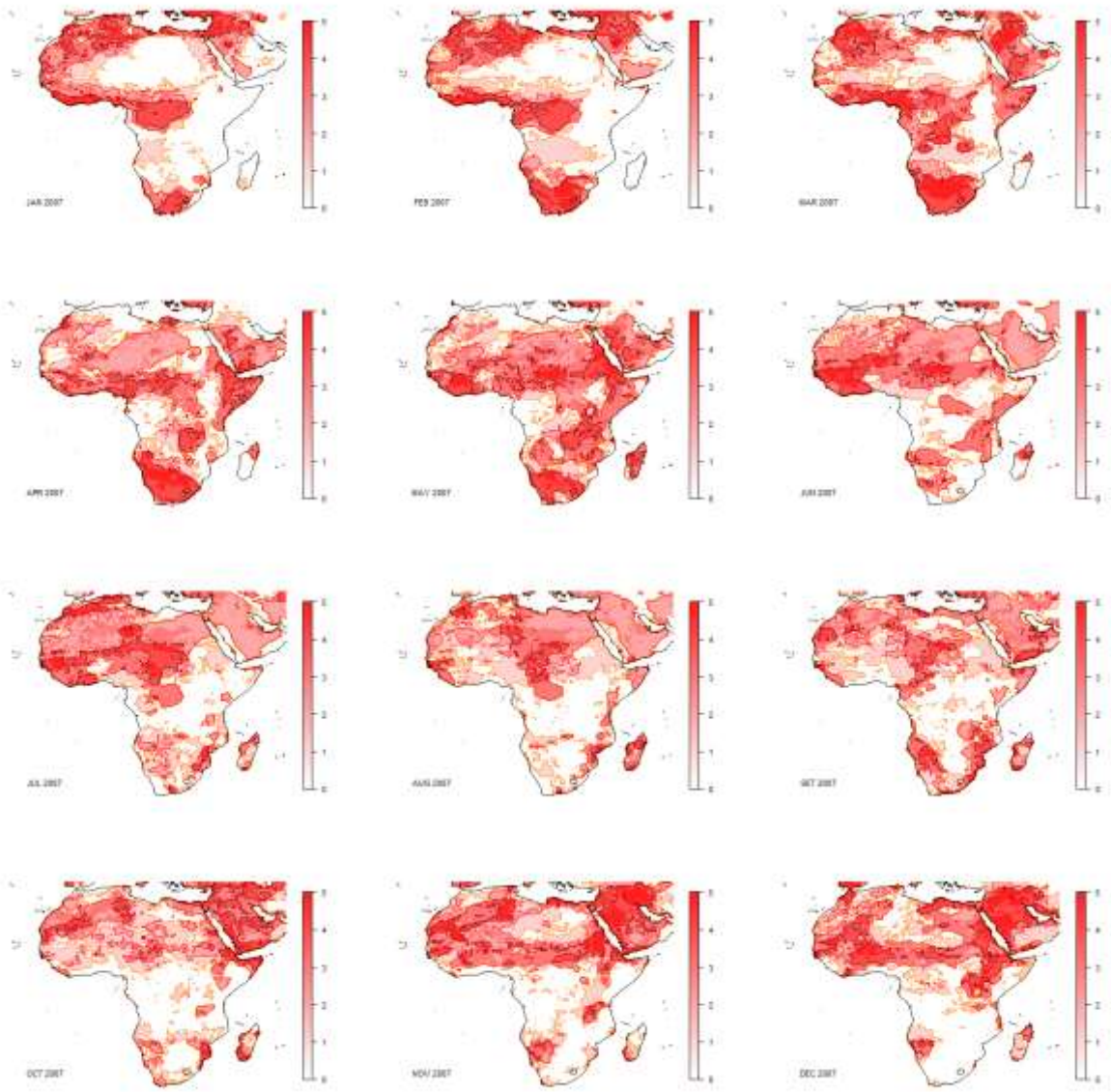

Figure 8-8 Same as Figure 8-1 but for 2007.

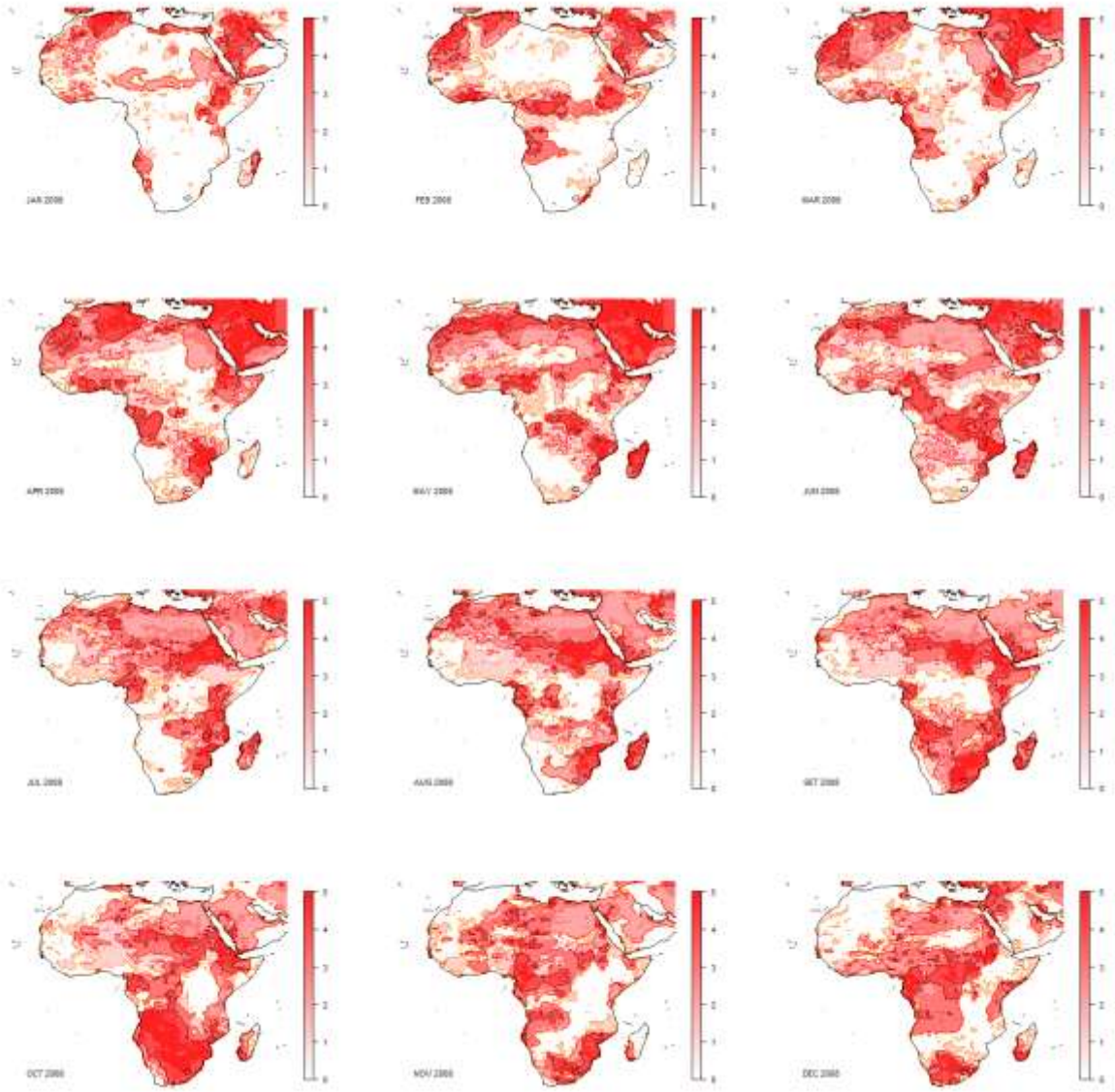

Figure 8-9 Same as Figure 8-1 but for 2008.

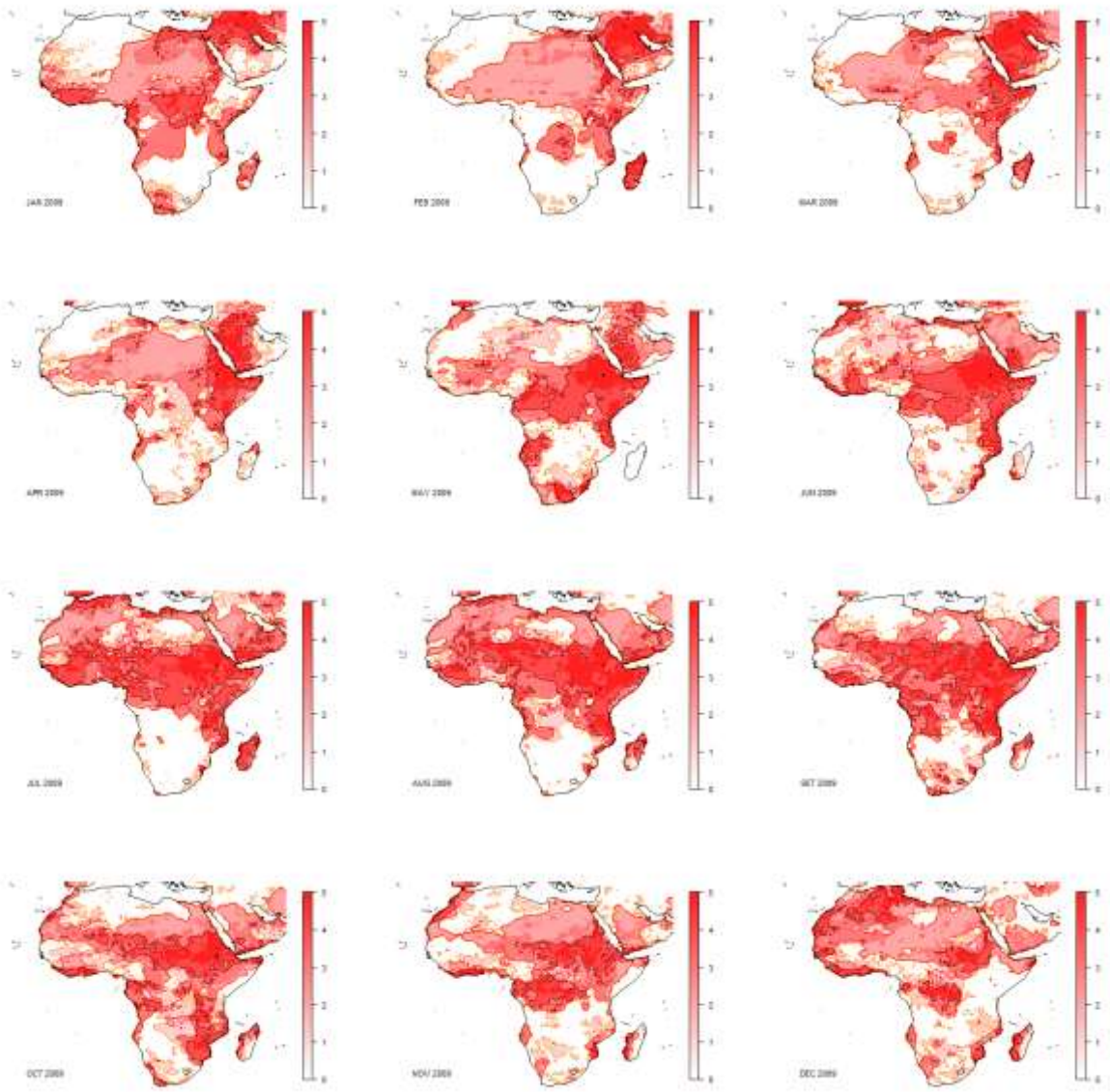

Figure 8-10 Same as Figure 8-1 but for 2009.

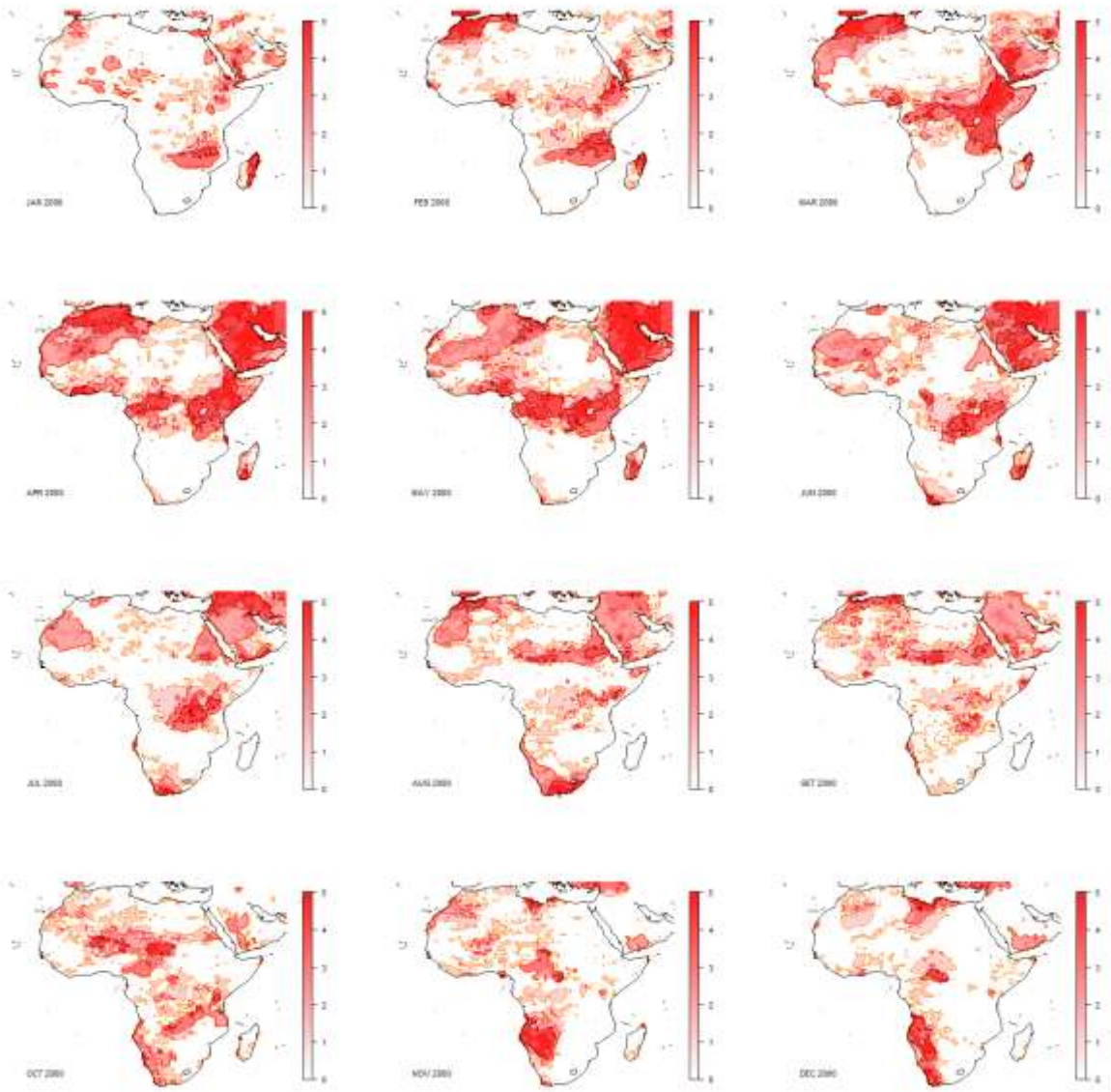

Figure 8-11 Spatial agreement between ERA-I, GPCP and TRMM SPI-3 and ERIA, GPCP SPEI-3 estimations for 2000. Grid cells with SPI-3 below -1.0 were considered. Values are ranged between 0 (no dataset with SPI below the threshold) and 5 (all datasets below the threshold).

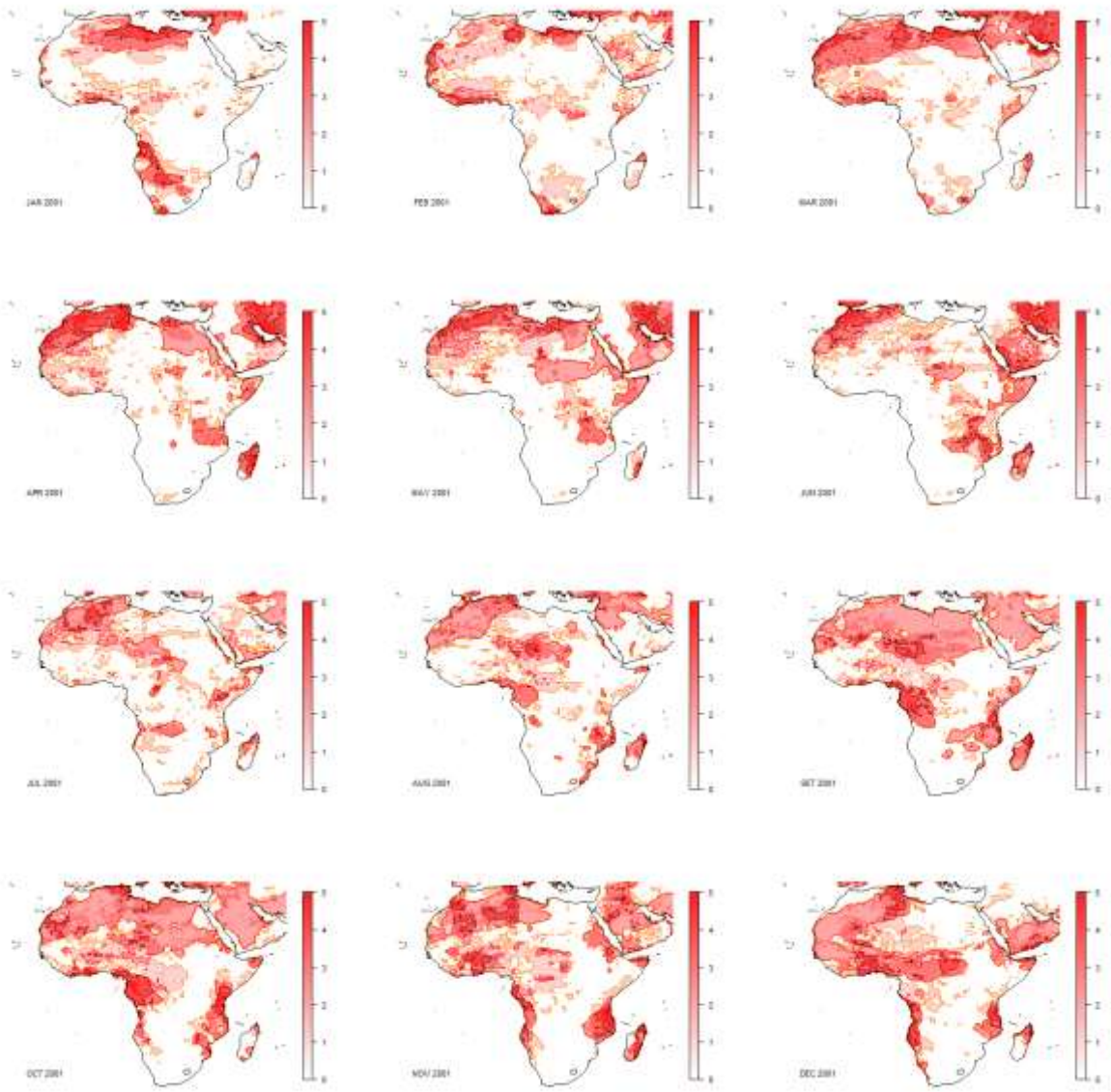

Figure 8-12 Same as Figure 8-11 but for 2001.

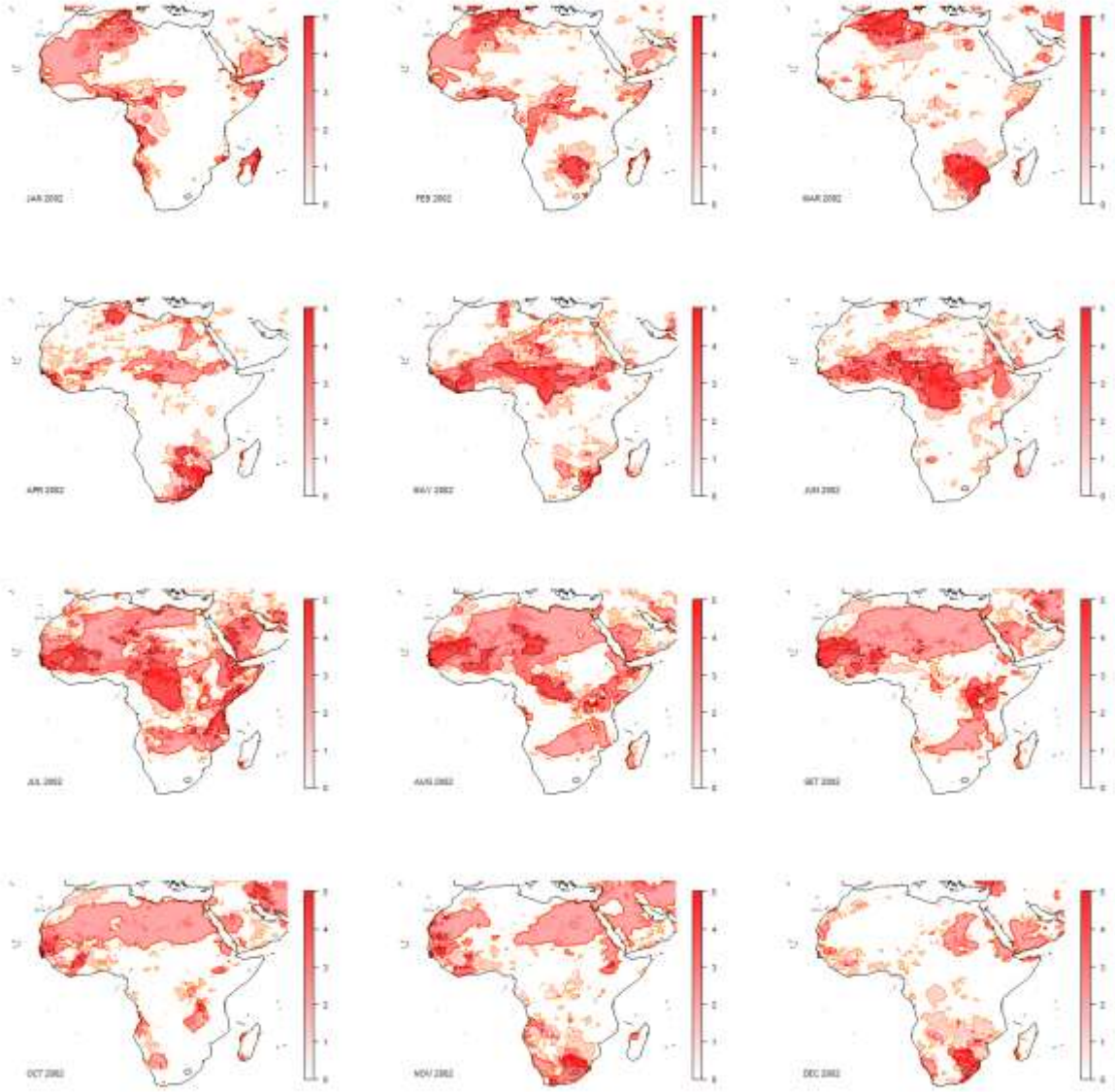

Figure 8-13 Same as Figure 8-11 but for 2002.

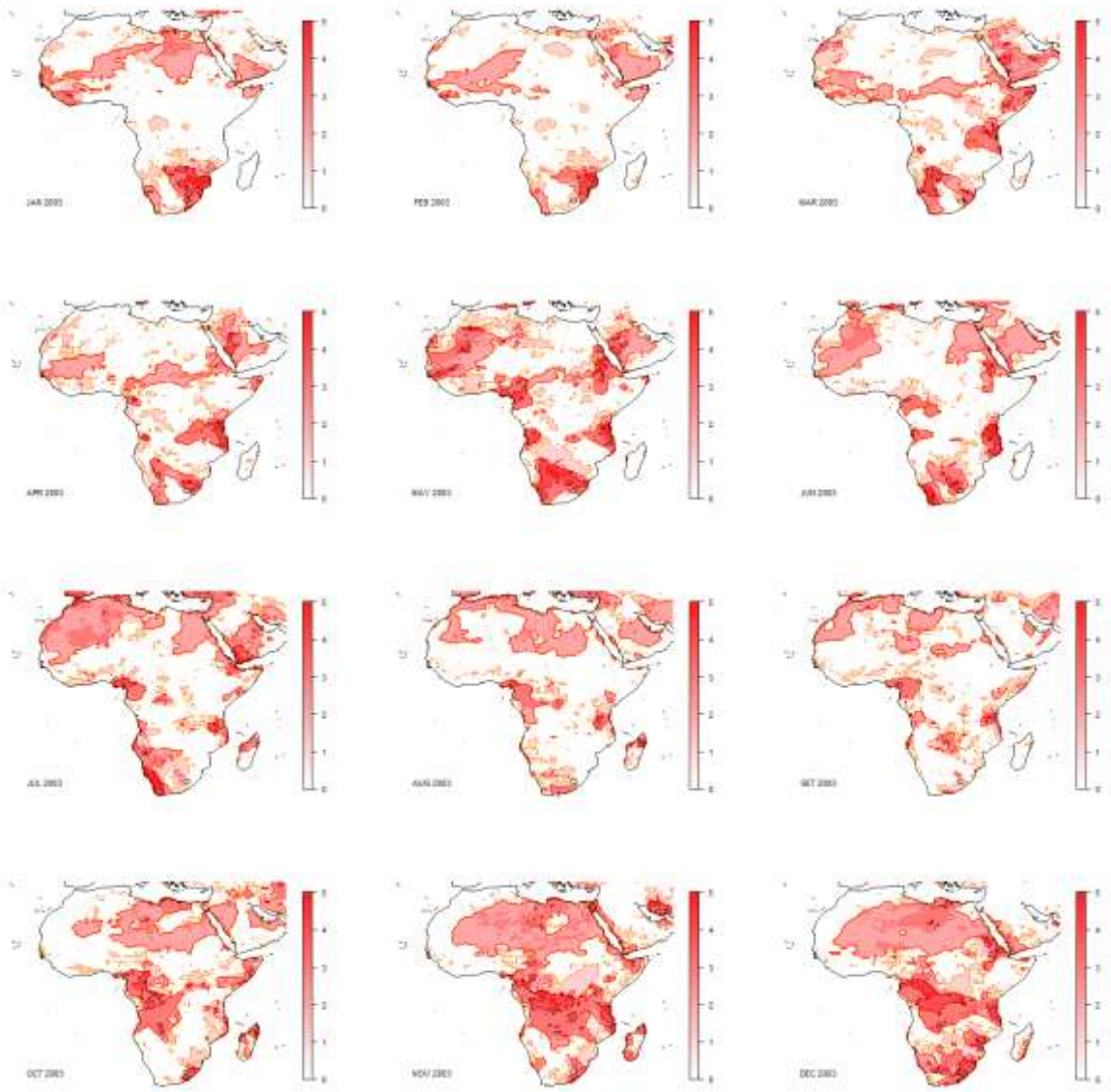

Figure 8-14 Same as Figure 8-11 but for 2003.

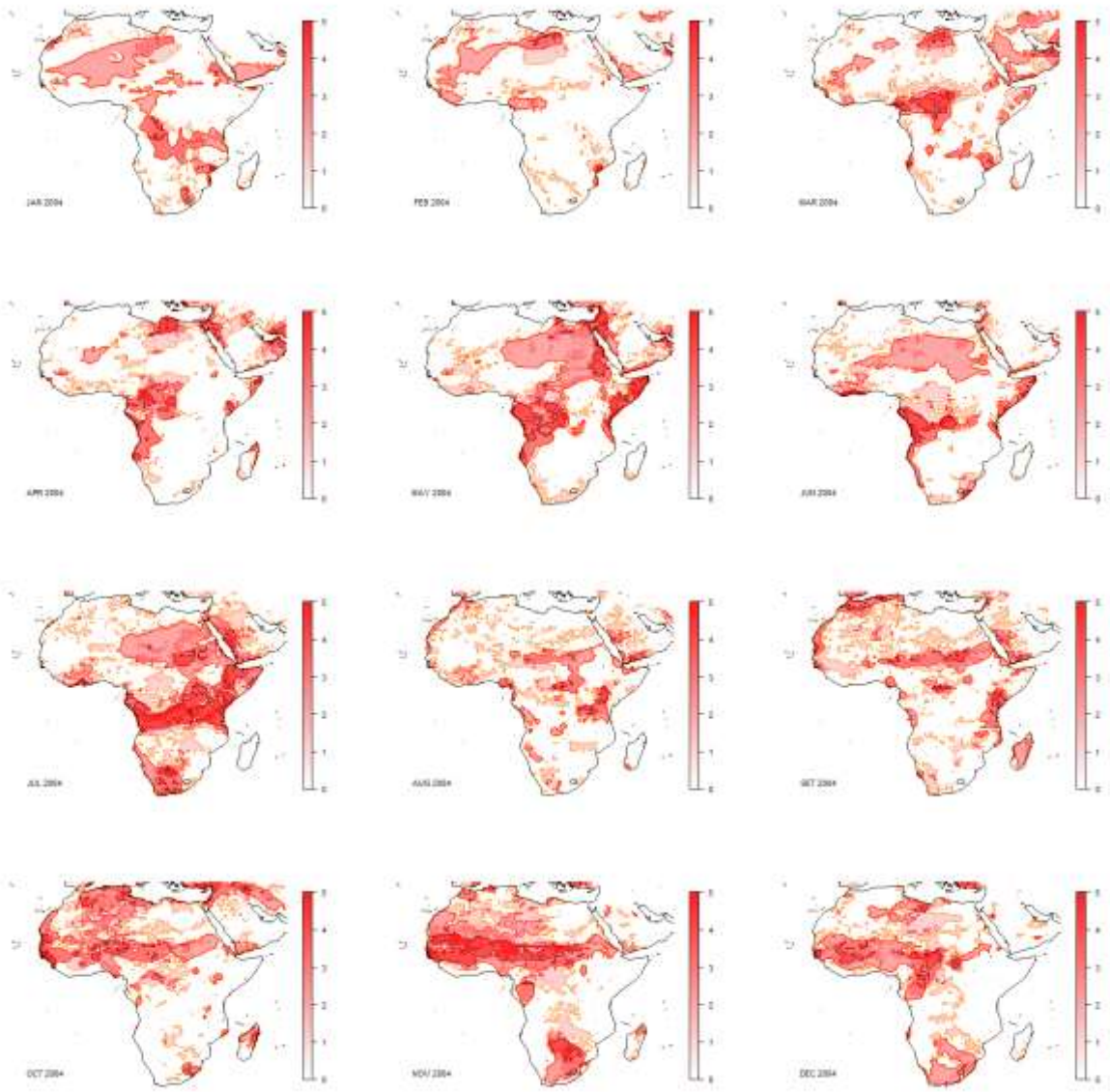

Figure 8-15 Same as Figure 8-11 but for 2004.

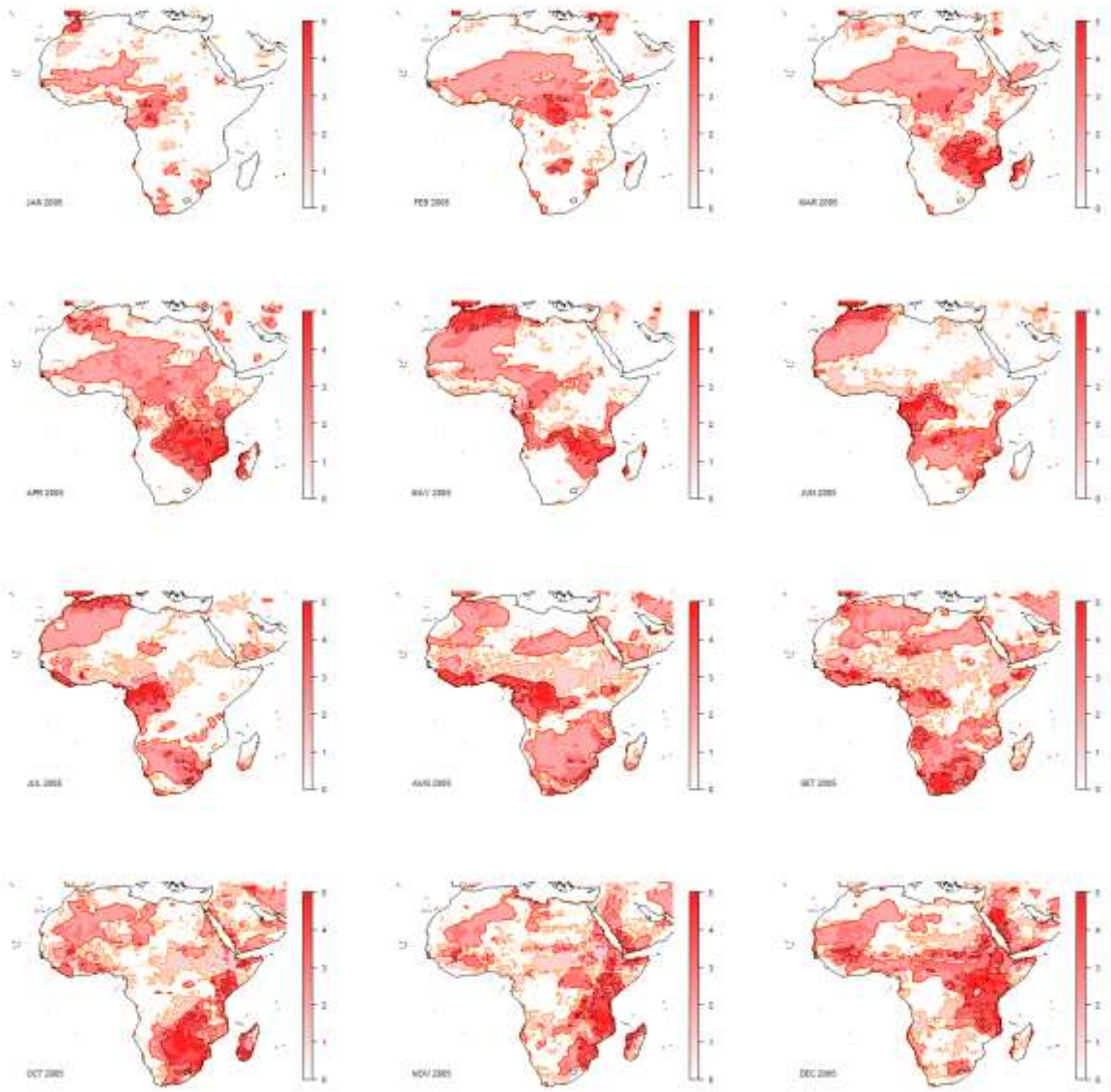

Figure 8-16 Same as Figure 8-11 but for 2005.

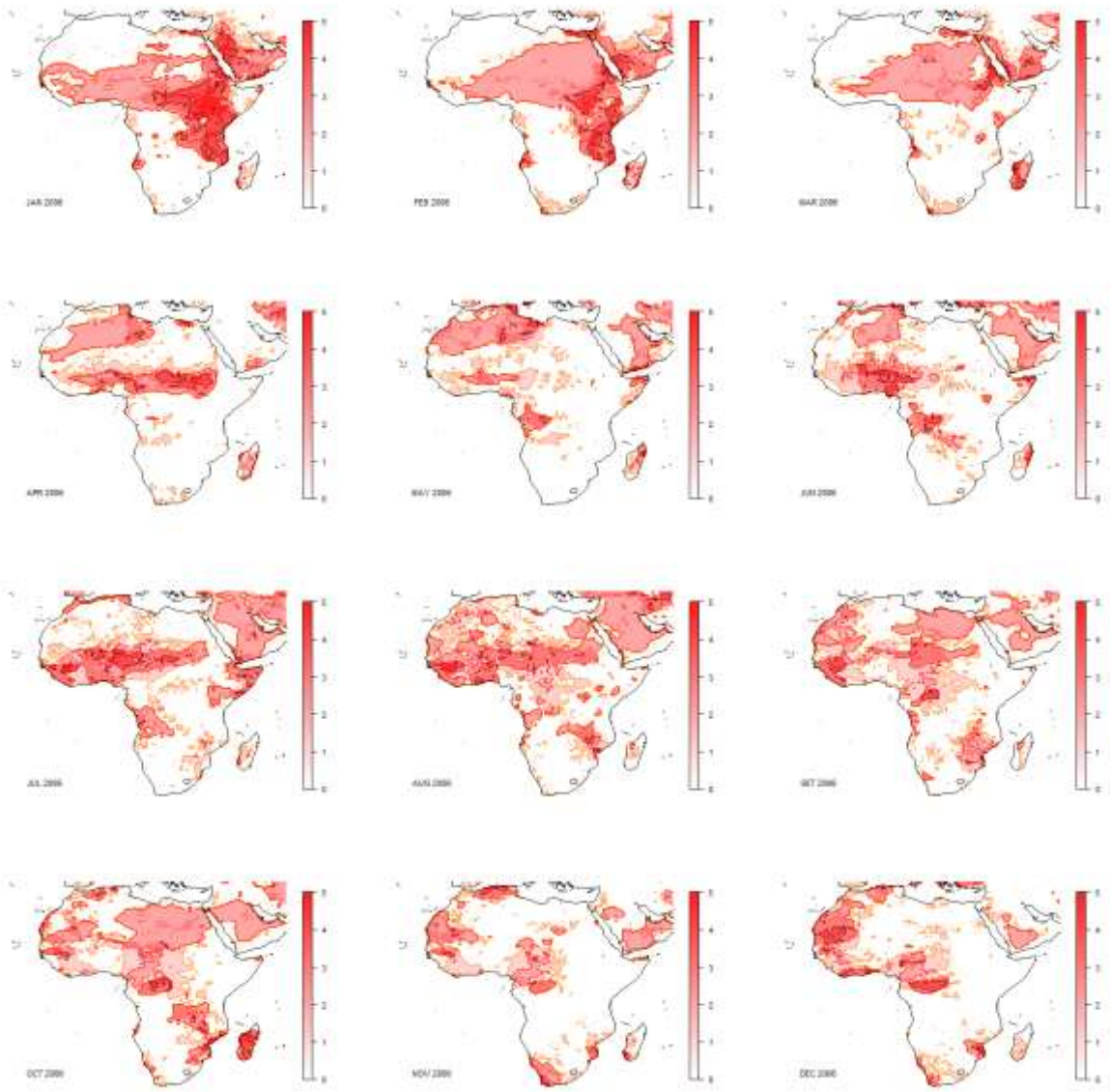

Figure 8-17 Same as Figure 8-11 but for 2006.

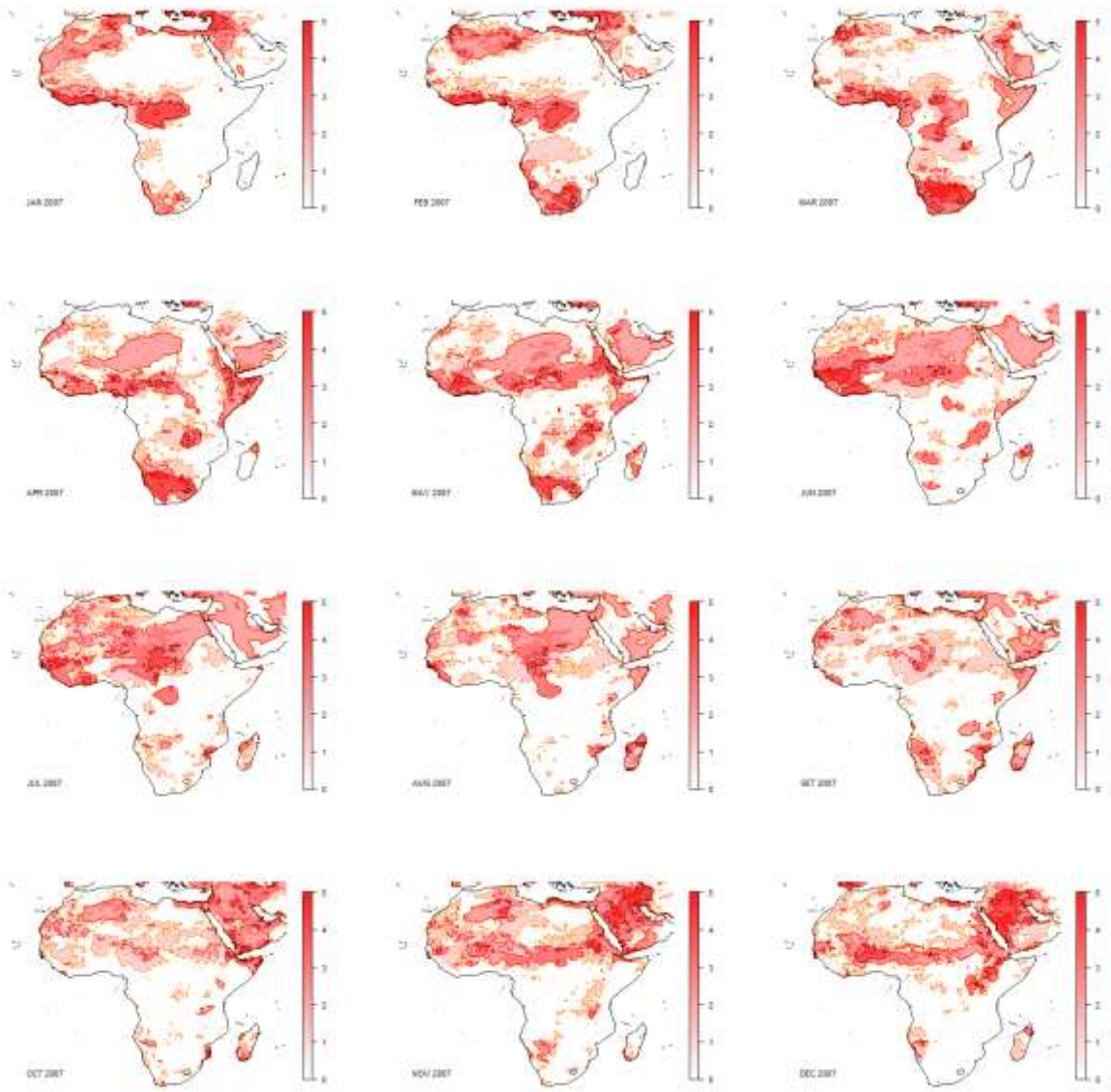

Figure 8-18 Same as Figure 8-11 but for 2007.

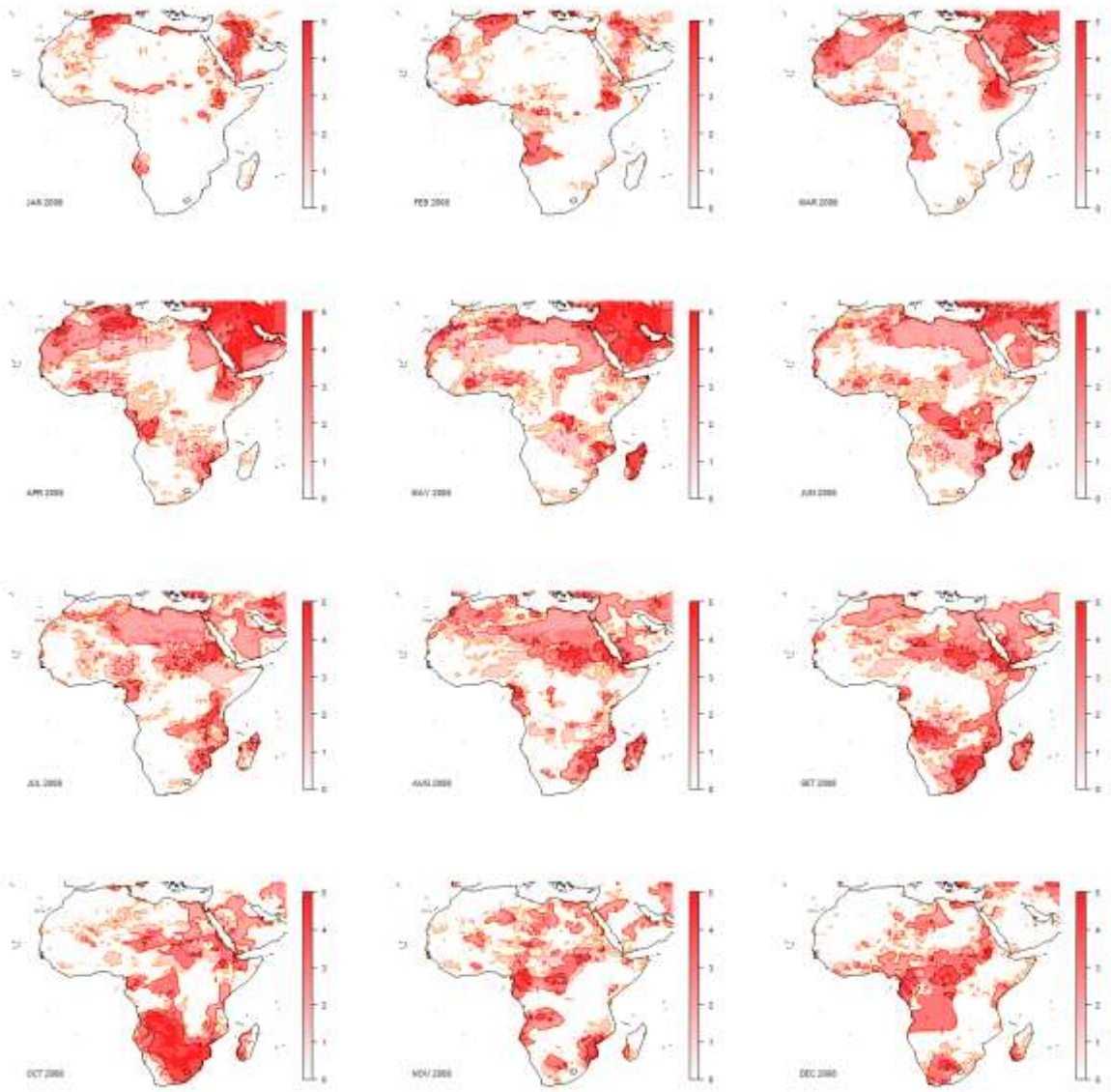

Figure 8-19 Same as Figure 8-11 but for 2008.

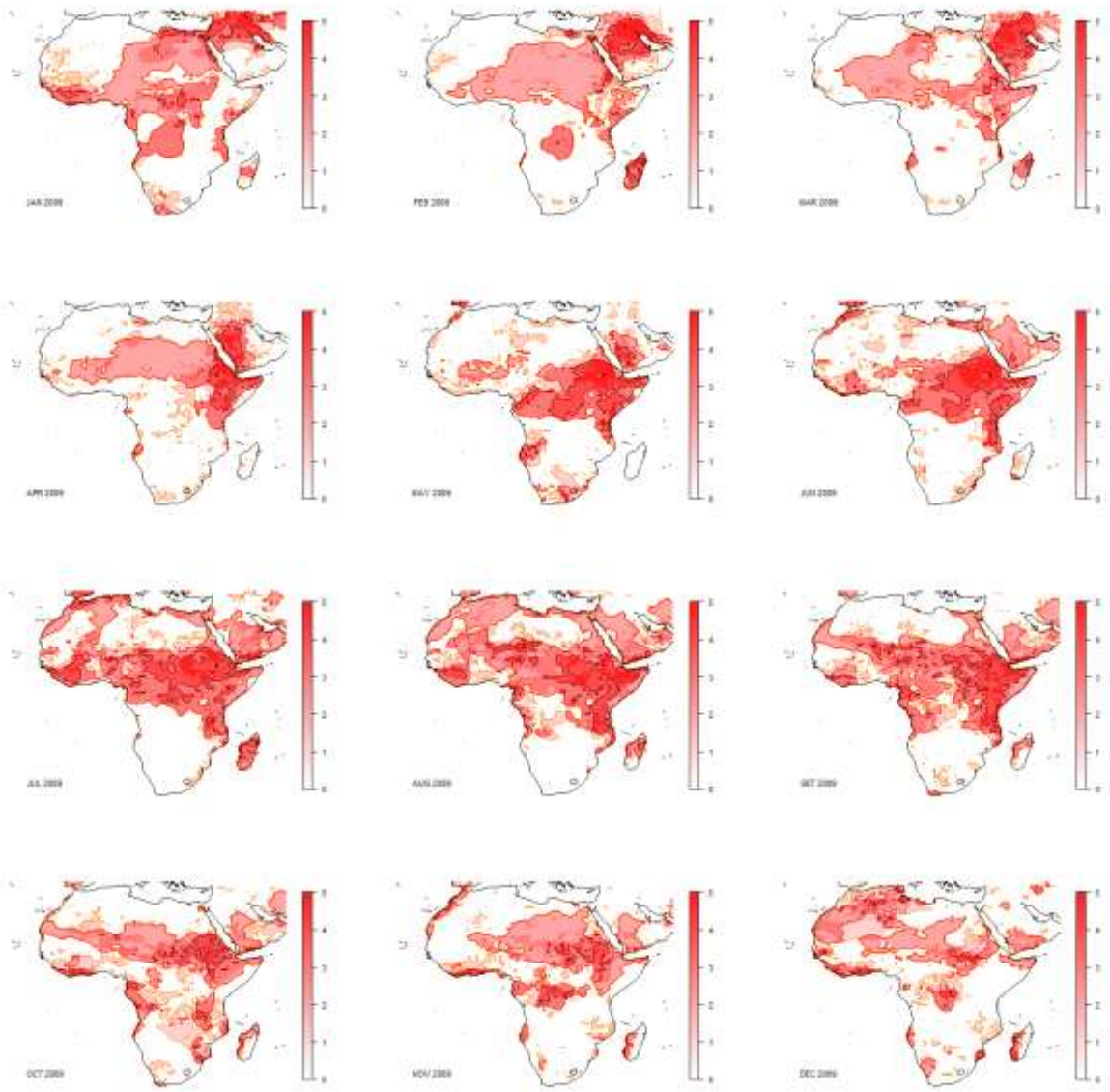

Figure 8-20 Same as Figure 8-11 but for 2009.